PRODUCTION OF RENEWABLE FUELS FROM DEOXYGENATION OF PALMITIC ACID OVER LEPIDOCROCITE TITANATE CATALYSTS

PORN-A-NAN ARSA

A THESIS SUBMITTED IN PARTIAL FULFILLMENT OF THE REQUIREMENT FOR THE DEGREE OF MASTER OF SCIENCE IN PETROCHEMICALS AND HYDROCARBON CHEMISTRY

DEPARTMENT OF CHEMISTRY
FACULTY OF SCIENCE
KING MONGKUT'S INSTITUTE OF TECHNOLOGY LADKRABANG

2016
KMITL-2016-SC-M-015-019

Thesis Title	Production of renewable fuels from deoxygenation of palmitic acid over lepidocrocite titanate catalysts
Student Name	Mr. Porn-a-nan Arsa
Student ID	56605049
Degree	Master of Science (Petrochemicals and Hydrocarbon Chemistry)
Department	Chemistry
Year	2016
Thesis Advisor	Assoc. Prof. Dr. Tawan Sooknoi
Thesis Co-advisor	Dr. Tosapol Maluangnont

ABSTRACT

This study investigated the deoxygenation of palmitic acid over several compositions of lepidocrocite titanate for the production of renewable fuels, including $K_{0.8}Li_{0.27}Ti_{1.73}O_4$, $K_{0.8}M_{0.4}Ti_{1.6}O_4$ (M = Mg^{2+}, Co^{2+}, Ni^{2+}, Cu^{2+}, Zn^{2+}), $K_{0.8}Fe_{0.8}Ti_{1.2}O_4$, $K_{0.8}Fe_{0.7}Mn_{0.1}Ti_{1.2}O_4$, $K_{0.8}Fe_{0.4}Mn_{0.4}Ti_{1.2}O_4$, $K_{0.8}Cu_{0.2}Ni_{0.2}Ti_{1.6}O_4$ and $K_{0.8}Cu_{0.2}Zn_{0.2}Ti_{1.6}O_4$. These catalysts were synthesized using a conventional solid state method from the corresponding mixture of K_2CO_3, TiO_2 and the metal oxides. Basic sites at the external and internal surfaces were evaluated by temperature-programmed desorption of CO_2 (CO_2-TPD) and by the liquid phase adsorption of palmitic acid, respectively. As an example, $K_{0.8}Zn_{0.4}Ti_{1.6}O_4$ has low basicity (0.04 mmol CO_2/g) is a weakly basic material (CO_2 desorption temperature of 50–300 $^{\circ}C$). However, it can intercalate as much as 37%wt of palmitic acid into the interlayer spaces, separating the titanate sheets by 0.1 nm further. The catalytic deoxygenation of intercalated palmitic acid was carried out in a semi-batch process at 350-500 $^{\circ}C$ under nitrogen atmospheric. It was found that linear long chain paraffins and α-olefins (C14 and C15) were obtained as the major products. C17 ketone and C16 aldehyde are also observed as minor products together with carbon dioxide and carbon monoxide. The liquid yield depends upon on the basicity of the catalysts, demonstrating the essential role of basic sites in the deoxygenation of palmitic acid. $K_{0.8}Li_{0.27}Ti_{1.73}O_4$ and $K_{0.8}Mg_{0.4}Ti_{1.6}O_4$ show a relatively high activity as compared to

other compositions of lepidocrocite titanate containing transition metals. $K_{0.8}Cu_{0.4}Ti_{1.6}O_4$ and $K_{0.8}Zn_{0.4}Ti_{1.6}O_4$ are selective for the decarboxylation of palmitic acid to C15 long chain paraffinic, while $K_{0.8}Fe_{0.8}Ti_{1.2}O_4$, $K_{0.8}Co_{0.4}Ti_{1.6}O_4$ and $K_{0.8}Ni_{0.4}Ti_{1.6}O_4$ facilitate the decabonylation of palmitic acid to C15 α-olefins. The incorporation of Mn enhances the ketonization activity. The co-substitution of two types of metals for titanium (as in $K_{0.8}Cu_{0.2}Ni_{0.2}Ti_{1.6}O_4$ and $K_{0.8}Cu_{0.2}Zn_{0.2}Ti_{1.6}O_4$) promotes the formation of C15 linear long chain paraffinic hydrocarbons. So, lepidocrocite titanate is a promising class of catalyst for the deoxygenation of fatty acids into renewable fuels.

Keywords: Deoxygenation, Lepidocrocite titanate, Palmitic acid, Renewable fuels

ACKNOWLEDGEMENT

The author wishes to gratefully thank the thesis advisor, Assoc. Prof. Dr. Tawan Sooknoi, and the thesis co-advisor, Dr. Tosapol Maluangnont, for their supervisions, inspiration, supports, suggestion and encouragement throughout. This thesis would not have been completely finished without their precious advice and supports.

I am grateful to Dr. Amnat Permsubsakul, Asst. Prof. Dr. Montree Thongkam and Assoc. Prof. Dr. Jatuporn Wittayakun for serving as the chairperson and the committee, and for valuable comments.

I would like to acknowledge the financial support from the Thailand Research Fund, granted to Assoc. Prof. Tawan Sooknoi (BRG5680007) and Dr. Tosapol Maluangnont (TRG5780160). I also appreciate the supports from the Department of Chemistry, Faculty of Science, King Mongkut's Institute of Technology Ladkrabang for the equipments, chemicals and facilities.

I would like to extend my thanks to Mr. Boonyawat Wuttitham, Mr. Thanasak Solos and Mr. Ayut Witsuthammakul for their help and advices in working the data analysis, support and encouragement.

I would like to extend my sincere appreciation to all teachers, friends and the member of this research group for their constant guidance, advice, support and encouragement.

Finally, I deeply appreciate and thank my parents and family for their love and supports.

Porn-a-nan Arsa

TABLE OF CONTENTS

TABLE OF CONTENTS (Continued)

TABLE OF CONTENTS (Continued)

LIST OF TABLES

LIST OF TABLES (Continued)

LIST OF FIGURES

LIST OF FIGURES (Continued)

LIST OF FIGURES (Continued)

LIST OF FIGURES (Continued)

CHAPTER 1

INTRODUCTION

1.1 Research Motivation

In recent years, the fuel prices are rising steadily because of the depletion of fossil fuel reserve. Therefore, the utilization of natural renewable resources has gained considerable attention for the production of fuel and related chemicals [1,2]. For example, triglyceride which can be easily obtained from vegetable oils, is an attractive renewable feedstock for agricultural country like Thailand.

Traditionally, biodiesel widely used as renewable fuel is obtained via the trans-esterification of triglyceride and alcohol [3,4]. However, such biodiesel is relatively polar, corrosive, and has low heating value. Since it is an alkyl ester, biodiesel can be readily hydrolyzed, showing low stability upon storage. Instead of performing the trans-esterification, the fatty acids produced from animal fats and vegetable oils can be alternatively converted to long chain hydrocarbons via the removal of an oxygen atom. Such reaction is called deoxygenation. The long chain hydrocarbons obtained via deoxygenation possess high stability and high heating value compared to the alkyl esters obtained via trans-esterification.

The fatty acids can be adsorbed on the surface of basic catalysts such as metal oxides, forming the respective carboxylates. Upon heating, the adsorbed fatty carboxylates can undergo decarboxylation, where long chain hydrocarbons are obtained together with the release of carbon dioxide. Meanwhile, the metal oxides could react with carbon dioxide forming metal carbonates. The metal carbonate can be further decomposed, and the active metal oxide catalyst is then recovered [5].

Decarboxylation of fatty acids has been extensively investigated over conventional metal oxide catalysts [6,7]. The reaction requires extremely high temperature and high pressure. Recently, the use of lepidocrocite titanates having a layered structure as the catalysts in the deoxygenation of fatty acid (palmitic acid) has been reported [8]. Pristine lepidocrocite titanate with good ordering along the stacking direction provides higher activity, as compared to re-assembled lepidocrocite titanate

where the registry between the layers was lost to some extent. However, details on the nature of the active sites have not been thoroughly studied.

In this research, lepidocrocite titanate catalysts of various compositions were prepared. The catalysts were tested for the deoxygenation of palmitic acid as a model compound for the production of long chain hydrocarbons i.e., diesel fuel, from renewable sources. The selectivity towards the elimination of the carboxylic group without breaking the hydrocarbon chain is focused.

1.2 Objectives of the study

1.2.1 To obtain long chain hydrocarbons from the deoxygenation of palmitic acid over lepidocrocite titanate catalysts.

1.2.2 To understand the role of basicity in lepidocrocite titanates on the activity and selectivity for the deoxygenation of palmitic acid.

1.2.3 To obtain optimum conditions for the deoxygenation of palmitic acid over the lepidocrocite titanate catalysts.

1.3 Scopes of the study

1.3.1 Preparation of lepidocrocite titanate catalysts by a conventional solid state synthesis from the mixture of the oxides/carbonates.

1.3.2 Characterization of lepidocrocite titanate catalysts by the following techniques:

1.3.2.1 X-ray Diffraction (XRD)

1.3.2.2 Gas adsorption analysis

1.3.2.3 CO_2-Temperature Programmed Desorption (CO_2-TPD)

1.3.2.4 H_2-Temperature Programmed Reduction (H_2-TPR)

1.3.2.5 Scanning Electron Microscopy (SEM)

1.3.2.6 Transmission Electron Microscopy (TEM)

1.3.2.6 Fourier Transform Infrared Spectroscopy (FTIR)

1.3.2.7 Thermogravimetric Analysis (TGA)

1.3.3 Investigation of the adsorption of the fatty acid and the respective swelling of lepidocrocite titanates using the solution of palmitic acid.

1.3.4 Investigation of the deoxygenation activity of prepared catalysts in a semi-batch reactor under nitrogen gas at atmospheric pressure.

1.3.4.1 Study on the reaction temperature

1.3.4.2 Study on the deoxygenation of palmitic acid over lepidocrocite titanate catalyst with various compositions.

1.3.4.3 Study on the deoxygenation of palmitic acid over co-substituted lepidocrocite titanate catalysts.

1.3.4.4 Study on the regeneration of catalyst.

1.3.5 Qualitative and quantitative analysis of liquid products by gas chromatography

1.4 Expected results

It is expected that this research will provide a new approach for the production of long chain hydrocarbons as fuels from renewable animal fats and vegetable oils available in Thailand.

CHAPTER 2

THEORY AND LITERATURE REVIEWS

2.1 Fatty acids

A fatty acid is a carboxylic (organic) acid, often with a long aliphatic tail containing 4 to 22 carbon atoms. The acid can be either saturated or unsaturated [9,10,11,12]. The fatty acid composition of lipids is particularly important in determining the physical, chemical and nutritional properties of lipids. Natural fatty acids can be obtained from the hydrolysis of triglycerides from several sources such as hard animal fats (tallow), coconut, palm kernel and soybean oils. They can also be obtained from the fractional distillation of crude tall oil, which is a byproduct of Kraft pulping of pine wood. Southeast Asia is the major source for coconut, palm and palm kernel oils [13], where several new plants have been built recently. Table 2.1 shows the composition of common fatty acids in vegetable oils (taken from [14]).

Saturated fatty acids do not contain any double bonds or other functional groups along the chain. The term "saturated" implies that all carbon atoms (apart from the carboxylic acid [-COOH] group) contain as many hydrogens as possible. On the other hand, unsaturated fatty acids contain at least one alkene group with double-bonded carbon atoms. The majority of naturally-occurring unsaturated fatty acids are in *cis*-form. Fatty acids in the *trans* configuration (trans fats) are usually not found in nature and are the result of human processing (e.g., hydrogenation) [12].

About 100,000 metric tons of the natural fatty acids are consumed in the preparation of various fatty acid esters. The simple esters of small-chain alcohols (methyl-, ethyl-, *n*-propyl-, isopropyl- and butyl esters) are used as emollients in cosmetics and other personal care products and as lubricants. Esters of fatty acids with more complex alcohols, such as sorbitol, ethylene glycol, diethylene glycol and polyethylene glycol are consumed in foods, personal care products, paper, water treatment, metal working fluids, rolling oils and synthetic lubricants [15]. Some chemical reactions known to transform these renewable materials into fuels, taken palmitic acid as a representative for fatty acids, are summarized below.

Table 2.1: Fatty acid compositions (wt%) of common vegetable oils [14]

Fatty acid	Notation*	Palm	Olive	Peanut	Soybean	Rape	Sunflower	Grape	H.O.sunflower	Almond	Corn
Lauric	C12:0	0.1	0.0	0.0	0.0	0.0	0.0	0.0	0.0	0.0	0.0
Myristic	C14:0	0.7	0.0	0.1	0.0	0.0	0.0	0.1	0.0	0.0	0.0
Palmitic	C16:0	36.7	11.6	8.0	11.3	4.9	6.2	6.9	4.6	10.4	6.5
Palmitoleic	C16:1	0.1	1.0	0.0	0.1	0.0	0.1	0.1	0.1	0.5	0.6
Stearic	C18:0	6.6	3.1	1.8	3.6	1.6	3.7	4.0	3.4	2.9	1.4
Oleic	C18:1	46.1	75.0	53.3	24.9	33.0	25.2	19.0	62.8	77.1	65.6
Linoleic	C18:2	8.6	7.8	28.4	53.0	20.4	63.1	69.1	27.5	7.6	25.2
Linolenic	C18:3	0.3	0.6	0.3	0.1	7.9	0.2	0.3	0.1	0.8	0.1
Arachidic	C20:0	0.4	0.3	0.9	0.3	0.0	0.3	0.3	0.3	0.3	0.1
Godoleic	C20:1	0.2	0.0	2.4	0.3	9.3	0.2	0.0	0.0	0.0	0.1
Behenic	C22:0	0.1	0.1	3.0	0.0	0.0	0.7	0.0	0.7	0.1	0.0
Erucic	C22:1	0.0	0.0	0.0	0.3	23.0	0.1	0.0	0.0	0.0	0.1
Lignoceric	C24:0	0.1	0.5	1.8	0.1	0.0	0.2	0.0	0.3	0.2	0.1
Nervenic	C24:1	0.0	0.0	0.0	0.0	0.0	0.0	0.0	0.0	0.4	0.0

*This notation indicates the number of carbon atoms and the number of double bond. For example, C12:0 indicates a fatty acid with a total number of 12 carbon atoms, without any double bond.

2.1.1 Palmitic acid

Palmitic acid $CH_3(CH_2)_{14}CO_2H$, or hexadecanoic acid in IUPAC nomenclature with the structure shown in Figure 2.1, is the most common saturated fatty acid found in animals, plants and microorganisms [16]. As the name indicates, palmitic acid is a major component of the oils from palm trees (palm oil, palm kernel, and palm kernel oil), although it can also be found in meats, cheeses, butter, and dairy products. Palmitate is a term for the salt and ester of palmitic acid. The palmitate anion is formed when palmitic acid is put into a condition with basic pH values [17].

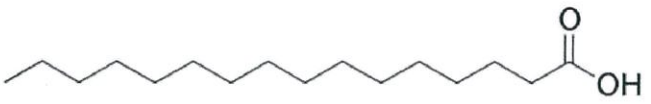

Figure 2.1 The molecular structure of palmitic acid.

Palmitic acid can be prepared by treating fats and oils with water at a high pressure and temperature (above 200 °C) leading to the hydrolysis of triglycerides. The resulting mixture is then distilled [18].

2.2 Reactions of fatty acids

2.2.1 Esterification

Esterification refers to the production of an ester from the reaction between alcohols and acids as shown in Figure 2.2. The most common esterification processes involve nucleophilic acyl substitution, where the carbonyl group of the acid acts as an electrophile and gets attacked by a nucleophilic alcohol. However, other processes are possible; esterification by alkylation reverses the roles of "classic" carbonyl chemistry: a carboxylate anion is used as a nucleophile that displaces a halide ion in an S_N2 reaction.

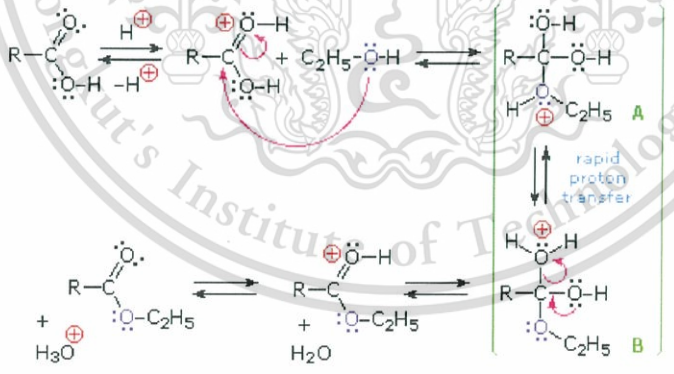

Figure 2.2 Acid-catalyzed esterification of fatty acids. (Taken from [19])

Currently, there is a great interest in the esterification reaction because of its application to several industries [20]. Organic esters are frequently used in the production of plastic derivatives, in the solvent industry, perfumery, agro-chemistry and other branches of fine chemistry [21]. One of the main products obtained by the

esterification of long chain fatty acids is biodiesel, the use of which has several environmental benefits [22].

2.2.2 Deoxygenation

Deoxygenation is a chemical reaction involving the removal of oxygen atoms from a starting molecule. In this context, a carboxyl group (-COOH) is split off as carbon dioxide (CO_2) and/or carbon monoxide (CO) as shown in Eq. 2.1 and 2.2 respectively. It is a novel method for the production of diesel-like fuels from renewable resources such as vegetable oils and animal fats. Here, linear hydrocarbons are produced from the fatty acid alkyl group [23]. Chemical decarboxylation without a catalyst often requires extensive heating in a high-boiling solvent.

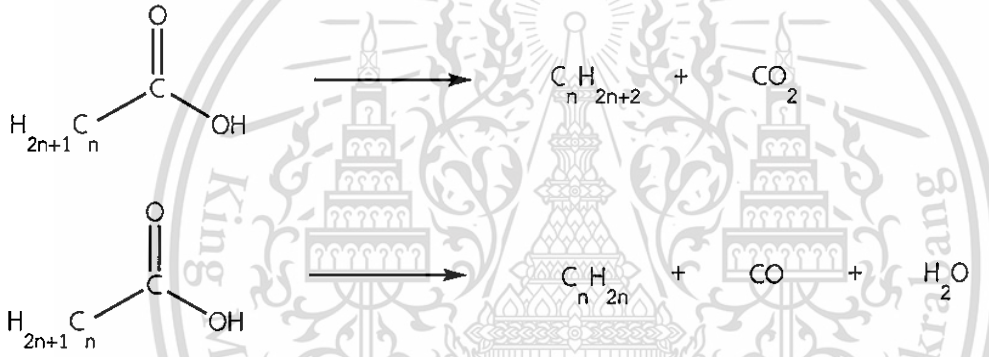

(Eq. 2.1)

(Eq. 2.2)

As an example, the catalytic decarboxylation of lauric acid (Eq. 2.3) has been studied over Pd/C catalyst in a continuous process at 255-300°C. Very high selectivity (>95 %) to the desired products, namely C_{11} hydrocarbons, can be achieved [24].The use of expensive Pd metal, however, makes the process unattractive. The conversion of lauric acid declined substantially within 10-20 minutes of the time-on-stream. The initial concentration of lauric acid was decisive for the catalyst deactivation; the higher the initial concentration of fatty acids, the more extensive catalyst deactivation.

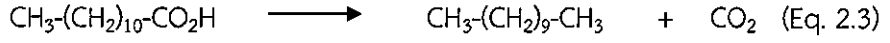

(Eq. 2.3)

2.2.3 Ketonization

Ketonization or ketonic decarboxylation is a reaction in which two molecules of carboxylic acid are converted into a symmetric ketone, carbon dioxide and water as shown in equation (2.4). This reaction is catalyzed by bases. The reaction mechanism likely involves the formation of carbanions as the intermediate from the decarboxylation of one acid group, followed by a nucleophilic attack by another acid group as a concerted reaction (S_N2). This reaction is different from the oxidative decarboxylation which proceeds through a radical mechanism [25].

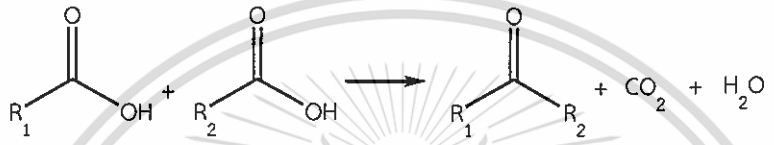

(Eq. 2.4)

2.3 Solid base catalysts

The use of a solid base catalyst instead of a basic solution offers several process advantages. Solid bases can be either of Brønsted- or Lewis-type. There are specific sites or centers, called "basic sites" that function as base on the surface of such solids. The advantages of using solid bases include the elimination of a quenching step (with the associated reduction in the aqueous waste), and the opportunity to operate in a continuous process. Several types of heterogeneous catalysts with base functionality are known as shown in Table 2.2 [26]. A major group of basic catalysts is supported or unsupported metal oxides. The basicity originates from O^{2-} anions on the surface, having different coordination numbers dependent on the crystalline planes where those oxygen atoms belong to.

Table 2.2 Materials of solid base catalysts (Taken from [25])

Metal oxides	MgO, CaO, Al_2O_3, ZrO_2, Rare earth oxides (La_2O_3 etc.), Alkali metal oxides
Mixed oxides	SiO_2-MgO, SiO_2-CaO, Al_2O_3-MgO (calcined hydrotalcite)
Alkali or alkaline earth oxides loaded on a support	MgO/SiO_2, Cs_2O on zeolites
Alkali compounds on Al_2O_3	KF/Al_2O_3, K_2CO_3/Al_2O_3, KNH_2/Al_2O_3, NaOH/Al_2O_3, KOH/Al_2O_3
Amides and imines loaded on a support	KNH_2/Al_2O_3, K, Y, Eu supported on zeolites from ammoniacal solution
Alkali metals loaded on a support	Na/Al_2O_3, K/Al_2O_3, K/MgO, Na/zeolite
Anion exchangers	Anion exchange resins Hydrotalcite and modified hydrotalcites
Zeolites	K, Rb, Cs-exchanged X-zeolites, ETS-10
Clays	Sepiolite, Montmorillonite
Phosphates	Hydroxyapatite, natural phosphates
Amines or ammonium ions tethered to a support	Aminopropyl group /silica or MCM-41 Alkylammonium group/MCM-41

The catalytic activity of BaO, SrO, CaO and MgO in the trans-esterification of vegetable oils into biodiesel has been reported [27]. One of the limitation of these common oxides is their low surface areas which limit the number of active sites available for the reaction. Also, some of them are slightly soluble in methanol which is used as a solvent of the fatty acid, thereby reducing the lifetime of a catalyst [28]. Considering that K_2O, MgO, ZnO and TiO_2 are known as basic catalysts (Table 2.2), it is interesting to see what would be the catalytic activity of oxides having these active cations altogether in a crystal. Recently, lepidocrocite titanates consisted of potassium, zinc (magnesium), and oxygen have been studied as catalysts for the deoxygenation of palmitic acid [8]. It was found that pristine lepidocrocite titanate with good ordering along the layers provided higher activity, as compared to re-assembled lepidocrocite

whose the registry between the layers was lost to some extent. Lepidocrocite titanates will be described in Section 2.3.1.

2.3.1 Lepidocrocite titanate

Lepidocrocite-type structure refers to the structure of γ-FeOOH. We will describe here the structure of the lepidocroite titanate $H_xTi_{2-x/4}\square_{x/4}O_4$ ($x \sim 0.7$; $\square$ is the vacancy) as an example. The structure can be constructed from the edge sharing of $(Ti,M)O_6$ octahedra, which extend into the sheets (or layers) along the *a*- and *c*-direction of the orthorhombic unit cell [29] as shown in Figure 2.3. These sheets stack along the *b*-direction like a pile of paper, resulting in 2-dimensional crystallites with the preferred orientation along the *b*-axis. The sheet as an elementary unit is roughly one-nanometer thick, having only 3 layers of atoms [30]. In a more general description, lepidocrocite titanates have the formula $A_xM_yTi_zO_4$, where A is an alkali metal, M is a transition metal having the valence not equal to +4 such as Li^+ [31], Zn^{2+} or Mg^{2+} [32], or Fe^{3+} [33], or the cation vacancy. The subscripts x, y and z indicates appropriate stoichiometry. Because of the substitution of M^{n+} ($n < 4$) or the formation of the cation vacancy, the $(Ti,M)O_6$ layers become negatively charged. In order to preserve charge neutrality, alkali metal cations A^+ are usually incorporated between the layers.

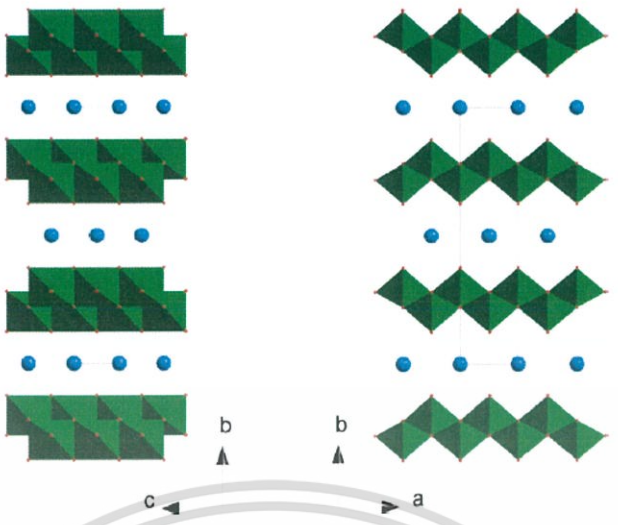

Figure 2.3 The crystal structure of lepidocrocite titanate viewed on the *bc* plane (left) and on the *ab* plane (right). The green polyhedral represent the $(Ti,M)O_6$ units, whereas the blue dots represent the alkali metal cations located between the layers. Taken from [34].

Lepidocrocite titanates exhibit chemical reactivities such as ion-exchange, intercalation, and swelling characteristics of layered materials. The A^+ cations originally located between the layers can be ion exchanged with a wide variety of guest species such as inorganic and/or organic cations, protons, and surfactants. For example, the ion exchange of K^+ in $K_{0.8}Li_{0.27}Ti_{1.73}O_4$ with H^+ results in $H_{1.07}Ti_{1.73}O_4{\cdot}H_2O$ where $H^+{\cdot}H_2O$ residing between the layer. For the mentioned composition, the repeating distance along the *b*-direction increased from 1.55 nm to 1.84 nm as a result of the ion exchange [31]. The ion exchange of guest species into the layers with a change in the distance between the layers is specifically called *intercalation*. The intercalation of large guest species could lead to the ultimate separation of the sheets, resulting in the colloidal suspension of atomically-thin nanosheets [31]. The process leading to such ultimate separation is called *exfoliation*.

Lepidocrocite titanates are of interest in a variety of applications [35]. However, the basicity of lepidocrocite titanates has not been reported so far, despite the fact that they have layered structure similar to hydrotalcites which are the well-known examples to exhibit basicity [36]. In this research, lepidocrocite titanate catalysts of various compositions will be prepared. The adsorption of palmitic acid and the respective

swelling of the titanates will be investigated. The deoxygenation of palmitic acid will be studied as a model reaction for the production of long chain hydrocarbons i.e., diesel fuel, from renewable sources. The characteristic of fuel oils will be discussed in Section 2.4.

2.4 Fuel oils

The fuel products derived from petroleum supply account for more than half of the world's total supply of energy [37]. These products include gasoline, kerosene, and diesel oil, serving as the fuel for automobiles, tractors, trucks, aircraft, and ships. Besides, fuel oil and natural gas are used to heat homes and commercial buildings, as well as to generate electricity. The constant demand for these products is the main driving force behind the petroleum industry. Other products, such as lubricating oils, waxes and asphalt, have also added to the popularity of petroleum as a national resource. The boiling range, carbon atom and phase of petroleum products are shown in **Table 2.3**.

Table 2.3 Boiling range of petroleum products [37]

Product	Boiling range, ^{o}C	Phase	Carbon atoms
Gas petroleum	< 10	Gas	1-4
Gasoline	30-185	Liquid	4-13
Kerosene	170-250	Liquid	10-14
Diesel	175-350	Liquid	14-19
Lubricant	350-500	Liquid	19-35
Wax	350-500	Solid	19-35
Fuel oil	> 500	Liquid	> 35
Bitumen	> 500	Solid	> 35

2.4.1 Kerosene

Kerosene, also called paraffin or paraffin oil, is a flammable pale-yellow or colorless oily liquid with a characteristic odor. It is obtained from petroleum sources and has found several uses such as burning in lamps and domestic heaters or furnaces, as a fuel or a fuel component for jet engines, and as a solvent for greases and insecticides. Kerosene is a refined petroleum distillate having a flash point of about 25

^{o}C. It is obtained from the straight-run petroleum fraction that boiled between approximately 205 and 260 ^{o}C. The term kerosene is often incorrectly applied to various fuel oils. In fact, a fuel oil is actually any liquid or liquid petroleum product that produces heat when burned in a suitable container, or that produces power when burned in an engine. Chemically, kerosene usually consists of about 10 different hydrocarbons, each containing from 10 to 16 carbon atoms per molecule; the constituents include *n*-dodecane (*n*-$C_{12}H_{26}$), alkyl benzenes, and naphthalene and its derivatives [38,39]. Since kerosene is used as a burning oil, it must be free from aromatic and unsaturated hydrocarbons, as well as from the more harmful sulfur compounds. Kerosene is a stable product, and additives are not required to improve its quality.

2.4.2 Diesel

Diesel fuel oil is a blend of straight-run gas oil and cracked gas oil, resulting in a product boiling in the range of 175-345^{o}C. [40]. Cetane number is a measure of the tendency of a diesel fuel to knock in a diesel engine. The scale is based upon the ignition characteristics of two hydrocarbons, *n*-hexadecane (cetane) and heptamethylnonane, whose the structures are shown in Figure 2.4.

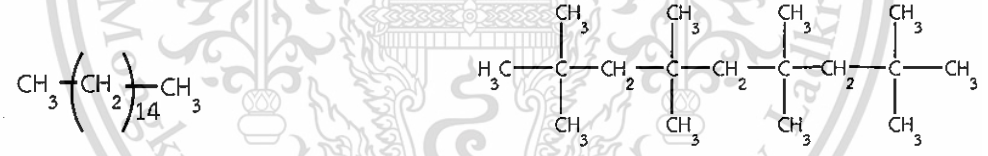

n-hexadecane (cetane) octametylnonane

Figure 2.4 The chemical structure of n-hexadecane (cetane) and octamethylnonane

Cetane has a short delay period during ignition and is assigned a cetane number of 100; heptamethylnonane has a long delay period and is assigned a cetane number of 15. Just as the octane number is meaningful for automobile fuels, the cetane number determines the ignition quality of diesel fuels. Cetane number is equivalent to the percentage by volume of cetane in the blend with heptamethylnonane, which matches the ignition quality of the test fuel.

2.5 Literature reviews

Catalytic decarboxylation is a well-established chemical reaction in an industrial process and has also been widely applied in organic synthesis on a smaller scale. It has been studied in broad reaction conditions and over various types of catalyst. However, works on the deoxygenation of fatty acid over metal oxides as the catalyst are rather limited.

Maki-Avera *et al* [41] studied the decarboxylation/decarbonylation of a fatty acid and their esters over Pd metal supported on activated carbons in a semibatch reactor. The main studied parameters were catalyst acidity, type of the feed, effect of the solvent, and the type of carrier gas. High yields of the desired product, *n*-heptadecane, were achieved from the decarboxylation of stearic acid at 300 $^{\circ}$C and 17.5 bar under helium gas. Similar work was reported by Snare *et al* [42] on the catalytic deoxygenation of stearic acid over palladium supported on carbon catalyst. A completed conversion of stearic acid with 98% selectivity toward the deoxygenated C17 products was obtained in a semibatch reactor at 300-360 $^{\circ}$C, 15-27 bar.

Also, the catalytic deoxygenation of palmitic and steric acids mixture has been reported over 1 wt%Pd supported on mesoporous carbon in a semibatch reactor using dodecane as the solvent. The reaction conditions are the temperature of 260-300 $^{\circ}$C, under an overall pressure of 17.5 bar of 5 vol% H_2/He. The main liquid products were *n*-pentadecane and *n*-pentadecane, which were formed in parallel [43].

Besides precious metal catalysts with or without the support, there are reports on oxide catalysts. For example, Chang Hyun *et al*. reported that oxides derived from hydrotalcite were active for the decarboxylation of oleic acid without hydrogen gas in an autoclave reactor at 300-400 $^{\circ}$C [44]. It was proposed that oleic acid might undergo saponification on MgO surface. This catalyst showed 100 % conversion of oleic acid at 400 $^{\circ}$C.

Additionally, there are reports in 2006, that ZrO_2, Y_2O_3, and CeO_3 can decompose steric acid in supercritical water at 400 $^{\circ}$C, 25-40 MPa in a batch reactor. The catalyst was stable in the reaction using supercritical water and the major product is C16 alkene and CO_2. An addition of alkali hydroxide (NaOH and KOH) in the supercritical water reaction enhanced the decarboxylation of steric acid with the main products being C17 alkane and CO_2 [45].

Tweesin [7] has reported the deoxygenation of palmitic acid over MgO, CaO, SrO and BaO in semi-batch reactor. The reaction was conducted using a 1/1 or 0.5/1 by mole of catalysts/palmitic acid at 460 °C for 6 hours and with nitrogen gas as carrier gas. The alkaline earth metal oxides showed high activity (>70%yield) for deoxygenation of palmitic acid.

Dararat *et al.* [46] studied the decarboxylation of palmitic acid to produce linear alpha olefins (LAOs) over cerium-metal mixed oxide catalysts. Catalytic activity testing showed that C_{31} ketone was produced as the major product from the ketonization of palmitic acid. This ketone can undergo cracking to a combination of C_{17} ketone, heavy ketone/alcohol and hydrocarbons including liquid and small hydrocarbons.

N. Asikin-Mijan *et al.* [47] reported that the deoxygenation of triolein over Co-CaO and W-CaO in batch reactor at reaction conditions; 350 °C reaction temperature, 45 min reaction time, 5 wt.% catalyst loading, 10 mbar pressure. The liquid product over Co-CaO and W-CaO yielded 32% and 22% of C8-C17 hydrocarbon with gasoline selectivity of 75% and 65% respectively. Co-CaO catalyst with positive effect on cracking-deoxygenation process was further investigated by study the effect of Co content from 10 to 40 wt.%. Results showed that paraffinic hydrocarbon yield was increased from 25% to 65%, while gaso-line selectivity increased from 56% to 84%.

Recently, Limsakul *et al.* [8] has reported the deoxygenation of fatty acid (palmitic acid) over lepidocrocite titanates. Pristine lepidocrocite with high ordering along the stacking direction provided higher activity, as compared to re-assembled lepidocrocite where the registry between the layers was lost to some extent. However, details on the nature of the active sites have not been thoroughly studied.

CHAPTER 3

RESEARCH METHODOLOGY

3.1 Reagents

1. Titanium dioxide (TiO_2) powder (APS Ajax Finechem), 99.5%
2. Potassium carbonate (K_2CO_3) powder (Carlo Erba), ≥99 %
3. Magnesium oxide (MgO) powder (Fluka), ≥98 %
4. Lithium carbonate (Li_2CO_3) powder (Acros), ≥99 %
5. Zinc oxide (ZnO) powder (Nano Materials Technology Co., Ltd.)
6. Copper(II) oxide (CuO) powder (Acros), ≥99+%
7. Nickel(II) oxide (NiO) powder (Acros), ≥97%
8. Cobalt(II) oxide (CoO) powder (Aldrich), ≥99+%
9. Iron(III) oxide (Fe_2O_3) powder (Sigma-Aldrich), ≥99%
10. Palmitic acid (Fluka), ≥97 %
11. Mesitylene (Acros), >99%
12. Isopropanol (Carlo Erba), analysis grade
13. Nitrogen gas, (PRAXAIR), high purity (99.99%)
14. Hydrogen gas, (PRAXAIR), high purity (99.99%)
15. Helium gas, (PRAXAIR), high purity (99.99%)
16. Air, (PRAXAIR), high purity (99.99%)

3.2 Apparatus

1. Catalytic testing rig
2. Horizontal tube furnace (Carbolite GHA Single Zone, Catalytic Chemistry Research unit, KMITL)
3. Muffle furnace (Cole-Parmer, Catalytic Chemistry Research unit, KMITL)
4. Tube reactor
5. Trap condenser
6. Clamp
7. Heating tape
8. Vials

9. Hot plate

10. Oven (Thermo Fisher scientific, Scientific Instrument Service Centre, KMITL)

11. Laboratory glassware

12. Laboratory plasticware

13. Magnetic stirrer

14. Mechanical shaker (Thermo Fisher scientific, Scientific Instrument Service Centre, KMITL)

15. Gas chromatograph (Hewlett Packard, HP 6890 series GC system, Scientific Instrumental Service Centre, KMITL)

16. X-ray powder diffractometer (Rigaku, DMAX 2200/Ultima+, Department of Chemistry, Faculty of Science, Chulalongkorn University)

17. Thermogravimetric analyzer (Perkin-Elmer, Scientific Instrument Service Centre, KMITL)

18. Fourier transforms infrared spectrometer (Perkin Elmer, Scientific Instrument Service Centre, KMITL)

19. Mass spectrometer (Agilent Technologies, 5973 inert/Mass Selective Detector, Scientific Instrument Service Centre, KMITL)

20. SEM (ZEISS, EVO/MA10, College of data storage innovation, KMITL)

21. TEM (Jeol, Jem 2010, National Metal and Materials Technology, NSTDA)

3.3 Experimental procedure

3.3.1 Preparation of catalyst

Lepidocrocite titanate was synthesized by a conventional solid state synthesis from mixtures of the oxides/carbonates. Potassium carbonate was dried at 120 °C in an oven overnight prior to use. Other chemicals were used as received. The procedure reported herein was slightly modified from that in the literature [28]. In a typical synthesis, the $K_{0.8}Li_{0.27}Ti_{1.73}O_4$ lepidocrocite titanate was synthesized from the physical mixture of K_2CO_3 (18.3332 g), Li_2CO_3 (3.3120 g) and TiO_2 (22.9234 g). The powder was ground together in a mortar for 30 minutes. They were then put into an alumina boat and heated in a tube furnace where the temperature was raised (10 °C/min) from room temperature to 800 °C followed by a hold for an hour. Next, the boat was immediately taken out from the furnace; the content was reground and subject to a heating at

800 °C for 20 hours twice, with grinding between each step. This material will be called "KLi" hereafter. The magnesium-containing lepidocrocite titanate can be made similarly, starting from the mixture of K_2CO_3 (18.2658 g), MgO (2.6639 g) and TiO_2 (21.1096 g) corresponding to the required stoichiometry for $K_{0.8}Mg_{0.4}Ti_{1.6}O_4$. This material will be called "KMg" hereafter.

Other lepidocrocite titanates $K_{0.8}M_{0.4}Ti_{1.6}O_4$ (M = Zn^{2+}, Cu^{2+}, Ni^{2+}, Co^{2+}) were accordingly synthesized in a muffle furnace from the mixture of K_2CO_3, MO, and TiO_2. After being ground in a mortar for 30 minutes, the mixture in an alumina crucible was heated to 800 °C for an hour, followed by another grinding for 30 minutes. After that, the mixture was re-heated at 900 °C for 20 hours. This material will be refered as "KZn", "KCu", "KNi" and "KCo" for lepidocrocite titanate $K_{0.8}M_{0.4}Ti_{1.6}O_4$ with M = Zn^{2+}, Cu^{2+}, $Ni^{2+}$and Co^{2+}, respectively. Lepidocrocite titanate catalysts $K_{0.8}Fe_{0.8}Ti_{1.2}O_4$ ("KFe") can be made similarly from the mixture of K_2CO_3, Fe_2O_3 and TiO_2. Some other compositions where Ti^{IV} was simultaneously substituted by two types of cations could also be prepared, including $K_{0.8}Cu_{0.2}Zn_{0.2}Ti_{1.6}O_4$, $K_{0.8}Cu_{0.2}Ni_{0.2}Ti_{1.6}O_4$, $K_{0.8}Fe_{0.7}Mn_{0.1}Ti_{1.2}O_4$ and $K_{0.8}Fe_{0.4}Mn_{0.4}Ti_{1.2}O_4$. They will be hereafter named "KCuZn", "KCuNi", "$KFe_{0.7}Mn_{0.1}$" and "$KFe_{0.4}Mn_{0.4}$", respectively.

3.3.2 Characterization of lepidocrocite titanate

3.3.2.1 Structural analysis using powder X-ray diffraction (PXRD)

The crystalline phase of the materials synthesized can be identified using PXRD measurement. The sample is prepared by packing the lepidocrocite titanate powder in the sample holder. A Cu-K_α X-ray beam is used for an analysis at 40 kV and 30 mA. The sample is scanned over the angle ranged from 5 to 65 degrees (2θ), at a 0.05 degree/step, and a detection time of 0.6 second/step.

3.3.2.2 Determination of specific surface area by nitrogen adsorption

Specific surface area of a lepidocrocite titanate can be determined by a gas adsorption analyzer (Autosorb-1C, Quantachrome). The sample was prepared by weighing approximately 100 mg of lepicrodocite titanate into a clean and dried sample cell. The sample cell was attached to the outgassing station where the temperature was raised to 350 °C at the rate of 5 °C/min under vacuum. After that, the sample cell was

removed from the outgassing station and was attached to the analysis station where the nitrogen gas can be filled. The equilibration time was set to 3 minutes and partial pressure (P/Po) range was varied from 10^{-6} to 1.0. The adsorption isotherm was recorded, and the corresponding surface area was analyzed using the method of Brunauer–Emmett–Teller (BET) [51].

3.3.2.3 Temperature-programmed desorption

Carbon dioxide temperature programmed desorption (CO_2-TPD) is the technique determining the basicity and basic strength of a catalyst. This technique was done according to the following procedure: the sample weighed approximately 200 mg was packed into a quartz tube reactor, which was located inside a temperature-regulated furnace. Prior to the measurement, each sample was calcined at 450 °C for 2 hours in air zero and cooled to room temperature under N_2 gas. Next, the sample was left in contact with 99.99% CO_2 at a flow rate 30 mL/min for an hour. Then, excess CO_2 physisorbed on the surface of the sample was removed by purging the sample with pure helium at a flow rate of 30 mL/min for an hour. The temperature was then raised from 35 °C up to 600 °C at the heating rate of 5 °C/min using pure helium as a carrier gas. The thermal conductivity detector (TCD) was used to detect desorbed CO_2 from sample. The CO_2 desorption peak was recorded and the basicity was calculated using the peak area obtained from a known amount of calcium carbonate as the standard. The basicity is expressed as mmol of CO_2 per g of a catalyst (Example C1).

3.3.2.4 Temperature-programmed reduction

Temperature-programmed reduction by hydrogen gas (H_2-TPR) provides the information on the reducibility of a species on the surfaces of a catalyst. The sample weighed approximately 100 mg was packed into a quartz tube reactor, which was then located inside a temperature-regulated furnace. Prior to the measurement, each sample was calcined at 450 °C for 2 hours in air zero and cooled to room temperature under N_2 gas. For TPR analysis, a 10% H_2 in Ar at a flow rate of 30 mL/min was fed through the reactor, and the temperature was raised from 50 °C up to 900 °C at a heating rate of 10 °C/min. Water molecules produced during the reduction was removed by a U-shape glass trap (cooled with the vapor of liquid N_2) before the carrier

gas entering the TCD detector. The reduction peak was recorded and the hydrogen consumption was calculated using a known amount of copper(II) oxide as a standard (Example D1).

3.3.2.5 Thermal stability of palmitic acid and the amount of adsorbed palmitic acid

The thermal decomposition of palmitic acid was investigated by a thermogravimetric analyzer. Approximately 30 mg of sample was placed in a platinum pan hanging from a microbalance, after which the exact mass was recorded by the instrument. The sample was then heated from room temperature to 900 $^{\circ}$C at the heating rate of 10 $^{\circ}$C/min under the flow of nitrogen gas (20 mL/min). The amount of organic molecules in the intercalation compound of lepidocrocite titanate (i.e., after the liquid phase adsorption) can be determined similarly assuming that the mass loss is solely ascribed to the loss of palmitic acid.

3.3.2.6 Infrared spectroscopy

The powder of the sample was mixed with potassium bromide. The mixed powder was pressed into a pellet. Infrared spectra of the pellets were collected using Spectrum GX (Perkin Elmer), from 400-4000 cm^{-1}.

3.3.2.7 Determination of catalyst morphology by Scanning Electron Microscopy (SEM) and Transmission Electron Microscopy (TEM)

The morphology of the catalyst was determined by SEM and TEM. For SEM, the powder was sonicated in acetone for 30 minutes. A few drops of the suspension were then deposited onto a glass slide. After drying, the dispersed solids on the glass slide were transferred to the carbon tape, followed by gold sputtering. After that, the sample was placed in a chamber which was evacuated from ambient pressure to below 10^{-4} Torr. For TEM, the powder was manually dispersed on a stub.

3.3.3. Adsorption of palmitic acid and the swelling of lepidocrocite titanate

An amount of 2.0 g of KZn lepidrococite titanate was heated with 150 mL of a 5%w/w palmitic acid in isopropanol at 60 °C for 36 hours. The liquid (1 mL) was taken out at certain intervals, and was filtered through the syringe filter to remove the KZn particles. The amount of adsorbed palmitic acid was calculated from the difference in the peak area of palmitic acid at any time *vs* that before the contact with KZn following equation 3.1.

$$\%\text{Adsorption} = \frac{[\text{Palmitic acid}]_{initial} - [\text{Palmitic acid acid}]_{time} \times 100}{[\text{Palmitic acid}]_{initial}} \quad \text{(Eq. 3.1)}$$

After completion of the adsorption, the solid was filtered, washed with isopropanol, and then dried at 70 °C overnight. The material obtained is called "KZn-Palmitic acid".

3.3.4 Preparation of substrates for catalytic activity testing

The intercalation compounds of palmitic acid and lepidocrocite titanate of several compositions catalyst were prepared as a substrate for testing the catalytic deoxygenation activity. The lepidocrocite titanate catalyst was activated at 450 °C for 2 h before adsorption with palmitic acid. The lepidocrocite titanate catalyst (1 mole) and palmitic acid (1 mole) were mixed in the Teflon-lined stainless steel autoclave at 280 °C for 6 hours without stirring. After completion of the adsorption, the mixture was washed with isopropanol at 70 °C for 8 hours by Soxlet extraction, and dried at 70 °C overnight. The amount of palmitic acid after the adsorption were analysed by thermogravimetric analysis (TGA) in a nitrogen atmosphere as described above.

3.3.5 Catalytic activity testing

The investigation on the catalytic activity of the lepidocrocite titanates was conducted in a semi-batch reactor under atmospheric pressure, using N_2 as a carrier gas. The intercalation compound was introduced into the glass reactor (length, 7 cm; outer diameter, 3.5 cm; inner diameter, 3.3 cm) as the substrate. The catalytic testing rig is illustrated in Figure. 3.1. The reactor was located inside a temperature-regulated tube furnace. The gas flow rate was controlled by a mass flow controller and was checked by a bubble flow meter. After that, it was heated to the reaction temperature (350-500 °C) under N_2 gas (30 mL/min). The gaseous mixture flowing out of the reactor passed through a gas sampling loop and was periodically sampled into an online gas chromatograph. The remaining gaseous mixture was trapped using liquid nitrogen trap (-77 °C). In order to prevent the condensation of products before trapping, the transfer-line after reaction is heated at 180 °C.

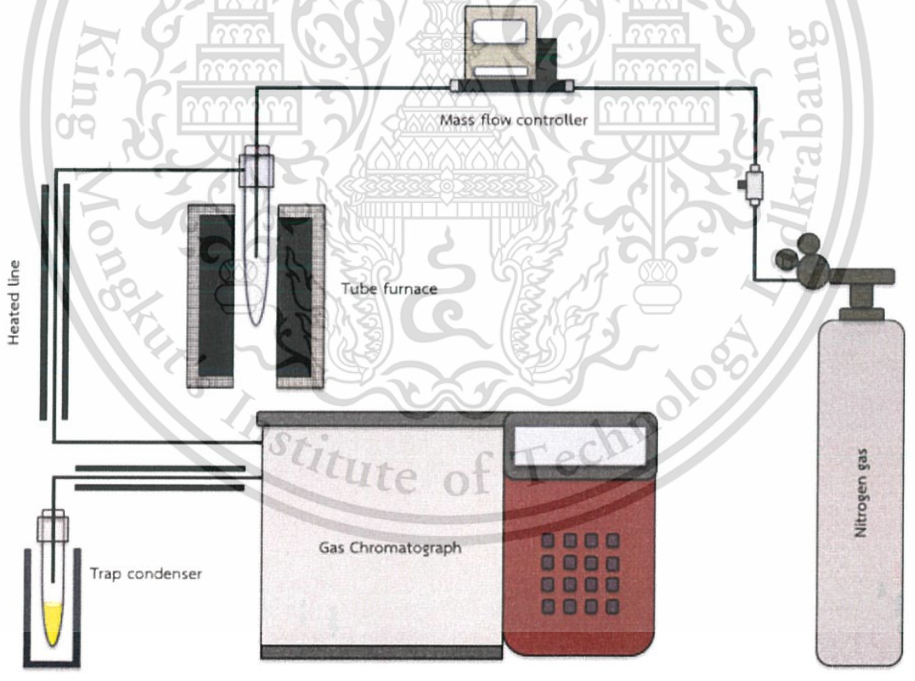

Figure 3.1 Schematic diagram of catalytic testing rig

3.3.6 Analysis of products

Products from the deoxygenation of palmitic acid were analysed online by a gas chromatograph (GC) (HP 6890 series) equipped with a DB-1 capillary column (length, 30m; internal diameter, 0.32 mm; film thickness, 5.00 μm) and a flame ionization detector (FID). The column temperature was initially 40 °C and was hold there for 5 min, followed by a ramp at 15 °C/min to 280 °C before another hold at this temperature for 24 minutes. The temperatures of the injection port and FID were kept constant at 275 °C during analysis. Identification of substances was performed by comparing the retention time with the comparison with databases from the analysis by a mass spectrometer coupled with a gas chromatograph (GC/MS).

3.3.7 Investigation of residue palmitic acid in spent KZn lepidocrocite titanate catalyst.

The spent KZn lepidocrocite titanate catalyst (1 g) after the reaction at 350 °C for an hour was digested by 4 mL of HF in a Teflon beaker. The mixture was gently heated on the hotplate until all solids were dissolved. Next, n-hexane (6 mL) was poured into the beaker to extract organic compounds from the HF solution. After that, the hexane layer was extracted by 10 mL of de-ionized water for the removal of fluoride ion. The hexane solution was transferred to the volumetric flask and was finally diluted to a volume of 10 mL. The residual palmitic acid in hexane was then investigated by GC-FID.

CHAPTER 4
RESULTS AND DISCUSSION

In this thesis, lepidocrocite titanate catalysts of several compositions were prepared and characterized. The adsorption of palmitic acid has been investigated. Finally, the deoxygenation of palmitic acid was studied as a model reaction for the production of long chain hydrocarbons.

4.1 Characterization of catalysts

4.1.1 Solid state synthesis

Lepidocrocite titanate $K_{0.8}Zn_{0.4}Ti_{1.6}O_4$ "KZn" was synthesized by a conventional solid state synthesis from the corresponding mixture of oxides/carbonates as described in Chapter 3. The white powder has the PXRD pattern shown in Figure 4.1. It possesses high crystallinity as inferred from the presence of several reflections with high intensity. The Miller indexes are shown on atop of each peak following the previous structure determination reported in ref [32]. The unit cell parameters of the orthorhombic symmetry with a = 0.380(6), b = 1.5(6), and c = 0.298(5) nm can be obtained, in agreement with the report by Groult et al [33]. The strongest peak at 2θ = 11.30 degree (d = 0.7824 nm) is ascribed to the 020 reflection, which is the repeating distance along the b-direction of the orthorhombic unit cell.

Lepidocrocite titanate of various compositions can be synthesized similarly. Besides "KZn" just mentioned, several samples made include $K_{0.8}Li_{0.27}Ti_{1.73}O_4$, $K_{0.8}Fe_{0.8}Ti_{1.2}O_4$, $K_{0.8}Co_{0.4}Ti_{1.6}O_4$, $K_{0.8}Ni_{0.4}Ti_{1.6}O_4$, and $K_{0.8}Cu_{0.4}Ti_{1.6}O_4$. Some other compositions where Ti^{IV} was simultaneously substituted by two types of cations could also be prepared, including $K_{0.8}Fe_{0.7}Mn_{0.1}Ti_{1.2}O_4$, $K_{0.8}Fe_{0.4}Mn_{0.4}Ti_{1.2}O_4$, $K_{0.8}Cu_{0.2}Zn_{0.2}Ti_{1.6}O_4$, and $K_{0.8}Cu_{0.2}Ni_{0.2}Ti_{1.6}O_4$. They will be hereafter named "KM" (where M is Li, Fe, Co, Ni, Cu, or a combination of Fe and Mn, Zn and Cu, Ni and Cu) for short. While these samples have different types of metal substituting into Ti^{IV} sites such as Li^{I}, Fe^{III}, several M^{II} cations, or the presence of more than one type of cations, the common feature among them is the

presence of the 0.8 negative charges per formula unit, which is balanced by K^+. Their PXRD patterns shown in Figure 4.2 resemble those of KZn, confirming the successful formation of lepidocrocite structure. In all cases, the first peak with very high intensity (assigned as the 020 reflection) was observed. No crystalline impurity phases exist in all compositions prepared. The unit cell parameters of lepidocrocite titanate are roughly in reasonable agreement with those reported in the literature (when available) [31,32,33]. The comparison of unit cell parameters of each composition synthesized in this work vs. the reported values can be found in Table A1.

The PXRD pattern of $K_{0.8}Mg_{0.4}Ti_{1.6}O_4$ "KMg" is shown in Figure 4.3. The pattern is similar to the reported pattern [33]. However, it has lower crystallinity than other materials synthesized. The attempt to increase the crystallinity by reheating KMg at 800°C for 20 h was unsuccessful, as peaks due to the impurity increase in intensity as shown in Figure A1. Also, the mixture of K_2CO_3, Mn_2O_3 (or Cr_2O_3) and TiO_2 corresponding to the composition $K_{0.8}Mn_{0.8}Ti_{1.2}O_4$ (or $K_{0.8}Cr_{0.8}Ti_{1.2}O_4$) was also heated in a similar manner. However, strong reflections due to the impurity phases were observed in $K_{0.8}Mn_{0.8}Ti_{1.2}O_4$ as shown in Figure A2. Also, the lepidocrocite $K_{0.8}Cr_{0.8}Ti_{1.2}O_4$ could not be formed under this experimental condition (Figure A3). The crystalline phase $K_{0.8}Cr_{0.8}Ti_{1.2}O_4$ was not assigned further.

The summary of the interlayer spacing (from the *020* reflections) of lepidocrocite titanates prepared in this work is shown in Table 4.1. In case of the substitution of Ti^{IV} by transition metal cations, it is found that the interlayer spacing of lepidocrocite titanates increases as the cationic radius of the cations increase. For example, the smallest d_{020} observed (0.7696 nm) is for KNi as Ni^{2+} has the smallest cationic radius of 69 pm among all cations studied. In another example, KFe exhibits the largest d_{020} (0.7847 nm) in agreement with the fact that Fe^{3+} has the largest cationic radius (75 pm).

However, the d_{020} of alkali- (KLi) and alkaline earth- (KMg) containing lepidocrocite titanate do not follow this trend. In fact, the opposite is observed where KLi having a

larger Li^+ shows a smaller d_{020}, and vice versa. This result might be explained considering the very ionic nature of Li^+ and Mg^{2+} in comparison to the transition metals. For these two compositions, it is found that the d_{020} is inversely proportional to the charge density. Here, charge density is equal to $0.8/(2ac)$, where 0.8 is the charge per unit, a and c are the unit cell parameters making the basal plane, and the factor 2 accounts for the fact that this charged is distributed between two basal planes. The charge density of KLi is 3.5807 nm^{-2}, higher than that of KMg (3.5363 nm^{-2}). Therefore, there is less electrostatic repulsion in KLi compared to KMg, such that the interlayer spacing of KLi is smaller than that of KMg.

Meanwhile, the d_{020} of lepidocrocite titanate having two types of metals substituted for Ti^{IV} is between that of the two end members. Consider $K_{0.8}Cu_{0.2}Zn_{0.2}Ti_{1.6}O_4$ as an example. Its interlayer spacing (d_{020}) of 0.7761 nm is between that of KZn (0.7824 nm) and KCu (0.7746 nm). This intermediate d_{020} strongly suggests that both Zn and Cu simultaneously substitute for Ti^{IV} making a solid solution, but not two separate phases of KZn and KCu.

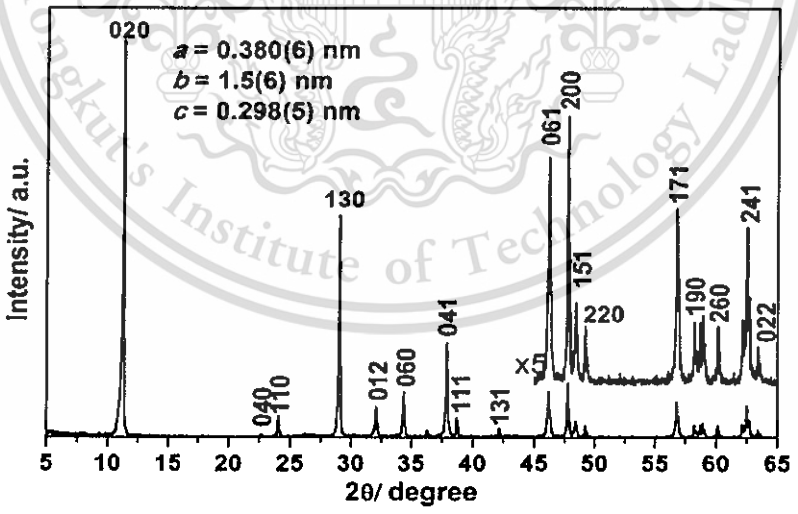

Figure 4.1 The PXRD patterns of $K_{0.8}Zn_{0.4}Ti_{1.6}O_4$ lepidocrocite titanate. The indexes of the orthorhombic symmetry of the unit cell are shown atop of each peak as an example.

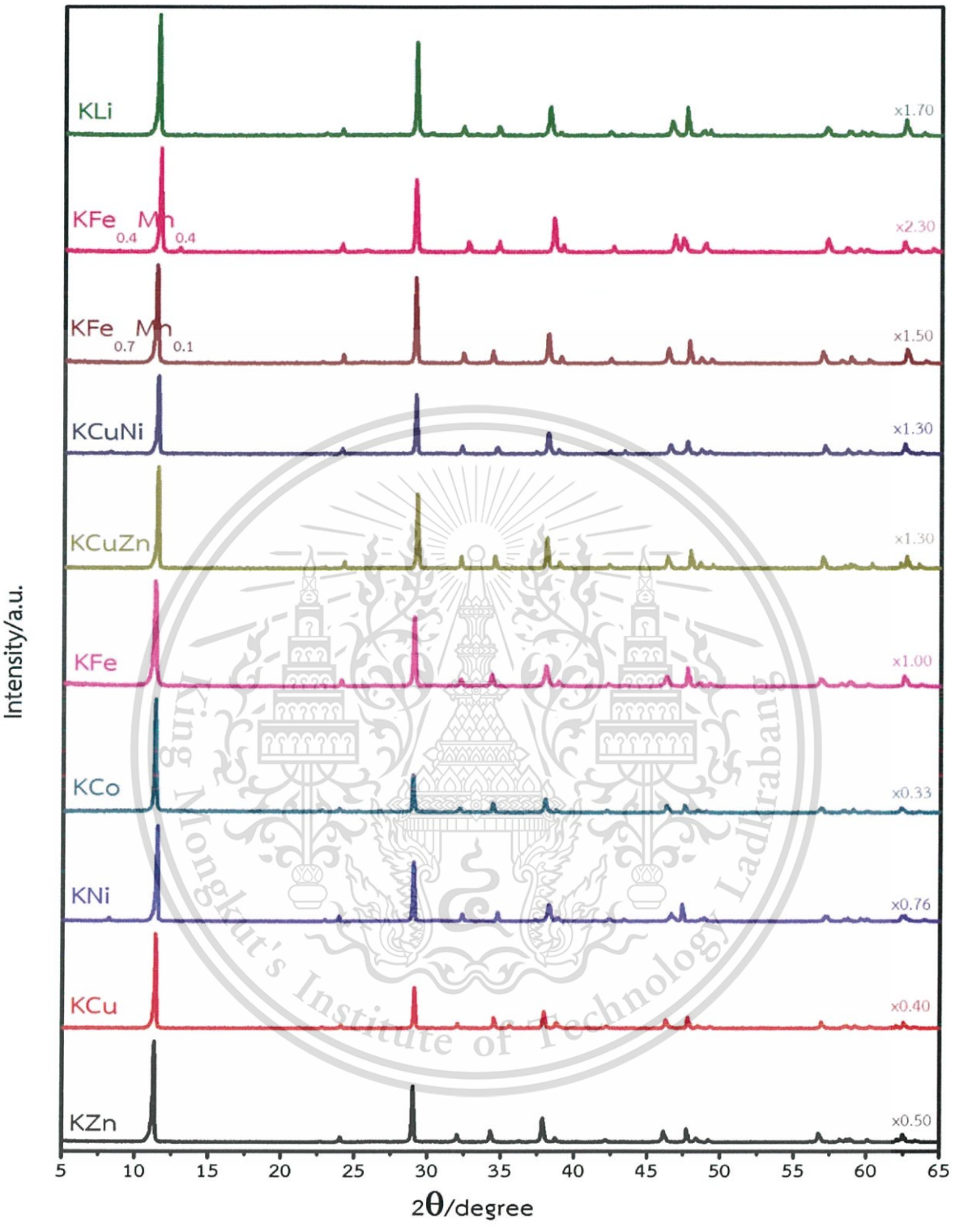

Figure 4.2 The PXRD patterns of various compositions of lepidocrocite titanate successfully synthesized in this work. The patterns in are rescaled such that the *020* peaks are of similar intensity.

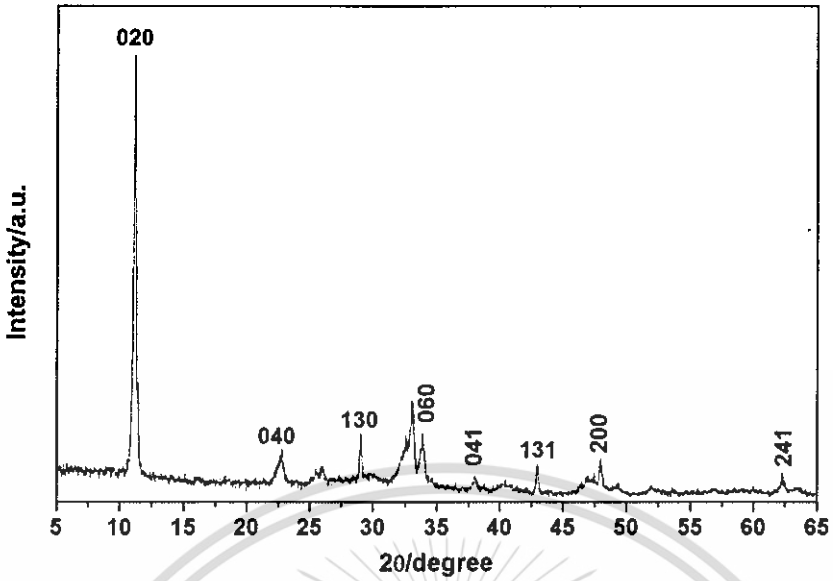

Figure 4.3 The PXRD patterns of KMg possessing low crystallinity.

Table 4.1 The interlayer spacing of catalysts calculated from the *020* reflection.

Catalysts	2θ (degree)	d (nm)	Cationic radius[a] (pm)
KLi	11.41	0.7746	76 (Li^{+})
KMg	11.16	0.7922	72 (Mg^{2+})
KFe	11.26	0.7847	75 (Fe^{3+})
KCo	11.30	0.7824	74 (Co^{2+})
KNi	11.48	0.7696	69 (Ni^{2+})
KCu	11.41	0.7746	73 (Cu^{2+})
KZn	11.30	0.7824	74 (Zn^{2+})
KCuNi	11.37	0.7761	69 (Ni^{2+}) 73(Cu^{2+})
KCuZn	11.37	0.7761	74 (Zn^{2+}) 73(Cu^{2+})
$KFe_{0.7}Mn_{0.1}$	11.34	0.7796	72 (Mn^{3+}) 75(Fe^{3+})
$KFe_{0.4}Mn_{0.4}$	11.56	0.7647	72 (Mn^{3+}) 75(Fe^{3+})

[a] *From literature [49-51].

The crystallite size and specific surface area of catalysts are shown in Table 4.2. The crystallite size of catalysts was calculated from Scherrer's equation, employing the FWHM of the *020* peak of lepidocrocite titanate. The crystallite size is in the range 41-78 nm, and is in the order KCu > KCuZn > KCuNi > KNi > KLi > KZn > KCo > $KFe_{0.7}Mn_{0.1}$ ≈ $KFe_{0.4}Mn_{0.4}$ > KFe > KMg. This difference might reflect the intrinsic textural property of each crystal. However, there are no significant differences in the surface area of lepidocrocite titanate samples of various compositions. Generally very small values of specific surface area for lepidocrocite titanates are obtained (not more than 6 m^2/g). A slightly larger value for KMg (13 m^2/g) could be due to its relatively poor crystallinity.

Table 4.2 Crystallite size and specific surface area of catalysts.

Catalysts	Crystallite size (nm)	Surface area (m^2/g)
KLi	60.9	5
KMg	41.0	13
KFe	46.6	6
KCo	57.5	3
KNi	64.0	3
KCu	78.2	3
KZn	60.5	3
KCuNi	65.0	3
KCuZn	69.0	3
$KFe_{0.7}Mn_{0.1}$	50.4	5
$KFe_{0.4}Mn_{0.4}$	50.8	6

4.1.2 Morphology

The SEM images (5000 times of magnification) of lepidocrocite titanates were shown in Figure 4.4. The layered-nature of the crystallites with tightly-stacked layers can be observed. The size of the particles was found to be 1-7 μm. The presence of these micron-size crystals is in agreement with the low specific surface area obtained

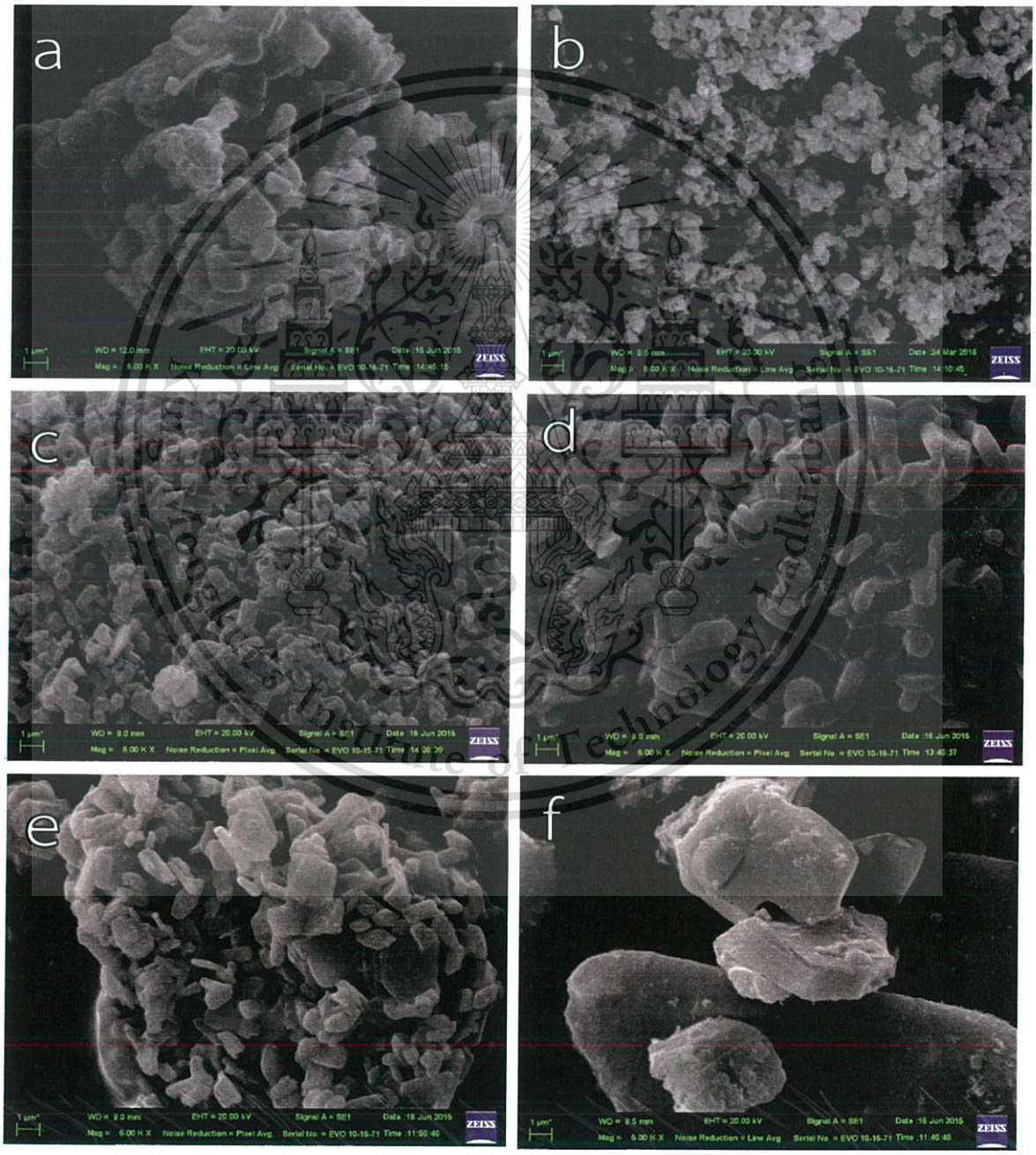

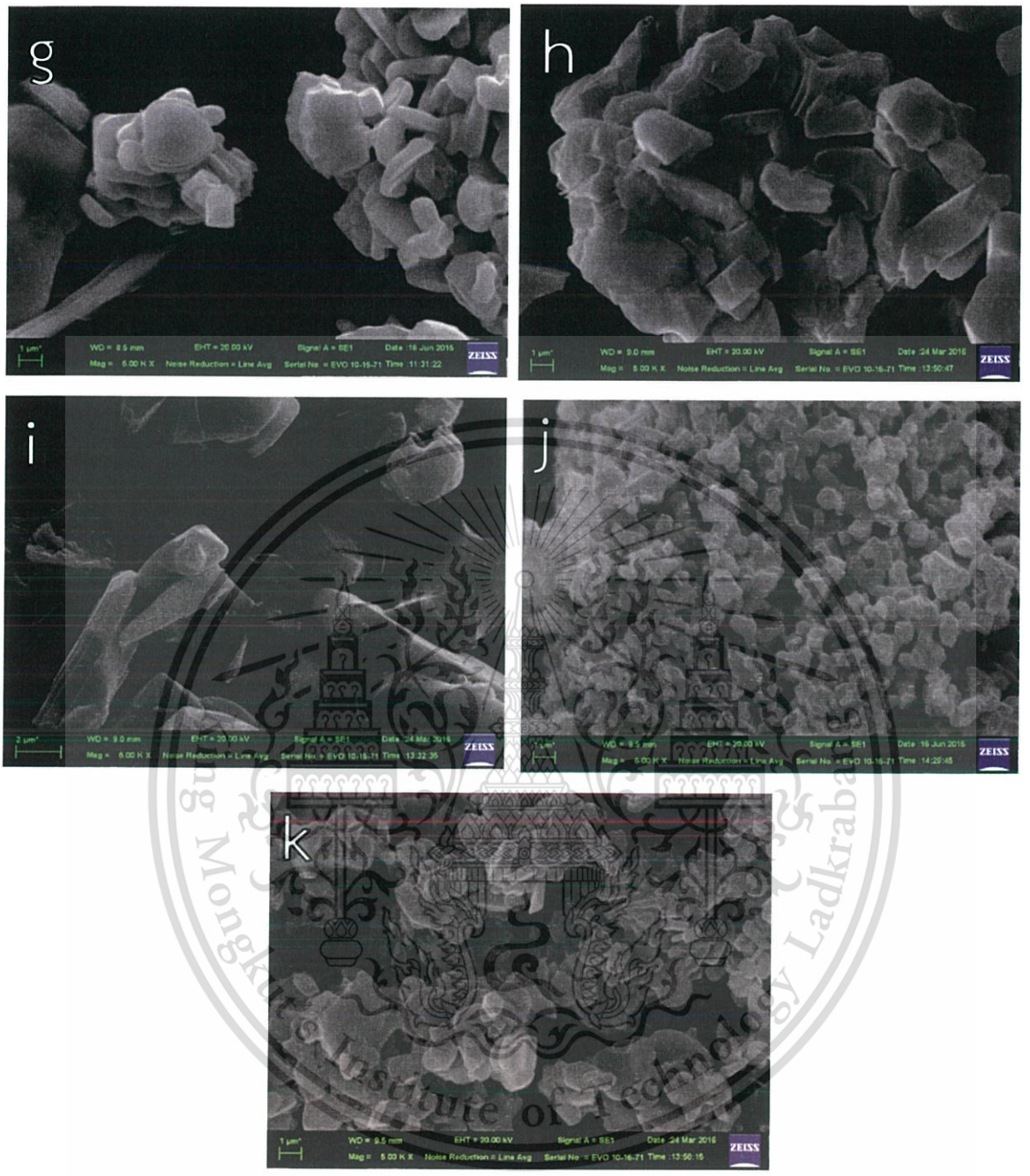

Figure 4.4 SEM images of (a) KLi, (b) KMg, (c) KFe, (d) KCo, (e) KNi, (f) KCu, (g) KZn, (h) KCuNi, (i) KCuZn, (j) $KFe_{0.7}Mn_{0.1}$ and (k) $KFe_{0.4}Mn_{0.4}$. The scale bar in all cases represent the distance 1 μm.

4.1.3 Elemental analysis

The chemical compositions of some materials prepared were determined by XRF. As shown in Table 4.3, the experimental compositions are in reasonable agreement with the theoretical compositions, thereby confirming the successful synthesis.

Table 4.3 Chemical composition of the lepidocrocite titanates prepared.

Catalysts	$\%K_2O$	%Metal oxide[a]	$\%TiO_2$
$K_{0.8}Zn_{0.4}Ti_{1.6}O_4$	19.0 (20.2)	16.3 (16.4)	63.0 (63.5)
$K_{0.8}Cu_{0.4}Ti_{1.6}O_4$	18.5 (20.3)	18.8 (16.1)	61.9 (63.7)
$K_{0.8}Ni_{0.4}Ti_{1.6}O_4$	18.7 (19.5)	15.2 (15.2)	65.4 (65.4)
$K_{0.8}Fe_{0.8}Ti_{1.2}O_4$	19.5 (19.3)	30.5 (32.3)	48.6 (48.5)

[a] "Metal oxide" refers to MO (M = Zn, Cu, Ni) or M_2O_3 (M = Fe) and value in parenthesis refers to the theoretical composition.

4.1.4 Basic strength and basicity

The CO_2-desorption temperature profiles of lepidocrocite titanates are shown in Figure 4.5. CO_2 desorbs from lepidocrocite titanate at temperature from 50 to 300 °C. The peak of CO_2 desorption below 100°C is the major fraction which was related to CO_2 physisorption, and the minor fraction desorbed in the range 100-300°C. Therefore, one can infer that lepidocrotite titanates are weakly basic material. For comparison, TiO_2 anatase desorbs CO_2 in a similar temperature range. The basic strength can be estimated from the peak temperature from the desorption profiles, and is in the order: $KFe_{0.4}Mn_{0.4}$ (120°C) > TiO_2 (119°C) > KLi (103°C) ≈ KCuNi (102°C) > KFe (96°C) = KNi (96°C) = KCuZn (96°C) = $KFe_{0.7}Mn_{0.1}$ (96°C) ≈ KCu (95°C) > KZn (86°C) > KCo (66°C) > KMg (49 and 59°C).

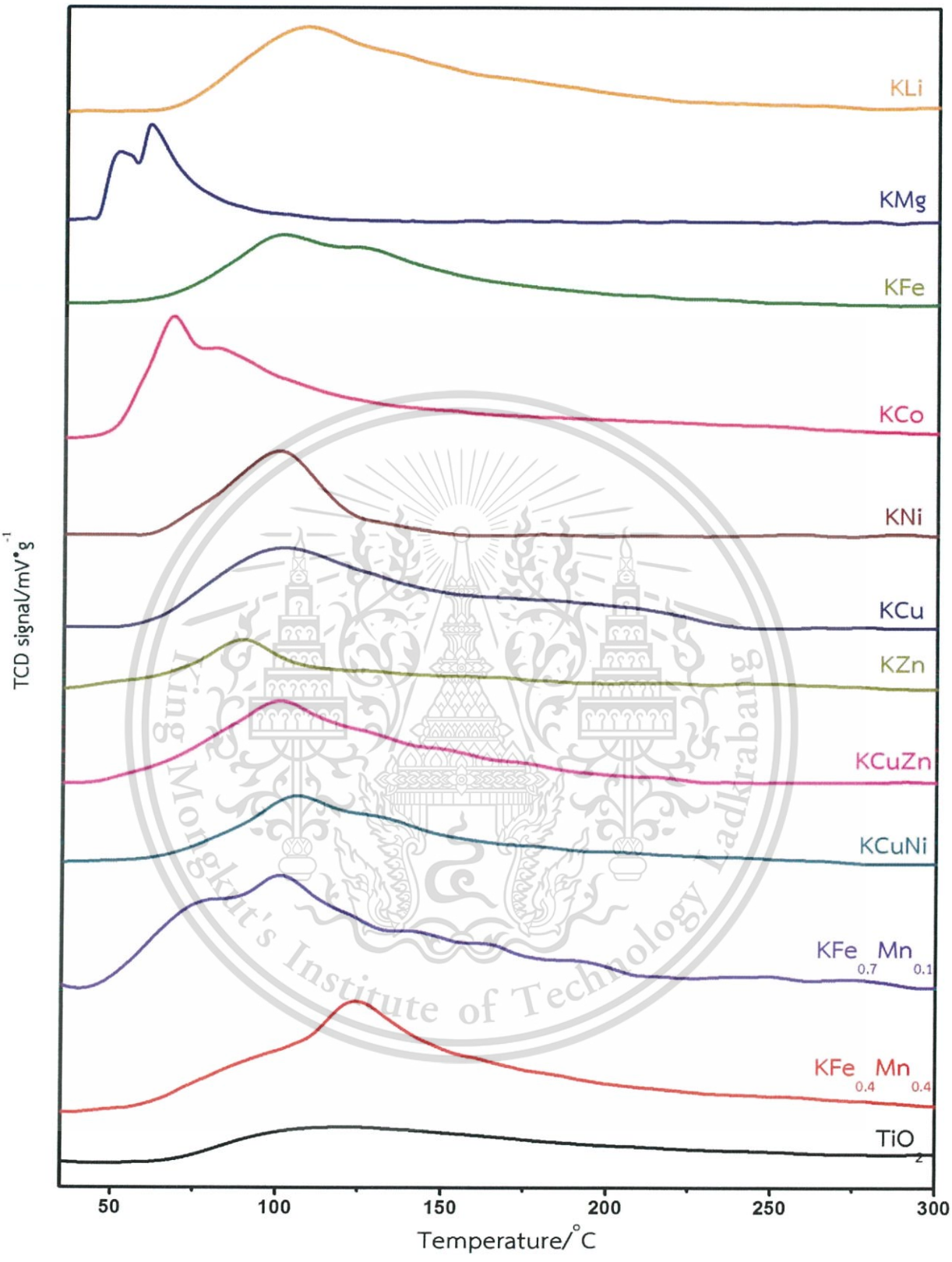

Figure 4.5 CO_2-TPD profiles of various compositions of lepidocrocite titanate. The y axis is the signal from TCD normalized by the mass of the sample.

The basicity of lepidocrocite titanates are shown in Table 4.4. The amount of CO_2 desorbs from lepidocrocite titanates was quite low (0.03-0.11 mmol CO_2/g), likely due to the low specific surface area of the solids. For comparison, the basicity of TiO_2 (anatase) is 0.07 mmolCO_2/g [54] similar to lepidocrocite titanates reported here. The basicity of titanium-based oxides is generally lower than that of some well-known basic materials such as the mixed (Mg/Al) oxide obtained from the decomposition of LDH with Mg/Al = 3 (0.82 mmol CO_2/g) [54]. Moreover, the very low surface area of lepidocrocite titanate calculated from the amount of CO_2 desorbs is related to the specific surface area from N_2 adsorption (Figure C2). So, one can infer that CO_2 gas do not interact with basic sites at interlayer region of lepidococrocite titanates as these sites are inaccessible to CO_2. In fact, the PXRD pattern of KZn after the CO_2 TPD experiment is compared to that of the as made one in Figure 4.6. The similarity of these two patterns is in agreement with the claim that the adsorption of CO_2 occurs on the external surfaces only.

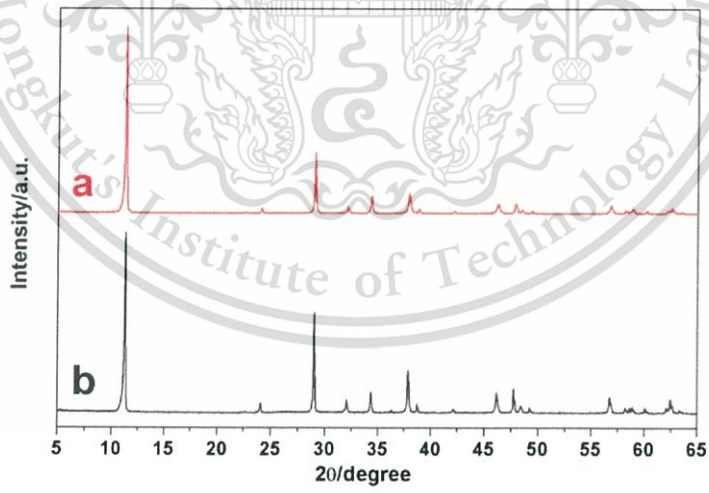

Figure 4.6 PXRD patterns of KZn (a) as made and (b) after the CO_2 desorption up to 600 °C.

The partial negative charges of framework oxygen calculated from Sanderson intermediate electronegativity are also shown in Table 4.4. (The example of the calculation is shown in Example C2.) Here, materials with high basicity are represented by the more negative charges at oxygen atoms. So, the ranking of basicity is in the order: KLi (-0.557) > KMg (-0.539) > KCo, KNi, KCu, KCuNi (-0.522 to -0.530) > KCuZn, KZn (-0.518 to -0.520) > KFe, $KFe_{0.4}Mn_{0.4}$, $KFe_{0.7}Mn_{0.1}$ (-0.516). The relationship between the partial negative charge of framework oxygen *vs.* the peak temperature and the partial negative charge of framework oxygen *vs.* the amount of CO_2 desorption are shown in Figure C3 and Figure C4, respectively. The high basicity of KLi suggested by the calculation of the partial charge agrees well with the high peak temperature in CO_2-TPD. The similar basicity of materials in the third group (KCo, KNi, KCu, KCuNi) is more or less in agreement with the results from CO_2-TPD, although the peak broadening makes the comparison more complicate. Of interest is the relatively high experimental basicity of $KFe_{0.4}Mn_{0.4}$ and $KFe_{0.7}Mn_{0.1}$, despite of their relatively small calculated partial charges. So, this result suggests that the co-substitution of metal atoms into the Ti site could modify the basicity. The low experimental basicity of KMg, in contrast to the partial charge, might be explained by its low crystallinity where the lepidocrocite structure is not well developed.

Table 4.4 Basicity of various catalysts prepared

Catalyst	Peak temperature (°C)	Surface area (m^2/g)	Basicity ($mmolCO_2/g$)	Basicity ($mmolCO_2/m^2$)	Partial negative charge of framework oxygen[a]
KLi	103	5	0.070	0.014	-0.556
KMg	49, 59	13	0.036	0.002	-0.539
KFe	96	6	0.038	0.006	-0.515
KCo	66	3	0.081	0.027	-0.529
KNi	96	3	0.043	0.014	-0.527
KCu	95	3	0.070	0.023	-0.522
KZn	86	3	0.039	0.013	-0.517
KCuNi	102	3	0.037	0.012	-0.526
KCuZn	96	3	0.036	0.012	-0.519
$KFe_{0.7}Mn_{0.1}$	96	5	0.091	0.018	-0.515
$KFe_{0.4}Mn_{0.4}$	120	6	0.108	0.018	-0.516

[a]Calculation from Sanderson intermediate electronegativity.

4.1.5 Reducibility

Figure 4.7 shows the temperature-programmed reduction profiles of lepidocrocite titanates. The reduction peak at 550 °C is widely ascribed to the reduction of Ti as reported in the reduction of TiO_2 anatase [55]. The TPR profile of KZn lepidocrocite titanate (Fig. 4.7a) shows a broad peak from 300 to 800 °C, likely due to the small reduction of the Ti. The H_2 consumption of KZn is low (0.41 mmol H_2/g, Table C1). The control experiment shows that ZnO itself is hardly reduced. So, Zn^{2+} could remain in the lepidocrocite structure.

The TPR profile of KCu (Figure 4.7b) shows an overlapping peak of high intensity in the temperature range of 300 to 700 °C. In general, the reduction of bulk

CuO particles in the absence of interactions with the support occurs at the temperature range of 220-350 °C [56]. The nonexistence of this peak indicates that the present KCu catalyst does not contain such bulk CuO particles. Instead, we assign the first reduction peak centered at 344 °C in KCu to the reduction of Cu^{2+} in the lepidocrocite structure having relatively weak interactions with the surroundings. It is difficult to explain the the second reduction peak at 496 °C at present. This peak could be either to the reduction of Ti, or to the reduction of Cu^{2+} species in the lepidocrocite structure with relatively strong interactions with the surroundings. The H_2 consumption of KCu (2.0 mmol/g) is 5 times that of KZn.

The reduction profile of KNi lepidocrocite titanate catalyst (Figure 7c) shows several peaks in the range 350 to 800 °C. The high peak value in the TPR profile (above 600 °C) has been reported in some materials such as $NiTiO_3$ [55]. Here, the first two peaks at 415 and 534 °C can be assigned to the reduction of Ni^{2+} having relatively weak and strong interactions with the surroundings. These two peaks are slightly shifted to the higher temperature compared to that in the NiO reference. The peak at 683 °C is likely associated with the removal of oxygen around Ti atoms. . The H_2 consumption of KNi is around 2.4557 mmol/g.

The TPR profile of KCo (Figure 7d) contains a broad peak a small peak at 280 °C followed by a board peak from 550-900 °C. The first one at 280 °C can be assigned to the reduction of Co^{2+}. The broad peak at the intermediate and high temperature apparently consisting of several overlapping reduction peaks can be de-convoluted into three peaks centered at 313 °C, 688 °C and 782 °C. These peaks could likely represent the reduction of Ti atoms in the structure. Similar reduction te,perature (720 °C) was observed in the reduction of cobalt titanate ($CoTiO_3$) [55]. The H_2 consumption of KCo is around 1.3284 mmol/g.

The TPR profile of KFe lepidocrocite titanate (Figure 7e) shows a broad peak from 350 to 900 °C. The reduction peaks can be de-convoluted into six peaks. These

peaks occur at similar temperature for the reduction of the Fe_2O_3 reference. So, they are most likely the reduction of Fe^{3+} in the lepidocrocite structure. The next broad maximum at 761 to 821 °C is attributed to the reduction of Ti in the lepidocrocite structure. The H_2 consumption of KFe is around 1.2720 mmol/g.

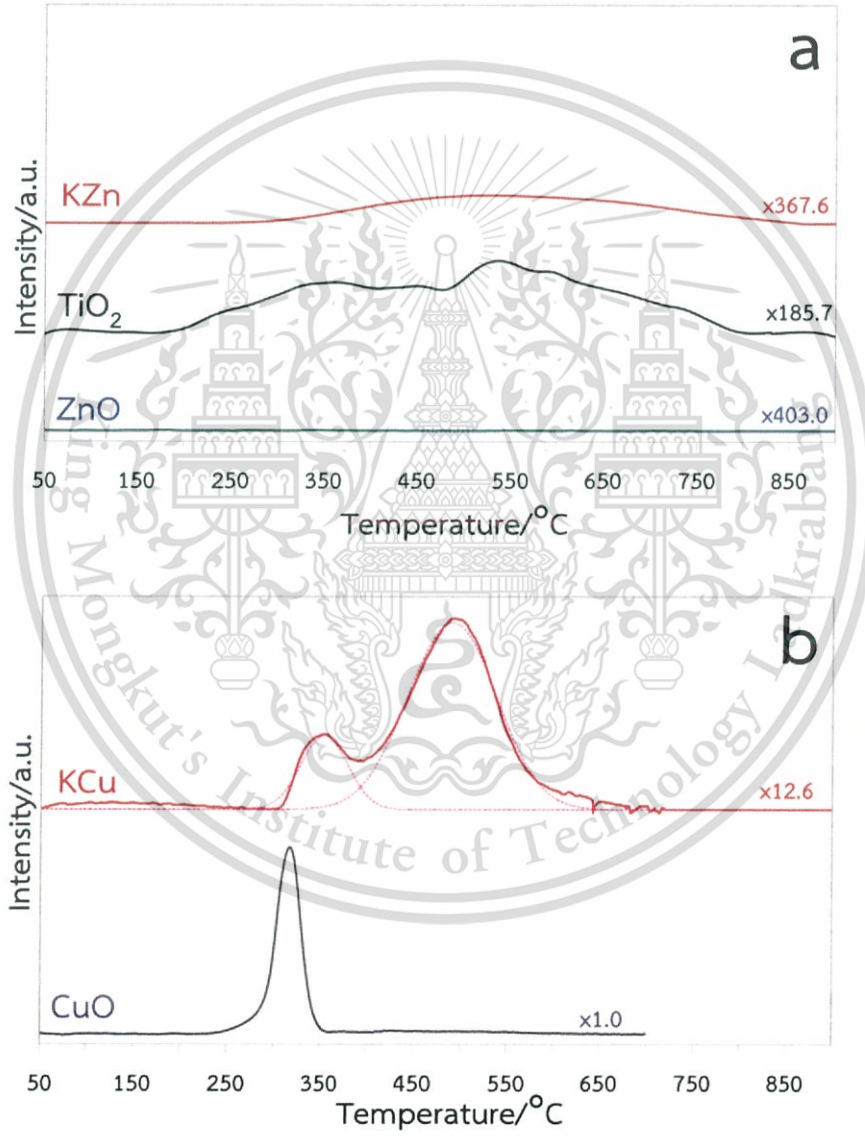

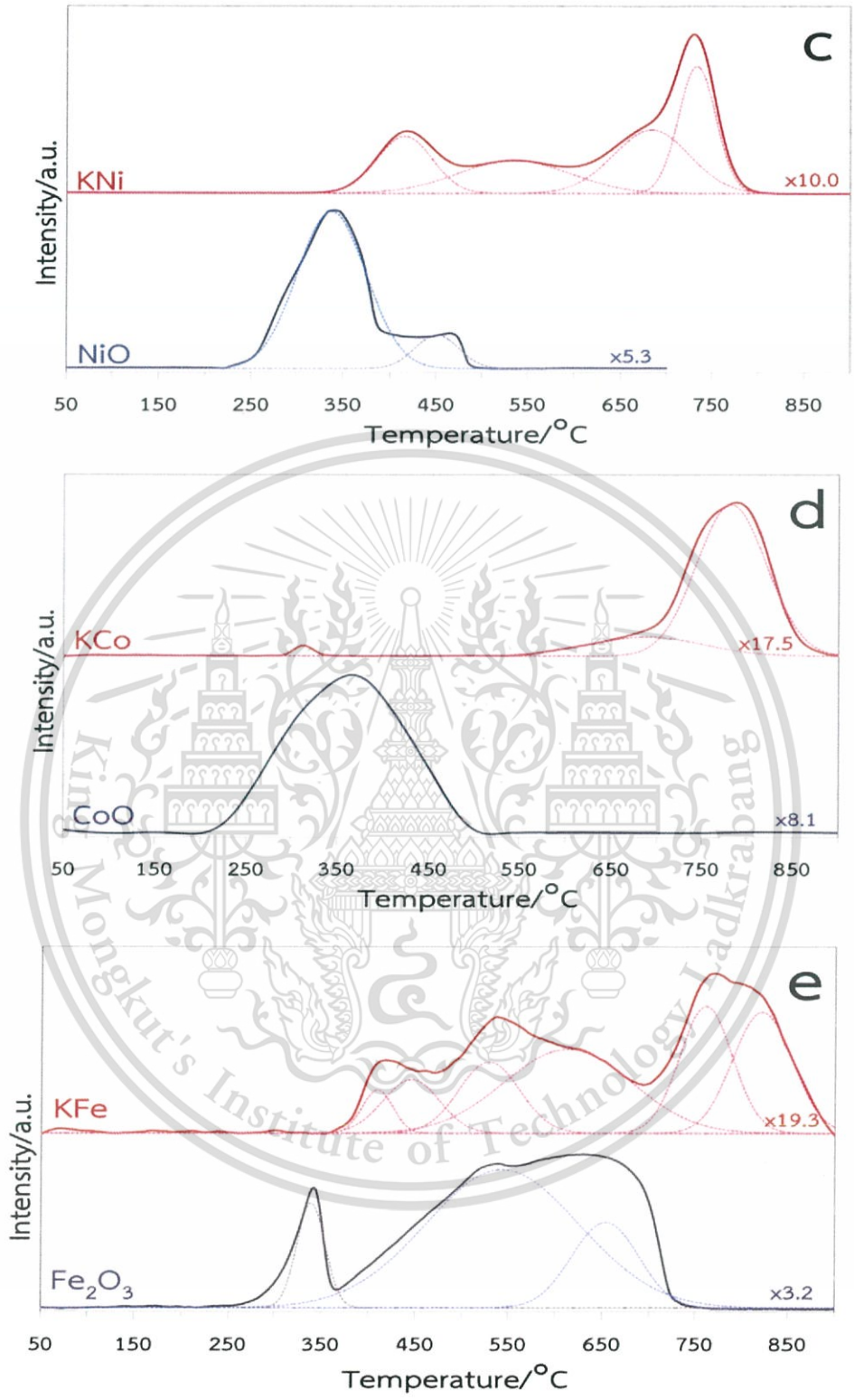

Figure 4.7 TPR profiles of metal oxide *vs.* various compositions of lepidocrocite titanate (a) KZn, (b) KCu (c) KNi, (d) KCo and (e) KFe. The y-axis is the signal from TCD normalized such that the signals are of similar intensity.

The H_2-consumption of lepidocrocite titanates are shown in Table 4.5. The amount of reducible sites can be estimated from the H_2 consumption per gram of the catalyst, and is in the order: KNi > KCu > KCo > KFe > KZn.

Table 4.5 The H_2-consumption of various catalysts prepared

Catalyst	Temp. of peak (°C)	H_2 consumption (mmol/g)	Total H_2 consumption (mmol/g)	Total H_2 consumption (mmol/m^2)
$K_{0.8}Zn_{0.4}Ti_{1.6}O_4$	550	0.408	0.408	0.136
$K_{0.8}Cu_{0.4}Ti_{1.6}O_4$	344	0.358	2.039	0.679
	496	1.680		
$K_{0.8}Ni_{0.4}Ti_{1.6}O_4$	415	0.465	2.455	0.818
	534	0.548		
	683	0.728		
	733	0.713		
$K_{0.8}Co_{0.4}Ti_{1.6}O_4$	313	0.020	1.328	0.442
	688	0.221		
	782	1.085		
$K_{0.8}Fe_{0.8}Ti_{1.2}O_4$	409	0.049	1.272	0.212
	445	0.115		
	529	0.167		
	612	0.404		
	761	0.261		
	821	0.273		

The PXRD patterns of KZn, KCu and KFe lepidocrocite titanate after the reduction at 500 °C for 2h are shown in Figure 4.8. Lepidocrocite titanates after reduction still preserve the high crystallinity similar to the "as made" catalyst. The reduced KCu and reduced KFe exhibit the impurity metal phase (Cu and Fe, respectively) as shown in Figure 4.8b and 4.8c, respectively. However, there is no impurity phase in KZn, in agreement with its low reducibility as shown in Figure 4.8a and Table 4.5. This result indicated that the metal impurity phase was occurred from the reduction of metal oxide in lepidocrocite titanated structure, and likely generating oxygen vacancy sites as demonstrated by the reduction of $K_{0.8}Cu_{0.4}Ti_{1.6}O_4$ lepidocrocite titanate shown in Scheme 4.1.

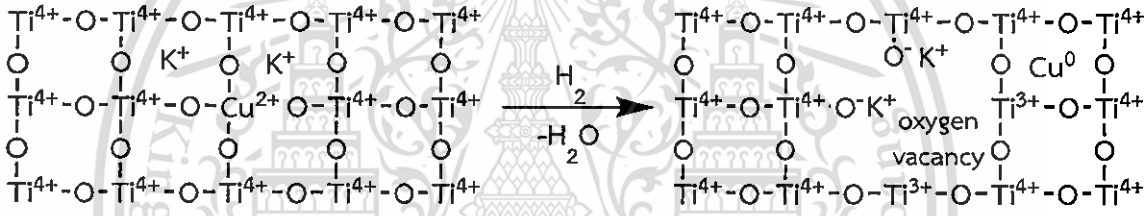

Scheme 4.1 Reduction of $K_{0.8}Cu_{0.4}Ti_{1.6}O_4$ lepidocrocite titanate (view from the top of surfaces).

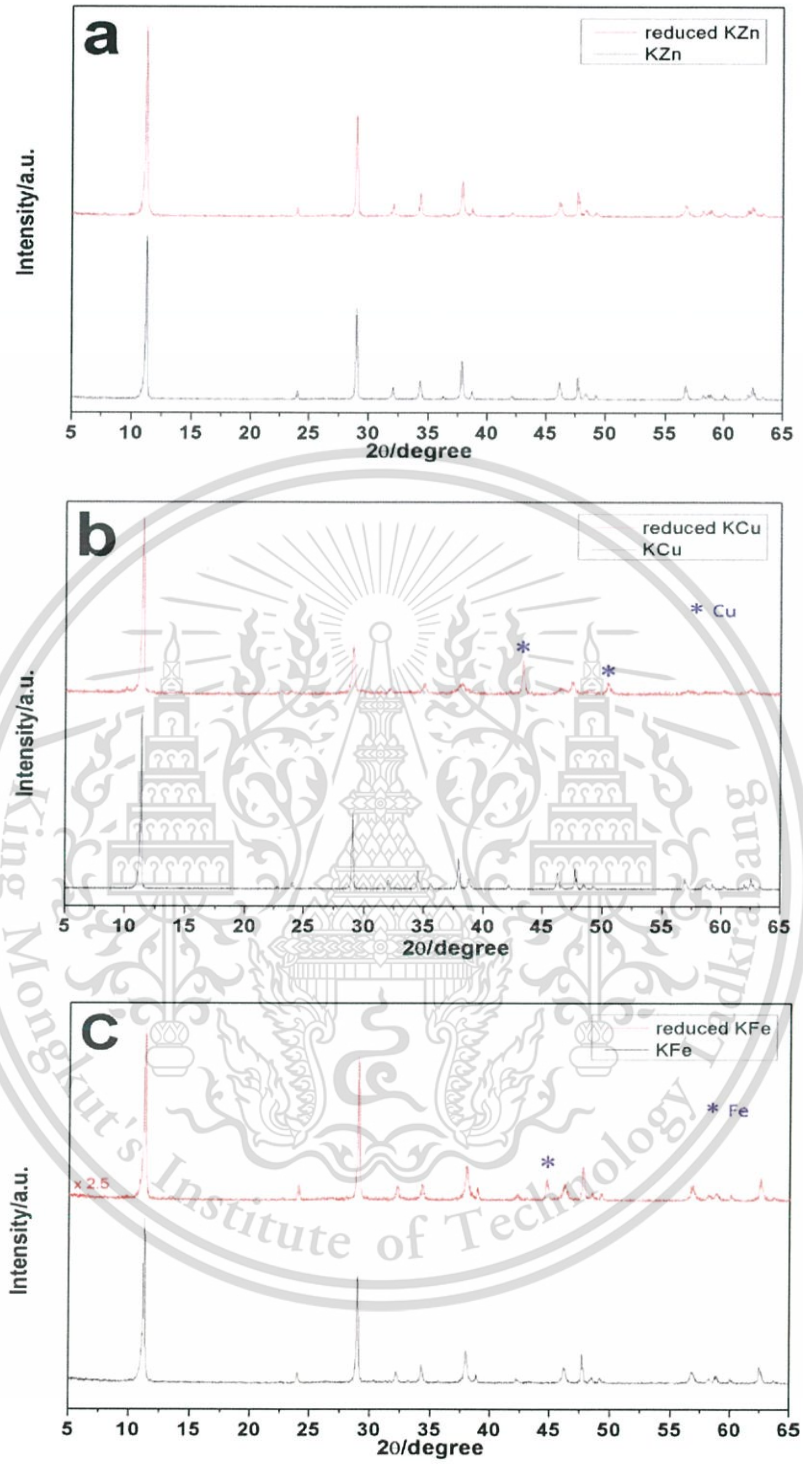

Figure 4.8 PXRD patterns of "as made" lepidocrocite titanate vs. lepidocrocite titanate after the reduction at 500 °C for 2h (a) KZn,, (b) KCu and (c) KFe. The patterns are rescaled such that the 020 peaks are of similar intensity. (The impurity peaks were marked with *.)

4.2 Adsorption of Palmitic acids and the swelling of KZn

The liquid phase adsorption of palmitic acid was employed to investigate the basic size at the internal surfaces of KZn lepidocrocite titanate as the representative. The %adsorption per mass after the adsorption of palmitic acid (5%w/w in isopropanol) at 60 °C and different adsorption times is shown in Figure 4.9. The adsorption of palmitic acid is increased to 34.5% by weight at 12 h and remains constant at 35% by weight up to 36 h. In agreement with %adsorption, the solid product after the adsorption has shown a 37% mass loss as shown in Figure 4.10b. This mass loss is ascribed to the loss of adsorbed palmitic acid in the range 200-400 °C (Figure 4.10c). Figure 4.10a shows negligible mass loss of the solid product from the control experiment with isopropanol only but in the absence of palmitic acid. The large amount of adsorption is rather unexpected considering the low surface area of KZn (3 m^2/g). Thus, the palmitic acid could have been adsorbed into the internal surfaces of lepidocrocite titanate as well.

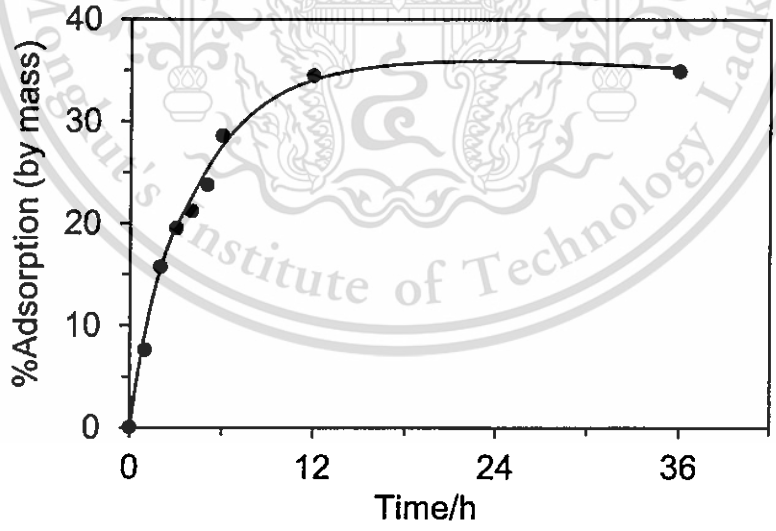

Figure 4.9 The %adsorption by mass of palmitic acid at 60 °C for 36 hours on KZn lepidocrocite titanate.

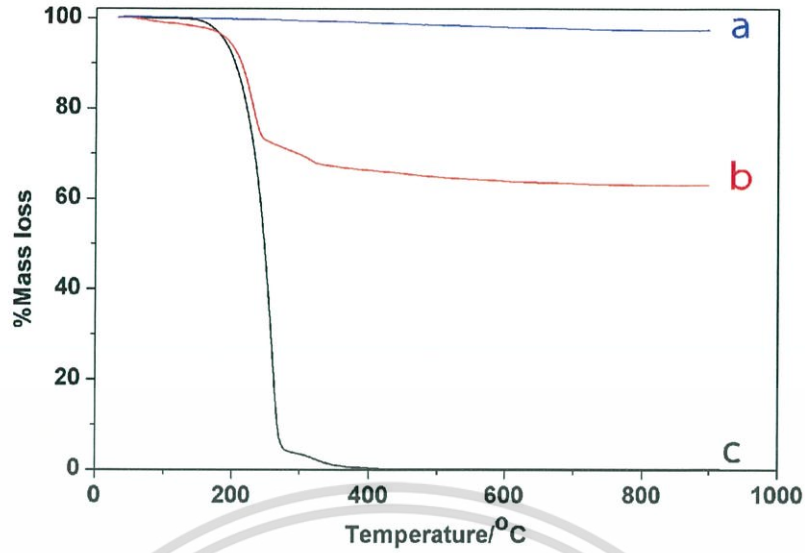

Figure 4.10 TGA mass loss curves of (a) the solid product the treatment with isopropanol only, (b) the solid product after the adsorption of 5%w/w palmitic acid in isopropanol at 60 °C for 36 h to KZn lepidocrocite titanate and (c) palmitic acid.

The PXRD pattern of the sample after the adsorption with palmitic acid is shown in Figure 4.11b. The unit cell parameters of the orthorhombic symmetry with a = 0.381(6), b = 1.7(6), and c = 0.296(6) nm can be obtained. The first peak (d_{020}) is shifted to the lower angle $2\theta = 10.09^{\circ}$ and the d spacing is larger to 0.8794 nm. This value is equivalent to the interlayer expansion of 0.1 nm in comparison to as made KZn. It is suggested that palmitic acid was adsorbed into the interlayer region and was ion-exchanged with charge balancing potassium cations to form potassium palmitate. The PXRD pattern of KZn after heated with isopropanol (Figure 4.11d) is similar to as made KZn, suggesting that palmitic acid is essential to the intercalation. Comparison of Figure 4.11b with the PXRD pattern of potassium palmitate in Figure 4.11c confirms that the product is not bulk potassium palmitate.

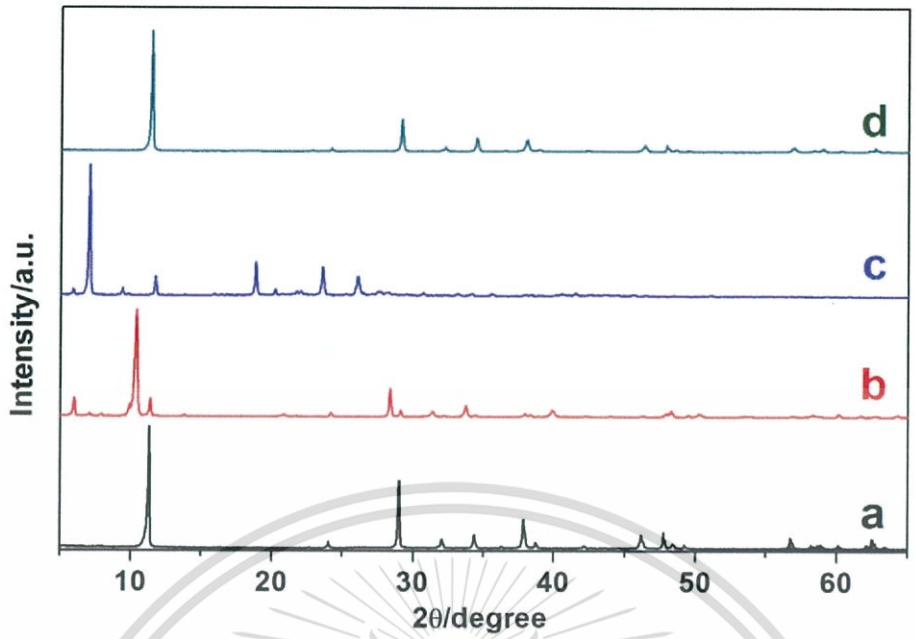

Figure 4.11 PXRD patterns of (a) KZn lepidocrocite titanate, (b) the solid product after the adsorption of 5%w/w palmitic acid in isopropanol at 60 °C for 36 h, (c) potassium palmitate and (d) the solid product the treatment with isopropanol.

The interactions between adsorbed palmitic acid and KZn can be investigated employing FTIR spectroscopy. In the spectrum of KZn (Figure 4.12a), the peak at 720 and 819 cm^{-1} characteristic of the Ti-O and Ti-O-K vibrations [34, 36] can be observed. The peaks at wavenumbers 1650 and 3441 cm^{-1} can be assigned to the vibration of a hydroxyl group of surface water or surface –OH. The peak at 1021 cm^{-1} can be assigned to hydroxyl group attached to the layered titanates. Several bands at 2850-3000 cm^{-1} are due to the CH stretching of the thin organic films coated on an FTIR window. The FTIR spectrum of KZn treated with isopropanol in Figure 4.12b is similar to as made KZn, with some variations in the relative peak intensities.

The characteristic peaks of palmitic acid in Figure 4.12d show the signature of the carboxylic acid, including the strong C=O stretching at 1711 cm^{-1}, OH stretching at 3441 cm^{-1}, and CH stretching at 1000-1290 cm^{-1}. As shown in Figure 4.12c, KZn-Palmitic acid shows several peaks at 1000-1290, 2850 and 2900 cm^{-1} (C-H stretching),

1471 cm^{-1} (O-H bending), and 3441 cm^{-1} (O-H stretching). The =C-O stretching and C=O stretching of the organics at 1600 and 1630 cm^{-1} respectively, suggest the formation of palmitate anion [58], possibly as a result of the surface basicity in KZn. The corresponding peaks in palmitic acid are at 1471 and 1711 cm^{-1}. In acid form, these two bands (~1471 cm^{-1} and 1700 cm^{-1}) are far apart. On the other hand, the stretching of C=O and =C-O in carboxylate anion becomes closer in energy due to the resonance effect. Therefore in carboxylate anions, the vibration of =C-O will shift to a higher wavenumber, while that of C=O will shift to a lower wavenumber, as compared to the respective vibrations in carboxylic acid [58]. Considering that the adsorbed species exists as palmitate, we therefore propose the complexation of K^+ with palmitate between the layers. To maintain charge neutrality, H^+ from the dissociation of palmitic acid might act as a cation balancing the negative charges at the titanate layers.

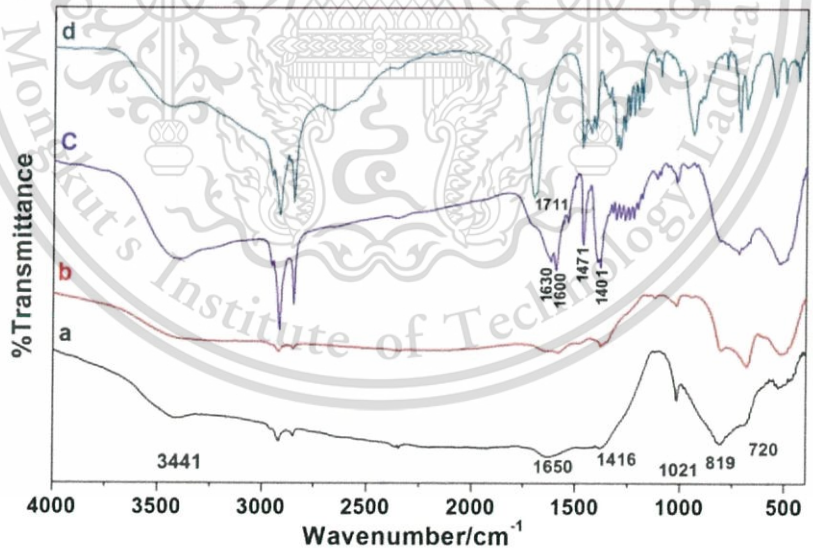

Figure 4.12 FTIR spectra of (a) KZn lepidocrocite titanate, (b) the solid product treated with isopropanol, (c) the solid product after the adsorption of 5%w/w palmitic acid in isopropanol at 60°C for 36 h solution to KZn lepidocrocite tittanate and (d) palmitic acid.

TEM images of the samples are shown in Figure 4.13. For the parent KZn prior to adsorption (Figure 4.13a), a layered structure can be observed. The distance between the layers is approximately 0.8 nm, in reasonable agreement with the distance calculated from d_{020}. Upon the adsorption of palmitic acid, the layered nature was preserved (Figure 4.13b). However, the distance between the layers increases to 1.0-1.2 nm. The expansion of 0.2-0.4 nm suggests that palmitic acid (or palmitate, as deduced from FTIR results) orients itself with the long molecular axis parallel to the sheets. The parallel orientation of an alkyl chain has been observed previously in graphite intercalation compounds [59].

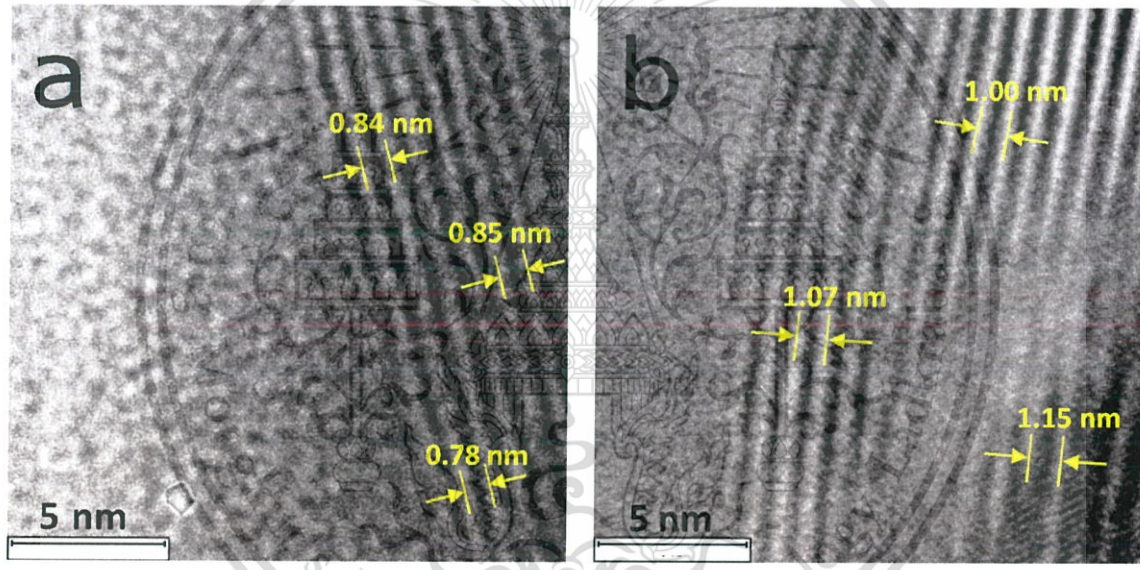

Figure 4.13 TEM images of (a) as made KZn and (b) the solid product after the adsorption of 5%w/w palmitic acid in isopropanol at 60°C for 36 h. The scale bars represent the distance of 5 nm.

4.3 Preparation of substrates for catalytic activity testing

The intercalation compound of palmitic acid and lepidocrocite titanate catalyst was prepared as a substrate for testing the catalytic deoxygenation activity. The amount of palmitic acid after the adsorption was analyzed by thermogravimetric analysis (TGA) in the nitrogen atmosphere. For example, the TGA mass loss curve of KZn lepidocrocite titanate is shown Figure 4.14a. The thermal decomposition of intercalated palmitic acid occurs at a temperature slightly higher than that of free palmitic acid (see Figure 4.14b). So, it is confirmed that palmitic acid is adsorbed into the interlayer region of lepidocrocite titanate. The TGA mass loss curves of other intercalation compounds can be found in Figure E1.

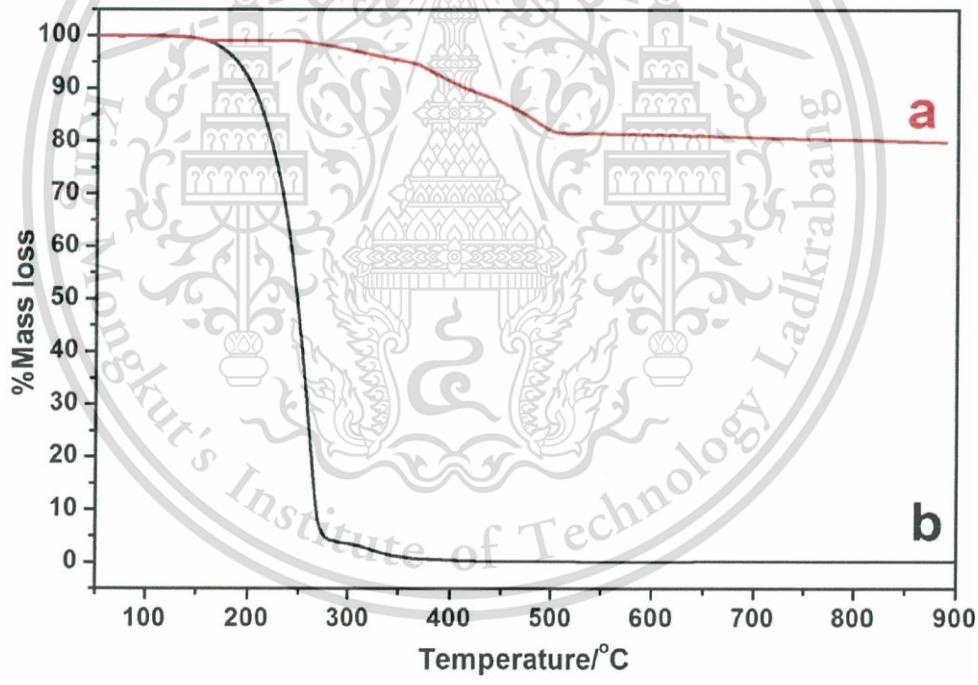

Figure 4.14 TGA mass loss curves of (a) the inter-calation compound of palmitic acid and KZn lepidocrocite titanate and (b) palmitic acid.

The amount of palmitic acid intercalated in several lepidocrocite titanate catalysts is shown in Figure 4.15 and Table 4.6. At the same adsorption condition, it is found that the amount of palmitic acid is increased when crystallite size is decreased. Here, the crystallite size was calculated employing the FWHM of the 020 peak. For example, the smallest %mass loss observed (15.115%) is for KCu with the largest crystallite size of 78.2 nm. In another example, KMg exhibits the largest %mass loss (25.28%) in agreement with the fact that it has the smallest crystallite size (41 nm).

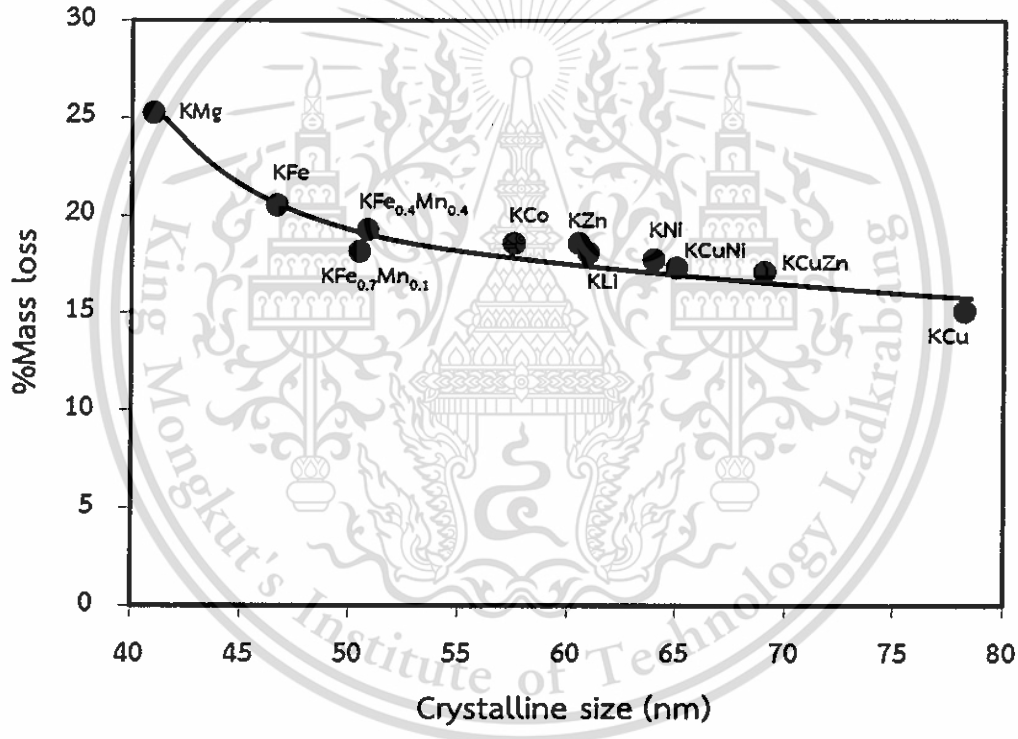

Figure 4.15 The dependence of the crystallite size on the uptake of intercalated palmitic acid (i.e., the %mass loss from TGA).

Table 4.6 The uptake of palmitic acid (wt%) in the intercalation compound from several compositions of lepidocrocite titanate.

Catalyst	Crystallite size (nm)	%Mass loss[a]
KLi	60.9	18.08
KMg	41	25.28
KFe	46.6	20.56
KCo	57.5	18.58
KNi	64	17.78
KCu	78.2	15.11
KZn	60.5	18.56
KCuNi	65	17.35
KCuZn	69	17.11
$KFe_{0.7}Mn_{0.1}$	50.4	18.19
$KFe_{0.4}Mn_{0.4}$	50.8	19.27

[a] From TGA mass loss curve.

4.4 Deoxygenation of palmitic acid over KZn lepidocrocite titanate catalyst.

The deoxygenation of palmitic acid over lepidocrocite titanate catalyst was studied using a semi-batch reactor. The reaction was first investigated using the intercalation compound of palmitic acid (~19 wt%) and KZn lepidocrocite titanate. The reaction temperature was 350 ^{o}C, the resident time was 1 h, and at the flow rate of 30 mL/min of nitrogen gas (as a carrier gas). The product distribution over KZn lepidocrocite titanate is shown in Figure 4.16 and Table 4.7.

As palmitic acid cannot be detected in the effluent during the catalytic activity testing, the conversion cannot be calculated. Therefore, the activity of the catalyst in this study is inferred by the total yields of the liquid products obtained. Here, the liquid yield is defined as the total liquid hydrocarbons obtained relative to the theoretical value of 100% conversion of palmitic acid. Even though C1-C4 hydrocarbon gas products are obtained from the deoxygenation of palmitic acid, the yields of these products are very low (<0.2%) such that they would be dissolved in the large amount of liquid hydrocarbon products. KZn lepidocrocite titanate exhibited the 52.6% yield of the liquid products. It is interesting that the relatively high activity is obtained despite the fact that KZn has extremely low surface area ($3 m^2/g$) and low basicity (0.04 mmolCO_2/g). If the reaction occurred only at the external surfaces only, a low activity should be expected. Hence, it is suggested that the reaction does not take place only at the external surfaces of the catalyst. The palmitic acid at the interlayer spaces undergoes deoxygenation to hydrocarbon products. The liquid products included both saturated and unsaturated hydrocarbons, as confirmed by GC-MS analysis (see Appendix H).

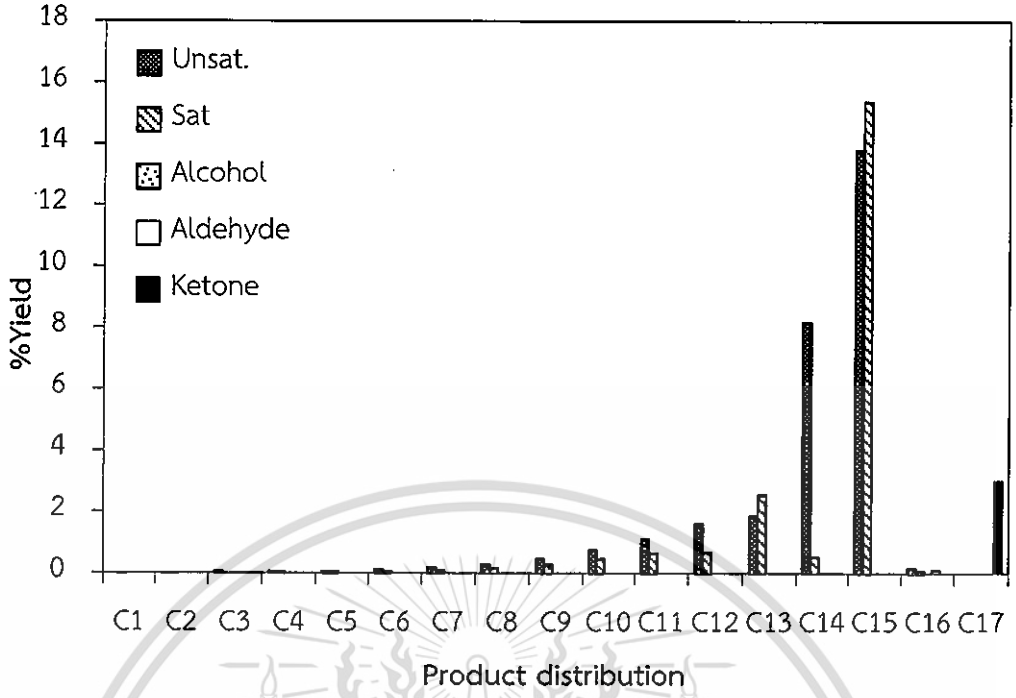

Figure 4.16 %Yield of hydrocarbon products from the deoxygenation of palmitic acid over KZn lepidocrocite titanate catalyst.

Reaction conditions: temperature 350 °C, 1 hour, 1 atm, 30 mL/min of nitrogen gas.

From Figure 4.16, the main products over KZn-palmitic acid are C15 hydrocarbons (>29% yield), consisting mainly of C15 saturated compounds (15.37% yield). The C15 saturated compounds would be obtained from the direct decomposition of the carboxylic group, forming the C15 saturated compounds and carbon dioxide via decarboxylation as shown in Scheme 4.2.

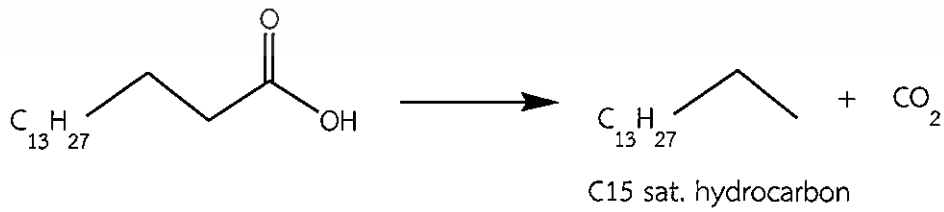

Scheme 4.2 Decarboxylation of palmitic acid.

The amount of C15 unsaturated hydrocarbon is slightly lower (13.77%). It is proposed here that palmitic acid undergoes decarbonylation to form C15 unsaturated compounds, carbon monoxide and water as demonstrated in Scheme 4.3.

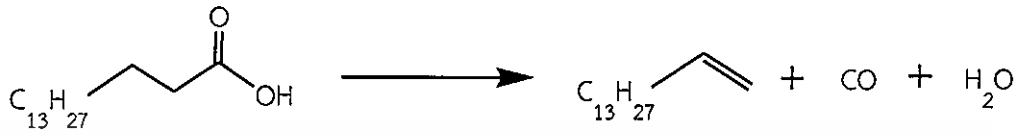

C15 unsat. hydrocarbon

Scheme 4.3 Decarbonylation of palmitic acid.

In fact, these two reaction pathways (decayboxylation and decarbonylation) can be confirmed by the observation of carbon dioxide and carbon monoxide in exhausted gas from the reaction as shown in Figure 4.17. The gas products contain a significant amount carbon dioxide from the decarboxylation, and a small amount of carbon monoxide from the decarbonylation of palmitic acid.

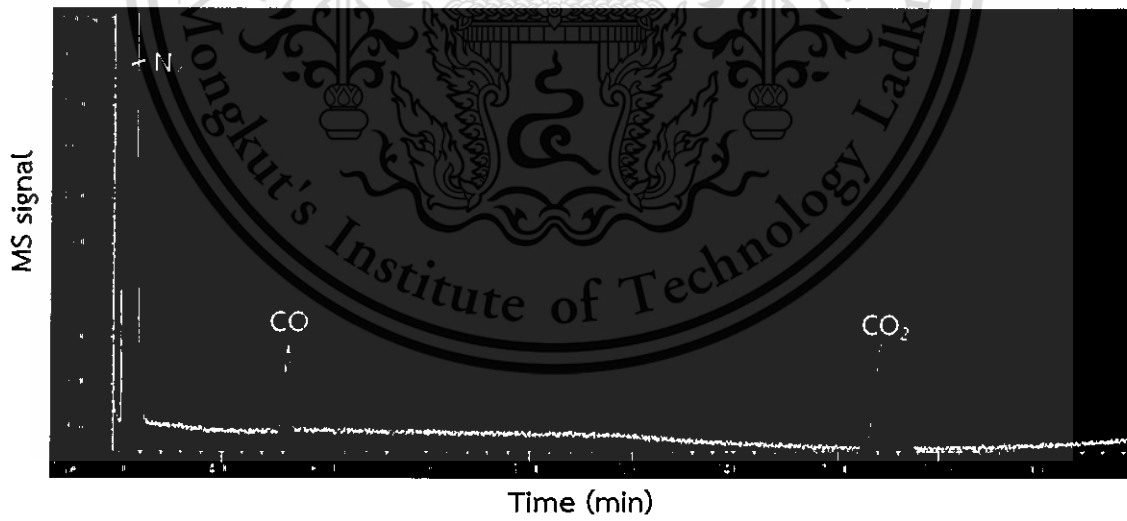

Figure 4.17 The chromatogram of gaseous products from the reaction of palmitic acid over KZn catalyst.

Table 4.7 Product distribution from the deoxygenation of palmitic acid over KZn lepidocrocite titanate catalyst.

Products	Catalyst (% by weight of palmitic acid in catalyst)	
	KZn (18.56)	
%Yield	52.60	
Product distribution	Unsat.	Sat.
C1	-	0.01
C2	0.01	0.01
C3	0.03	0.02
C4	0.03	0.03
C5	0.04	0.03
C6	0.10	0.05
C7	0.16	0.09
C8	0.26	0.15
C9	0.46	0.29
C10	0.75	0.46
C11	1.11	0.64
C12	1.61	0.67
C13	1.86	2.54
C14	8.18	0.51
C15	13.77	15.37
C16	0.16	0.08
C16 alcohol	0.00	
C16 aldehyde	0.11	
C17 ketone	3.01	

Another main products are C14 unsaturated hydrocarbon (8.18% yield) and C17 ketone (3.01% yield). Previous results from our group [8,57] suggest that, C14 unsaturated hydrocarbons and C17 ketone are the products from the catalytic cracking of C31 ketone. This ketone was obtained from the ketonization on the Ti-O-Ti surface of KZn lepidocrocite titanate catalyst. Two molecules of palmitic acid are adsorbed on the titanate surfaces and are subsequently coupled to form a symmetric ketone (C31 ketone). Meanwhile, carbon dioxide and water were released as depicted in Scheme 4.4.

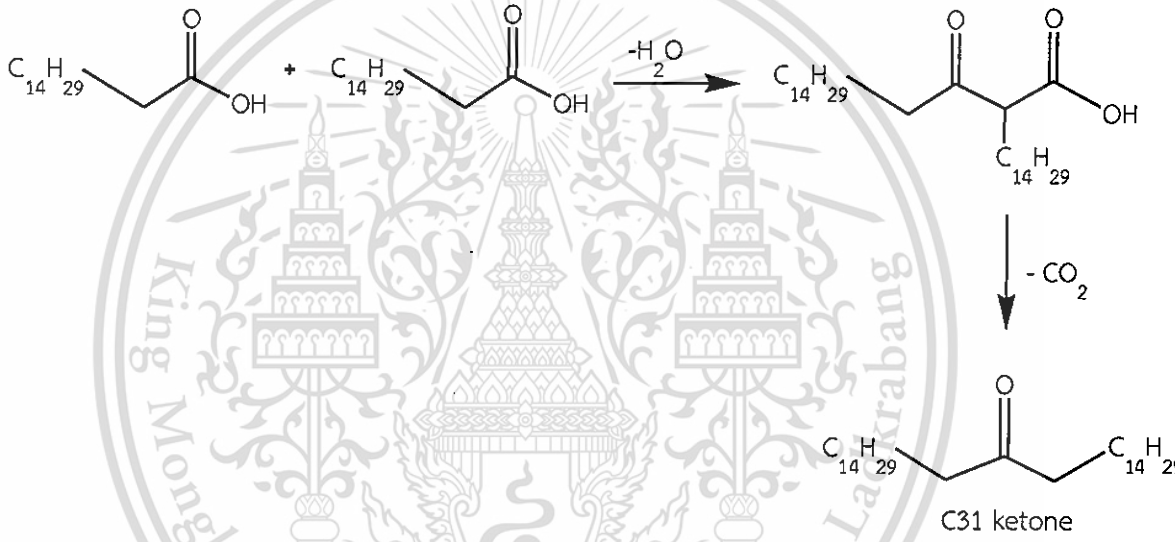

Scheme 4.4 Ketonization of palmitic acid

The cracking of C31 ketone likely takes place via a six-membered ring intermediate, which is stabilized by the intra-molecular hydrogen transfer to the carbonyl group as demonstrated in Scheme 4.5.

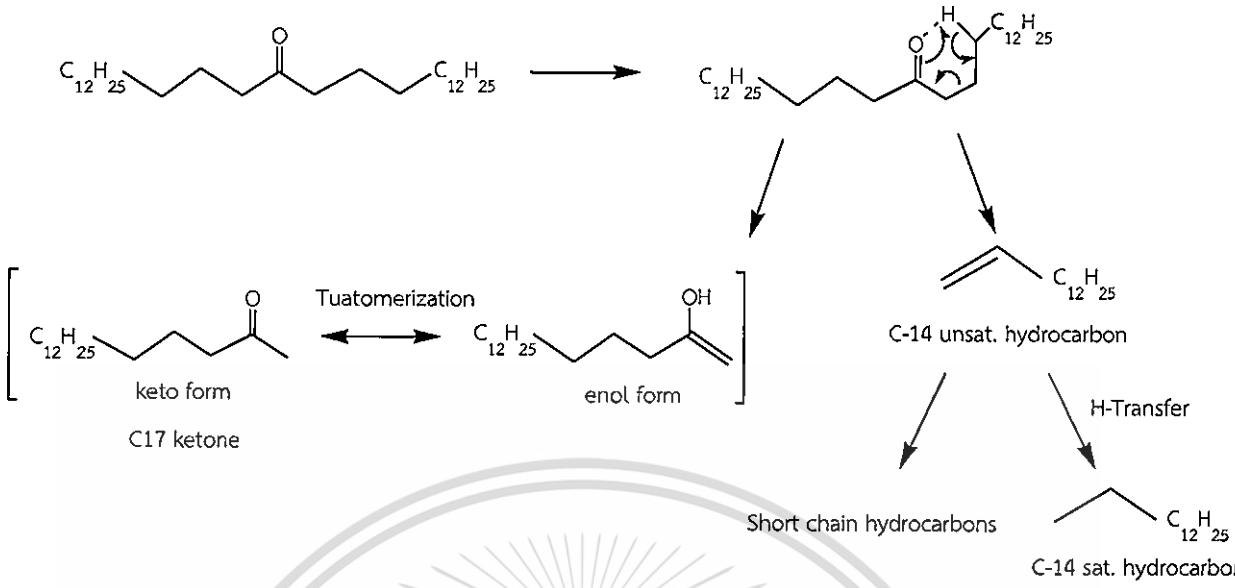

Scheme 4.5 Cracking of C31 ketone.

Hence C17 ketone is produced together with C14 unsaturated hydrocarbons. However, the C14 long chain hydrocarbons can abstract hydrogen from coke forming alkane, or it can be cracked to other short chain hydrocarbons.

According to the proposed reaction pathway in Scheme 4.5, the C14 long chain hydrocarbons and heptadecanone (C17 ketone) are produced in parallel from the cracking of C31 ketone. However, it was observed experimentally that the yield of C14 long chain hydrocarbons is higher than that of C17 ketone. This result indicates that the cracking of C-31 ketone is not the only production route of C14 long chain hydrocarbons. It is proposed here that palmitic acid undergoes deacetylation by the cleavage of the β carbon-carbon bond, forming C14 unsaturated hydrocarbons and acetic acid. Acetic acid could be further decomposed to coke, CO, CO_2 and water [60-62], as shown in Scheme 4.6.

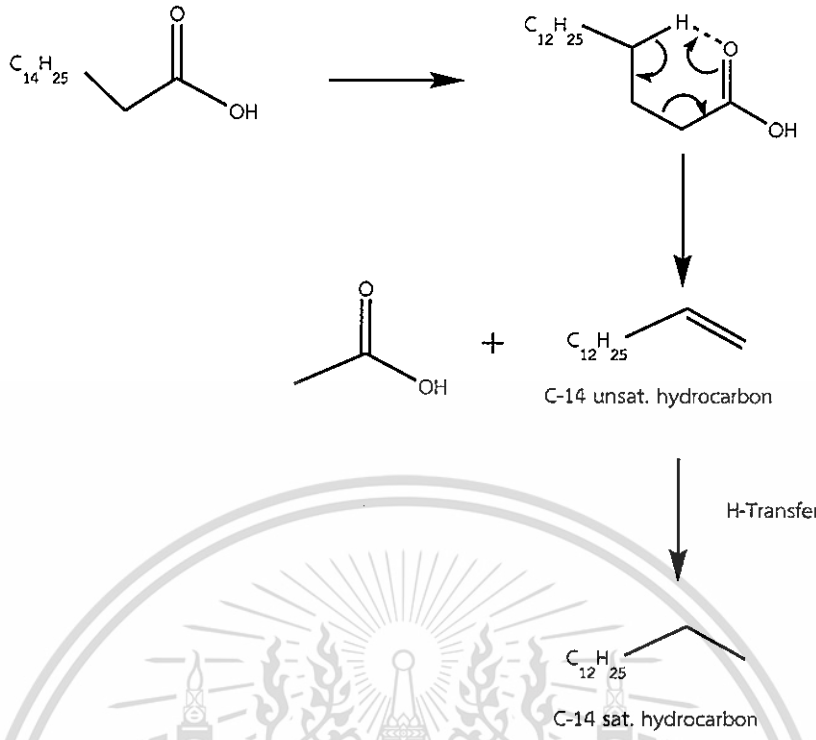

Scheme 4.6 The deacetylation of palmitic acid.

Moreover, the detectable yields of C16 long chain hydrocarbons and C16 aldehyde are also observed. It is proposed that palmitic acid was reduced on oxygen vacancy sites to form C16 aldehydes. However, this reaction is a non-catalytic process because the oxygen vacancy site is consumed. H-transfer, either from decarbonylation or coke formation, to C16 aldehyde intermediate would result in C16 alcohols that undergoes dehydration to C16 long chain hydrocarbons. Meanwhile, the decarbonylation of C16 aldehyde to C15 unsaturated hydrocarbon [63] can occur as well as depicted in Scheme 4.7.

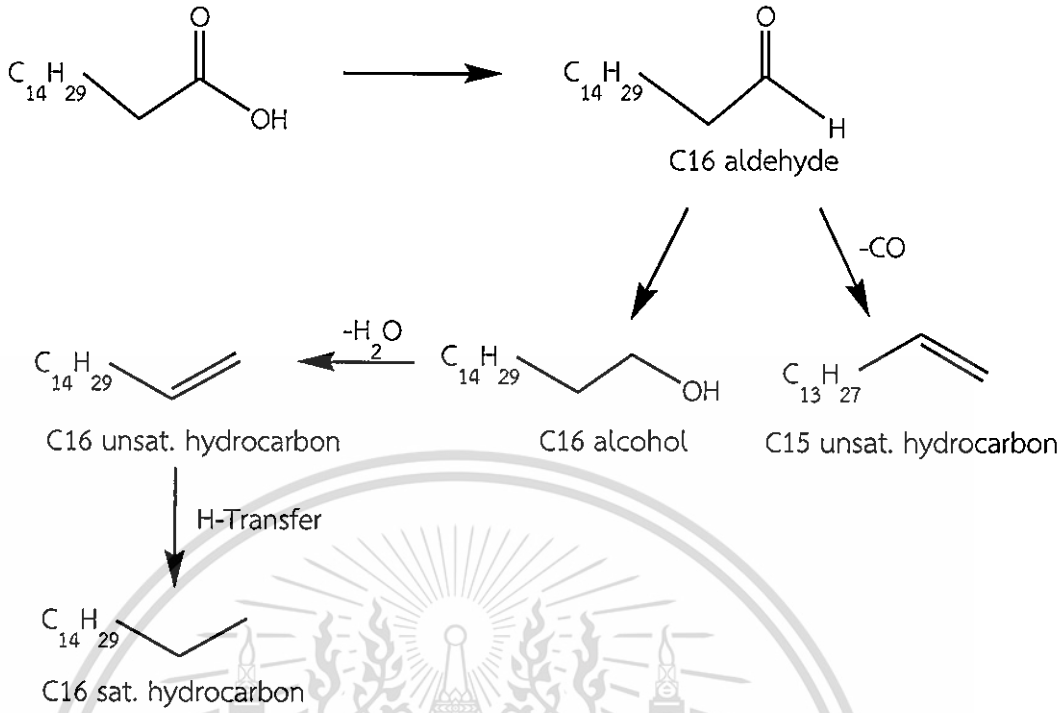

Scheme 4.7 The reduction of palmitic acid.

From the above observations and discussions, the overall reaction pathway for the deoxygenation of palmitic acid over lepidocrocite titanate can be proposed, as demonstrated in Scheme 4.8.

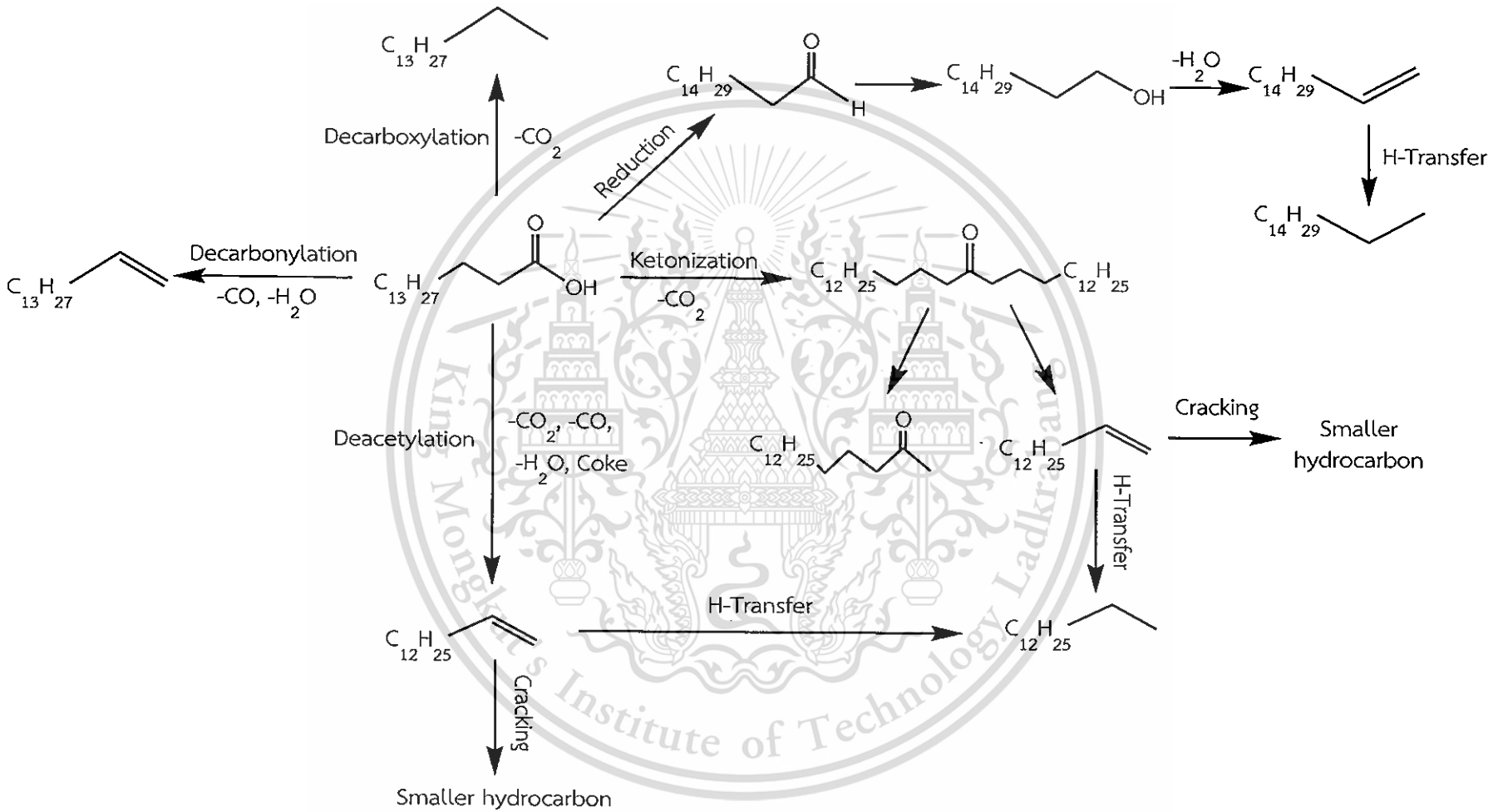

Scheme 4.8 The overall reaction pathway for the conversion of palmitic acid over lepidocrocite titanate.

4.5 Study on the reaction temperature

The effect of the reaction temperature for the deoxygenation of palmitic acid over KZn lepidocrocite titanate was studied at 350, 400, 450 and 500 °C. Results are shown in Figure 4.18 and Table 4.8.

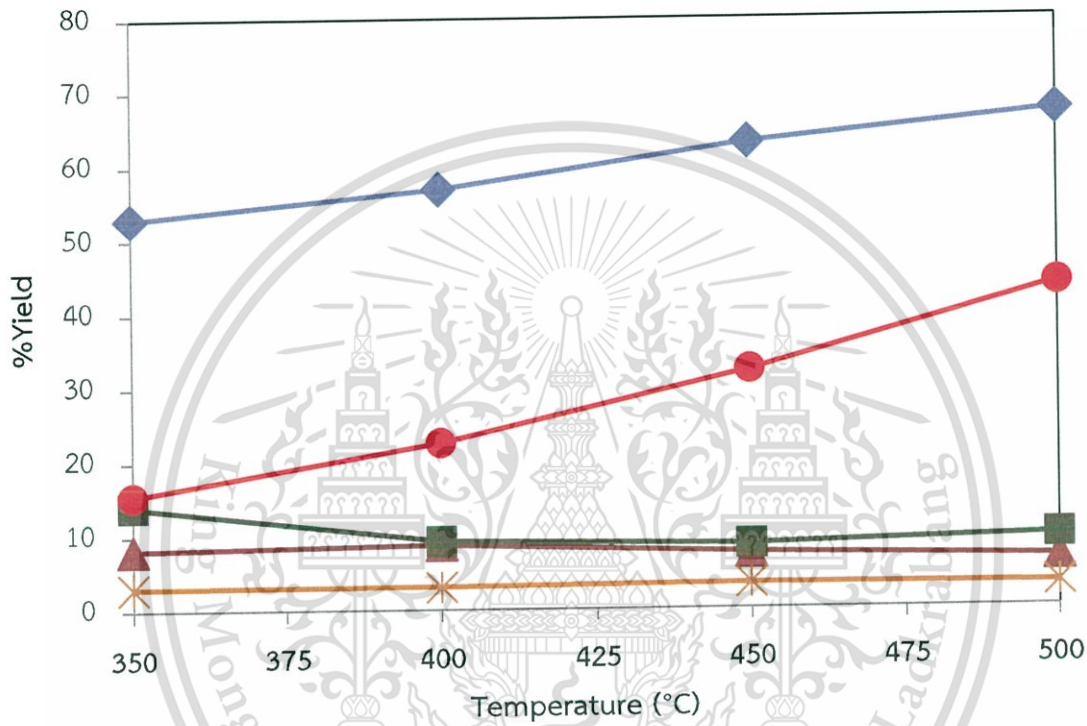

Figure 4.18 The effect of the reaction temperature on the conversion of palmitic acid and the yields of major products from the deoxygenation of palmitic over KZn.

Reaction conditions: temperature 350-500 °C, 1 hour, 1 atm, 30 mL/min of nitrogen gas, Total yield (◆), C14 unsat. (▲), C15 unsat. (■), C15 sat. (●), C17 ketone (*).

It can be seen that the yields of liquid products is increased with the reaction temperature. Results can be reasonably understood considering that at higher temperature, the reactant molecules possess higher thermal energy [64]. The increase in the liquid products yields with the reaction temperature also suggests that, the conversion of palmitic acid is not completed. This statement can be confirmed by the detection of residual palmitic acid (Figure 4.19), obtained from the digestion of the spent

catalyst after the reaction at 350°C for 1h. Details for analysis can be found in Section 3.3.7.

Table 4.8 Product distribution from deoxygenation of palmitic acid over KZn lepidocrocite titanate at various reaction temperatures

Products	Reaction temperature (°C)							
	350		400		450		500	
%Yield	52.6		56.9		63.1		67.3	
Product distribution	Unsat.	Sat.	Unsat.	Sat.	Unsat.	Sat.	Unsat.	Sat.
C1	-	-	-	-	-	-	-	-
C2	-	-	-	-	-	-	-	-
C3	-	-	-	-	-	-	-	-
C4	-	-	-	-	-	-	-	-
C5	-	-	-	-	-	-	-	-
C6	0.1	-	-	-	-	-	-	-
C7	0.2	0.1	-	-	-	-	-	-
C8	0.3	0.1	-	-	0.1	0.1	-	-
C9	0.5	0.3	0.1	0.1	0.1	0.1	-	-
C10	0.8	0.5	0.3	0.2	0.2	0.2	0.1	-
C11	1.1	0.6	0.7	-	0.4	0.5	0.3	-
C12	1.6	0.7	1.9	1.5	0.7	1.0	0.9	0.2
C13	1.9	2.5	3.3	3.1	1.6	3.5	1.1	0.6
C14	8.2	0.5	8.8	1.8	7.4	2.9	6.7	0.5
C15	13.8	15.4	9.3	22.6	8.5	31.8	9.7	43.8
C16	0.2	0.1	0.2	-	-	0.1	0.1	0.3
C16 alcohol	-		-		-		-	
C16 aldehyde	0.1		0.1		-		-	
C17 ketone	3.0		3.1		3.3		3.2	

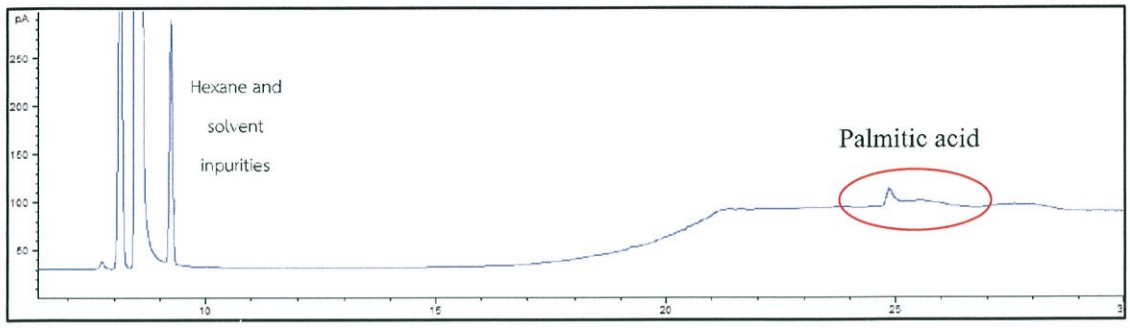

Figure 4.19 A representative chromatogram showing the liquid products obtained from the decomposition and extraction of spent KZn catalyst.

Moreover, one can see that the yields of C15 saturated hydrocarbon are increased with the reaction temperature. On the other hand, the yield of C15 unsaturated hydrocarbons is decreased from 15% yield at 350°C to a value of 10% at 400°C. This result suggests that the decarboxylation is largely promoted by increasing temperature, but the decarbonylation is not significantly affected. The yields of other products remain similar even the reaction temperature is increased. In order to validate all possible reaction pathways, the deoxygenation activity of other lepidocrocite titanate catalysts will be compared at the reaction temperature of 350°C.

4.6 Deoxygenation of palmitic acid over lepidocrocite titanate catalyst with various compositions.

The product distribution from the deoxygenation of palmitic acid was also performed with several compositions of lepidocrocite titanate catalysts possessing different basicity as referred by the partial negative charge of framework oxygen (Table 4.4). Results are shown in Table 4.9 and Figure 4.20.

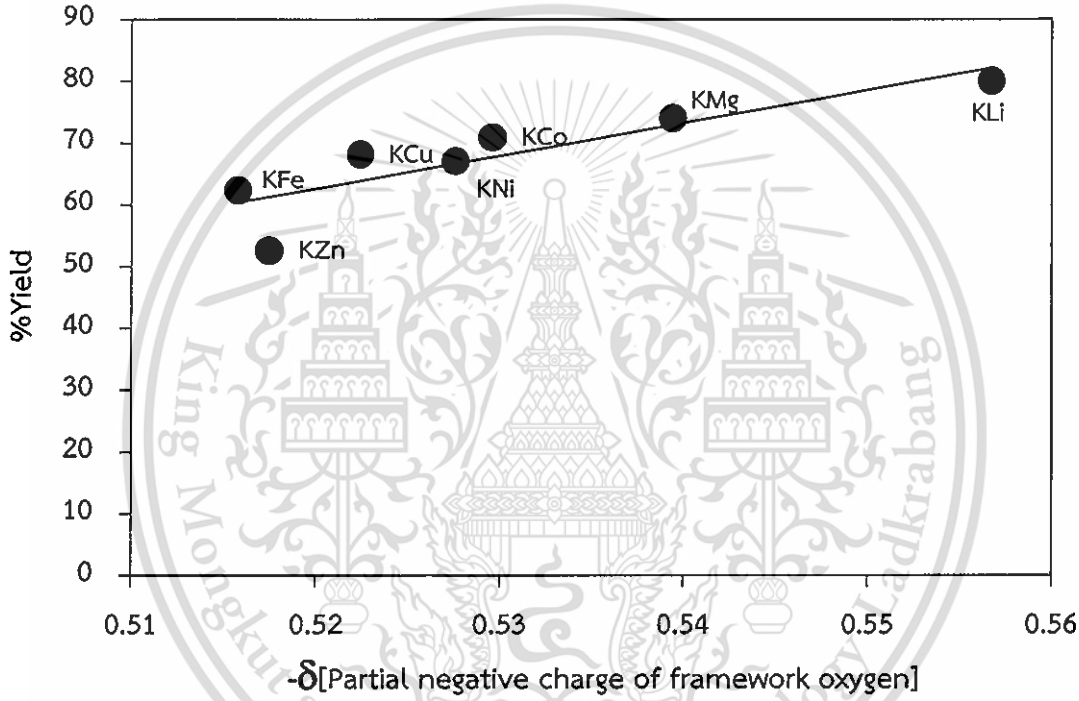

Figure 4.20 The partial negative charge of framework oxygen *vs.* the total yield of liquid hydrocarbons.

Reaction conditions: temperature 350 °C, 1 hour, 1 atm, 30 mL/min of nitrogen gas.

It can be clearly seen that there is a linear relationship between the yields of liquid hydrocarbon products and the partial negative charge of framework oxygen. This is because the high basicity facilitates the interaction with acidic molecule. The lepidocrocite titanates containing alkaline Li and alkaline earth Mg in the sheets ($K_{0.8}Li_{0.27}Ti_{1.73}O_4$ and $K_{0.8}Mg_{0.4}Ti_{1.6}O_4$) show a relatively high conversion than other

lepidocrocite titanate containing transition metals in the layers. Alkali and alkaline earth cations are usually considered as more ionic than the transition metals. These cations are also well known as promoters for basicity [65].

From Table 4.9, it can be seen that the high yield of C17 ketone and C14 unsaturated hydrocarbons are observed from the deoxygenation of palmitic acid over KLi and KMg catalyst. As discussed above, C14 unsaturated hydrocarbons and C17 ketones are obtained in parallel from the cracking of C31 ketone and the observed high activity of these two catalysts may well be derived from the increase in ketonization. It is suggested that KLi and KMg catalyst are selective to the ketonization of palmitic acid to form C31 ketone. Then, C31 ketone is cracked to C14 unsaturated hydrocarbons and C17 ketone. However, the yield of C14 unsaturated hydrocarbons is higher than that of C17 ketone. This result suggests that the deacetylation of palmitic acid that has occurred in parallel is also promoted. Moreover, the reaction over KLi gives a relative higher amount of short chain hydrocarbons as compared to $K_{0.9}Mg_{0.45}Ti_{1.55}O_4$, likely because of the higher basicity in the former.

Table 4.9 Product distributions from the deoxygenation of palmitic acid over several composition of lepidocrocite titanate.

Products	Catalyst (% by weight of palmitic acid in catalyst)													
	KLi (18.08)		KMg (35.28)		KFe (20.56)		KCo (18.58)		KNi (17.78)		KCu (15.11)		KZn (18.56)	
%Yield	80.0		73.9		62.3		70.9		67.0		68.1		52.6	
Product distribution	Unsat.	Sat.	Unsat.	Sat.	Unsat.	Sat.	Unsat.	Sat.	Unsat.	Sat.	Unsat.	Sat.	Unsat.	Sat.
C1	-	-	-	-	-	-	-	-	-	-	-	-	-	-
C2	-	-	-	-	-	-	-	-	-	-	-	-	-	-
C3	-	-	-	-	-	-	0.1	-	-	0.1	-	-	-	-
C4	-	-	-	-	-	-	0.0	-	0.1	0.1	-	-	-	-
C5	0.1	-	-	-	-	-	0.0	-	0.1	-	-	-	-	-
C6	0.2	0.1	0.1	-	0.1	-	0.3	0.1	1.3	0.6	-	-	0.1	-
C7	0.3	0.2	0.1	0.1	-	0.1	0.1	0.1	0.3	1.0	-	-	0.2	0.1
C8	0.6	0.5	0.2	0.2	0.1	0.1	0.4	0.3	0.1	0.8	-	-	0.3	0.1
C9	1.2	0.9	0.4	0.4	0.3	0.3	0.9	0.3	0.7	0.7	0.1	0.1	0.5	0.3
C10	2.5	1.8	1.0	0.9	0.3	0.3	0.7	0.3	1.4	0.7	0.2	0.1	0.8	0.5
C11	6.4	4.5	2.2	1.5	0.5	0.4	1.2	0.5	0.6	0.3	0.3	0.2	1.1	0.6
C12	5.9	5.9	2.9	2.0	0.8	0.7	2.3	0.9	0.8	0.9	0.3	0.3	1.6	0.7
C13	5.5	5.9	3.7	8.5	1.0	1.4	3.4	1.7	1.9	2.0	0.4	0.4	1.9	2.5
C14	11.3	5.3	23.6	2.7	4.1	5.4	4.2	6.6	4.8	2.0	1.7	3.3	8.2	0.5
C15	5.0	9.5	3.3	4.4	18.3	10.0	26.0	16.8	22.5	12.0	16.2	24.9	13.8	15.4
C16	0.2	0.1	0.2	-	0.9	1.9	1.1	0.3	3.3	2.7	0.4	0.3	0.2	0.1
C16 alcohol	0.2		0.1		1.1		0.6		1.1		2.6		-	
C16 aldehyde	0.2		0.1		13.4		1.0		3.6		15.8		0.1	
C17 ketone	5.5		15.0		0.7		0.5		0.7		0.5		3.0	

For lepidocrocite titanates incorporating the transition metals, it is found that the yield of C15 hydrocarbons is increased as the basicity of the catalyst is increased (Figure 4.21).

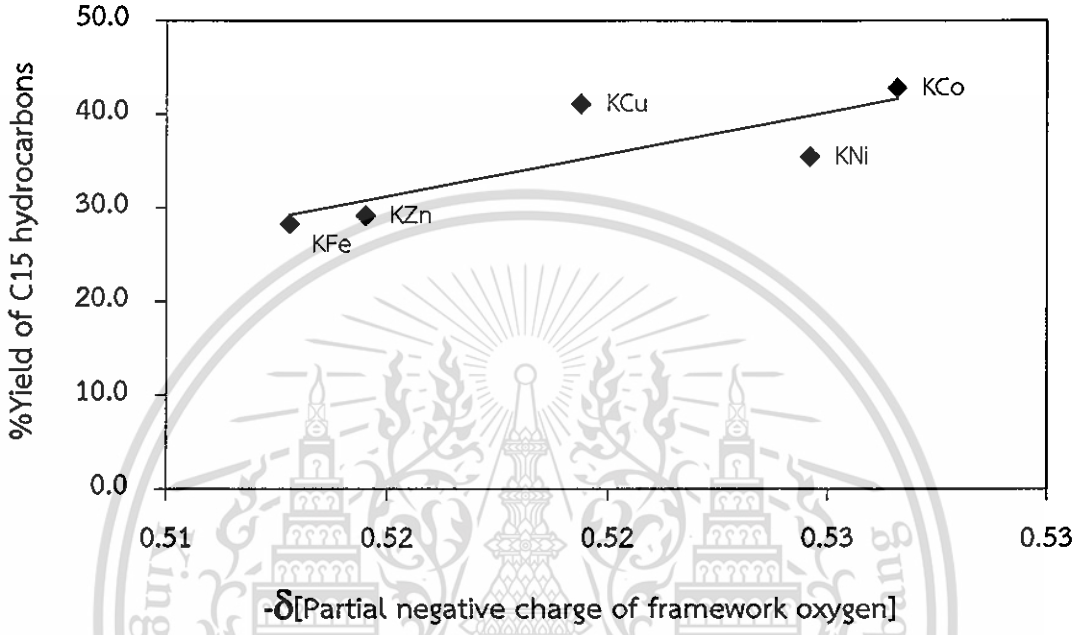

Figure 4.21 The relationship between the partial charge of framework oxygen *vs.* the yield of C15 hydrocarbons over several compositions of lepidocrocite titanate catalyst.

Reaction conditions: temperature 350 °C, 1 hour, 1 atm, 30 mL/min of nitrogen gas.

As discussed above, C15 hydrocarbons were obtained from the decarboxylation and decarbonylation of palmitic acid. It is suggested here that the decarboxylation and decarbonylation required the strong interaction of carboxylic group on the basic site of catalysts. However, from Table 4.9 and Figure 4.22, KCu and KZn give the higher yield of C15 saturated hydrocarbons, as compared to the unsaturated ones. This indicates that KCu and KZn are selective for the decarboxylation of palmitic acid to C15 saturated hydrocarbons. On the other hand, the high yield of C15 unsaturated hydrocarbon (larger than that of C15 saturated

hydrocarbons) is obtained from the deoxygenation of palmitic over KFe, KCo and KNi catalysts. It is suggested that KFe, KCo and KNi facilitates the decabonylation of palmitic acid to C15 unsaturated hydrocarbon. This is presumably because Fe, Co and Ni possess strong interaction with CO [66].

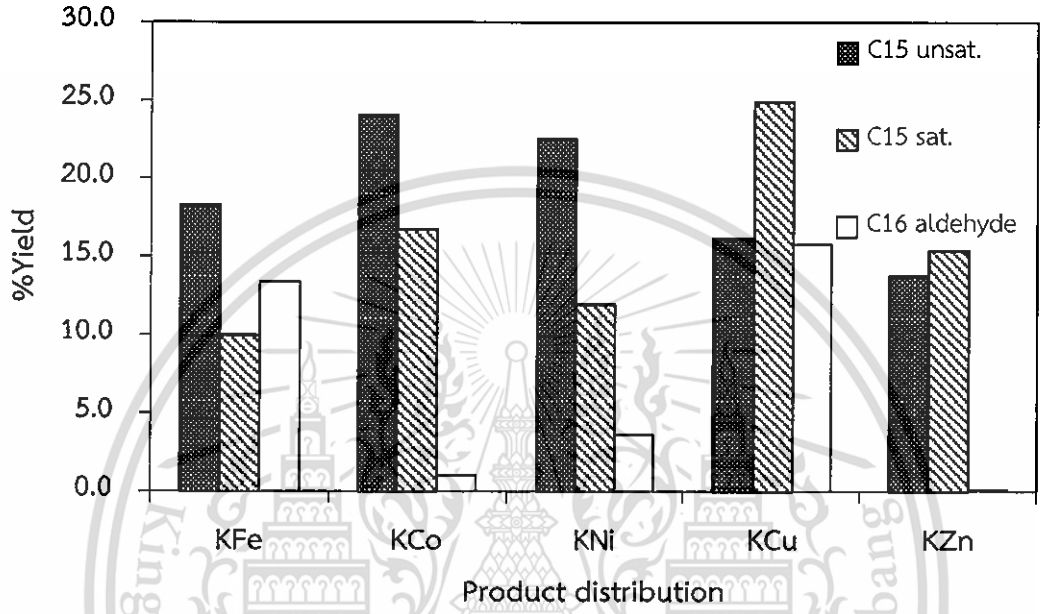

Figure 4.22 The yield of major products from the deoxygenation of palmitic acid over several compositions of lepidocrocite titanate incorporating transition metal cations into the layers.

Reaction conditions: temperature 350 °C, 1 hour, 1 atm, 30 mL/min of nitrogen gas.

Moreover, the high of C16 aldehyde from non-catalytic reaction is observed in the order of KCu (15.8) > KFe (13.4) > KNi (3.6) >KCo (1.0) > KZn (0.1). It is suggested that under the experimental condition (350°C), the incorporated transition metal is reduced by hydrogen from decarbonylation or coke formation to generate oxygen vacancy sites. Then, oxygen vacancy sites abstract an oxygen atom from palmitic acid to generate C16 aldehyde (Scheme 4.9).

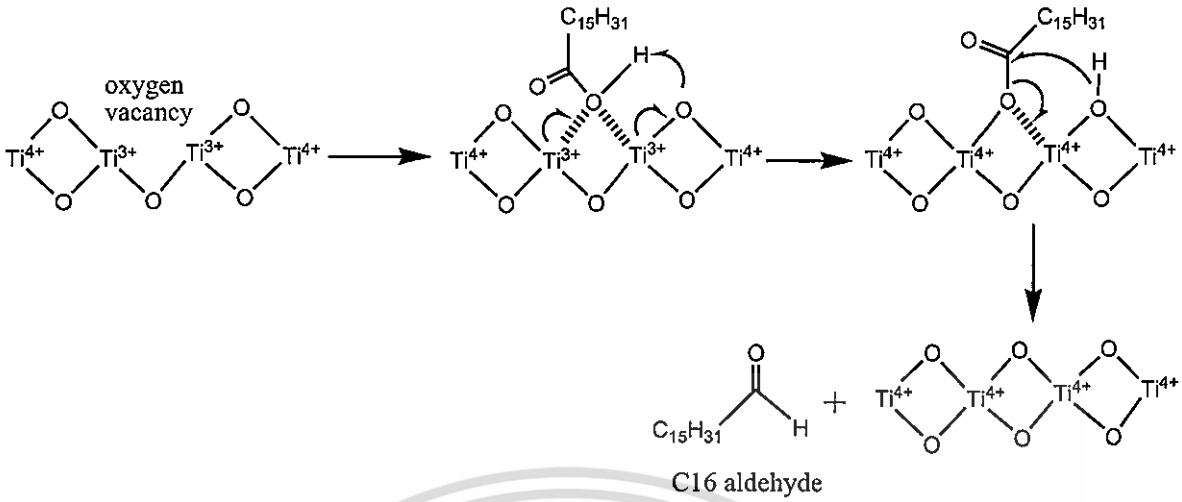

Scheme 4.9 The reduction of palmitic acid over oxygen vacancy site.

This statement is supported by the known reducibility of the catalysts under H_2 atmosphere at 350°C as shown in the TPR profiles (Figure 4.7). At 350 °C, it can be seen that KCu will be reduced to a higher extent than the KFe and KNi. Thus, C16 aldehyde is produced in a large amount by KCu compared to other catalysts. On the other hand, small amount of C16 aldehyde is observed for KCo and KZn because it is difficult to reduce KCo (i.e., high reduction temperature, Figure 4.7d) and KZn (i.e., very small H_2 consumption, Figure 4.7a).

It can be noticed that the yield of C15 unsaturated hydrocarbon is inversely proportional to the yield of C16 aldehyde (Figure 4.23). It is suggested that, C16 aldehyde can also be decarbonylated to C15 unsaturated hydrocarbons as shown in Scheme 4.7. Hence, the decarbonylation activity of KCo is higher than that of KNi, KFe and KCu respectively. This is not the case for KZn as it possesses no reducibility (Figure 4.7a). As KFe and KCu give relatively low long chain hydrocarbon, these catalysts are further modified for the conversion of C16 aldehyde to linear long chain hydrocarbons.

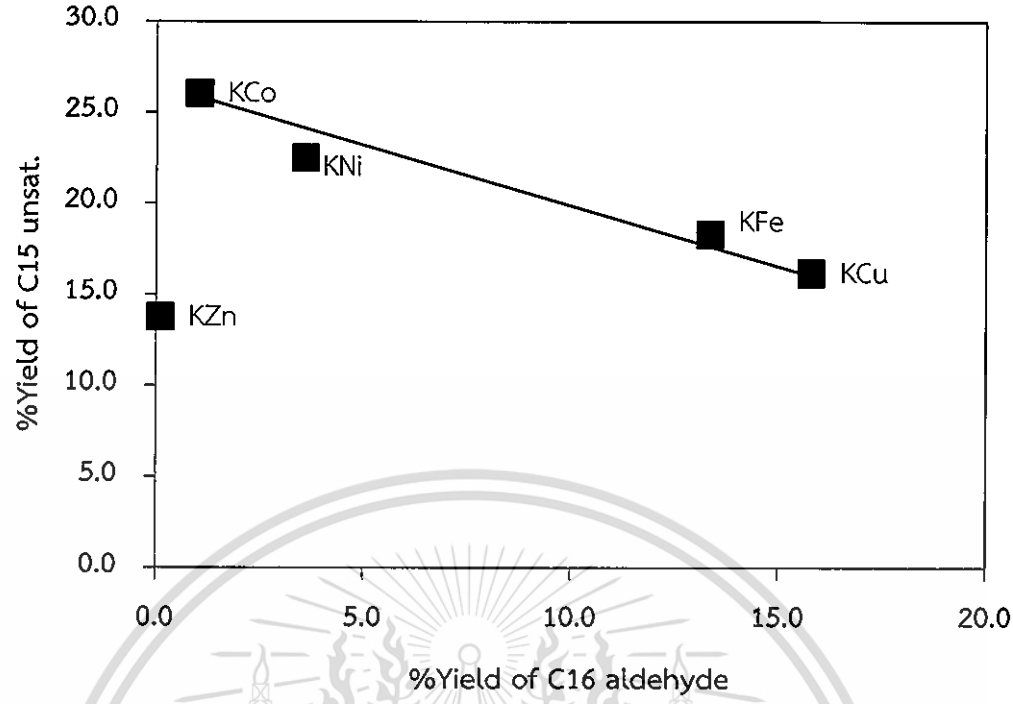

Figure 4.23 The yield of C16 aldehyde *vs.* the yield of C15 unsaturated hydrocarbons from the deoxygenation of palmitic acid over different transition metal incorporated lepidocrocite titanate catalysts.

Reaction conditions: temperature 350 °C, 1 hour, 1 atm, 30 mL/min of nitrogen gas.

4.7 Deoxygenation of palmitic acid over co-substituted lepidocrocite titanate catalysts

Lepidocrocite titanate where Ti was simultaneously substituted by two types of cations (including $K_{0.8}Fe_{0.7}Mn_{0.1}Ti_{1.2}O_4$, $K_{0.8}Fe_{0.4}Mn_{0.4}Ti_{1.2}O_4$, $K_{0.8}Cu_{0.2}Ni_{0.2}Ti_{1.6}O_4$, and $K_{0.8}Cu_{0.2}Zn_{0.2}Ti_{1.6}O_4$) were also tested for deoxygenation of palmitic acid at 350°C.

The product distributions obtained over KFe, $KFe_{0.7}Mn_{0.1}$ and $KFe_{0.4}Mn_{0.4}$ are compared in Table 4.10. It can be seen that the liquid product yield increased as the basicity increased as shown in Figure 4.24.

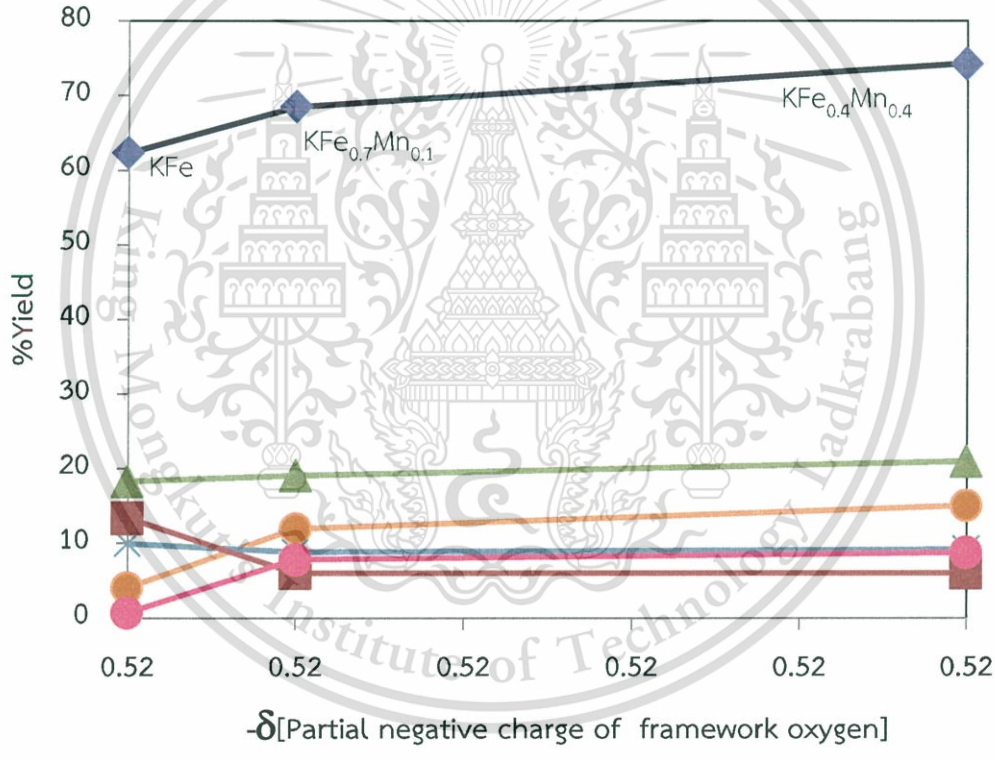

Figure 4.24 Yield of major products from the deoxygenation of palmitic acid over $K_{0.8}Fe_{0.8}Ti_{1.2}O_4$, $K_{0.8}Fe_{0.7}Mn_{0.1}Ti_{1.2}O_4$ and $K_{0.8}Fe_{0.4}Mn_{0.4}Ti_{1.2}O_4$ catalysts.

Reaction conditions: temperature 350 °C, 1 hour, 1 atm, 30 mL/min of nitrogen gas, Total yield (◆), C14 unsat. (●), C15 unsat. (▲), C15 sat. (X) ,C16 aldehyde (■), C17 ketone (●).

The decrease in yield of C16 aldehyde is observed when Mn is loaded. However, the high yield of C17 ketone and C14 unsaturated hydrocarbon are increased with Mn content. This result suggests that, the loading of Mn promotes the ketonization of C16 aldehyde and palmitic acid to form C31 ketone. Then, C31 ketone is cracked to C14 unsaturated hydrocarbons and C17 ketone. These results are in agreement with the report on ketonization of propanoic acid over Mn_2O_3 [67].

Table 4.10 Product distribution from the deoxygenation of palmitic acid over $K_{0.8}Fe_{0.8}Ti_{1.2}O_4$, $K_{0.8}Fe_{0.7}Mn_{0.1}Ti_{1.2}O_4$ and $K_{0.8}Fe_{0.4}Mn_{0.4}Ti_{1.2}O_4$ catalysts.

Products	Catalyst (% by weight of palmitic acid in catalyst)					
	KFe (17.78)		K $Fe_{0.7}Mn_{0.1}$(18.19)		$KFe_{0.4}$ $Mn_{0.4}$(21.07)	
%Yield	62.3		68.51		74.3	
Product distribution	Unsat.	Sat.	Unsat.	Sat.	Unsat.	Sat.
C1	-	-	-	-	-	-
C2	-	-	-	-	-	-
C3	-	-	-	-	-	-
C4	-	-	-	-	-	-
C5	-	-	-	-	-	-
C6	0.1	-	-	-	-	-
C7	0.0	0.1	-	-	-	0.1
C8	0.1	0.1	-	-	0.1	0.1
C9	0.3	0.3	0.1	0.1	0.3	0.3
C10	0.3	0.3	0.4	0.3	0.5	0.5
C11	0.5	0.4	1.2	0.9	0.9	0.8
C12	0.8	0.7	1.4	1.1	1.3	1.2
C13	1.0	1.4	2.4	2.3	2.1	3.7
C14	4.1	5.4	11.9	1.8	15.0	1.4
C15	18.3	10.0	19.1	8.8	21.0	9.2
C16	0.9	1.9	0.5	0.7	0.3	1.5
C16 alcohol	1.1		1.8		1.0	
C16 aldehyde	13.4		6.0		4.0	
C17 ketone	0.7		7.8		8.8	

As discussed above, one can infer that KCu shows the high yield of C16 aldehyde, while KNi is selective to the decarbonylation of palmitic acid to C15 unsaturated hydrocarbon. Co-incorporation of these two transition metals into lepidocrocite titanate may lead to the improved decarbonylation of C16-aldehyde to

C15 unsaturated hydrocarbons. The product distributions of KCu, KNi and $KCu_{0.2}Ni_{0.2}$ are compared in Table 4.11.

Table 4.11 Product distribution from the deoxygenation of palmitic acid over $K_{0.8}Cu_{0.4}Ti_{1.6}O_4$, $K_{0.8}Ni_{0.4}Ti_{1.6}O_4$ and $K_{0.8}Cu_{0.2}Ni_{0.2}Ti_{1.2}O_4$ catalysts.

Products	Catalyst (% by weight of palmitic acid in catalyst)					
	KCu (15.11)		KNi (17.78)		$KCu_{0.2}Ni_{0.2}$ (17.35)	
%Yield	68.1		67.0		68.8	
Product distribution	Unsat.	Sat.	Unsat.	Sat.	Unsat.	Sat.
C1	-	-	-	-	-	-
C2	-	-	-	-	-	-
C3	-	-	-	0.1	-	-
C4	-	-	0.1	0.1	-	-
C5	-	-	0.1	-	-	-
C6	-	-	1.3	0.6	-	-
C7	-	-	0.3	1.0	-	-
C8	-	-	0.1	0.8	-	0.1
C9	0.1	0.1	0.7	0.7	-	-
C10	0.2	0.1	1.4	0.7	0.1	-
C11	0.3	0.2	0.6	0.3	0.1	0.1
C12	0.3	0.3	0.8	0.9	0.1	0.2
C13	0.4	0.4	1.9	2.0	0.1	0.2
C14	1.7	3.3	4.8	2.0	0.4	0.6
C15	16.2	24.9	22.5	12.0	14.7	51.1
C16	0.4	0.3	3.3	2.7	0.0	0.1
C16 alcohol	2.6		1.1		0.4	
C16 aldehyde	15.8		3.6		0.4	
C17 ketone	0.5		0.7		-	

It can be seen that the liquid products yield from the deoxygenation of palmitic acid over $Cu_{0.2}Ni_{0.2}$ catalyst are somewhat similar to KCu and KNi. Although

the yield of C16 aldehyde is decreased when Cu and Ni are co-incorporated, the yield of C15 unsaturated hydrocarbon are not increased. However, the high yield of C15 saturated hydrocarbon is obtained, suggesting that Cu and Ni co-incorporation promotes the decarboxylation of palmitic acid. This result implies that the activity of Cu is dominating over Ni when the two metals are co-incorporated. This behavior are in line with those reported previously [68].

As KCu and KZn are selective to the decarboxylation of palmitic acid to C15 saturated hydrocarbon, the co-incorporation of Cu and Zn was also tested for the deoxygenation of palmitic acid. The product distributions over KCu, KZn and $KCu_{0.2}Zn_{0.2}$ are compared in Table 4.12.

Table 4.12 Product distribution from the deoxygenation of palmitic acid over $K_{0.8}Cu_{0.4}Ti_{1.6}O_4$, $K_{0.8}Zn_{0.4}Ti_{1.6}O_4$ and $K_{0.8}Cu_{0.2}Zn_{0.2}Ti_{1.2}O_4$ catalysts.

Products	Catalyst (% by weight of palmitic acid in catalyst)					
	KCu (15.11)		KZn (18.56)		$KCu_{0.2}Zn_{0.2}$ (17.11)	
%Yield	68.1		52.6		53.9	
Product distribution	Unsat.	Sat.	Unsat.	Sat.	Unsat.	Sat.
C1	-	-	-	-	-	-
C2	-	-	-	-	-	-
C3	-	-	-	-	-	-
C4	-	-	-	-	-	-
C5	-	-	-	-	-	-
C6	-	-	0.1	-	-	-
C7	-	-	0.2	0.1	-	-
C8	-	-	0.3	0.1	-	-
C9	0.1	0.1	0.5	0.3	-	-
C10	0.2	0.1	0.8	0.5	-	-
C11	0.3	0.2	1.1	0.6	-	-
C12	0.3	0.3	1.6	0.7	0.1	0.1
C13	0.4	0.4	1.9	2.5	0.1	0.1
C14	1.7	3.3	8.2	0.5	0.2	1.1
C15	16.2	24.9	13.8	15.4	13.9	37.5
C16	0.4	0.3	0.2	0.1	0.0	0.1
C16 alcohol	2.6		-		0.2	
C16 aldehyde	15.8		0.1		0.4	
C17 ketone	0.5		3.0		0.1	

It can be seen that liquid product yields from the deoxygenation of palmitic acid over $KCu_{0.2}Zn_{0.2}$ are not increased significantly. However, the yield of C15 saturated hydrocarbon is increased from 15.4% (KZn) or 24.9% (KCu) to 37.5%. This is presumably because the reduction activity of Cu is suppressed when Zn is incorporated. This is in line with a significant decrease in C16 aldehyde.

4.8 Regeneration of catalyst

The spent KCo and KCu were collected from the reaction after being used at the reaction temperature of 350 °C and the resident time of 1 h. These spent catalysts were recalcined in air at 600 °C for 8 h for the removal of coke deposited. The TGA mass loss curve of spent KCu is shown in **FigureG1**. The palmitic acid was intercalated over these regenerated catalysts. The catalytic activity of the regenerated catalysts was investigated under the same reaction conditions as with the fresh catalysts. The yield of hydrocarbons is shown in Table 4.13.

Table 4.13 Product distribution from the deoxygenation of palmitic acid over $K_{0.8}Co_{0.4}Ti_{1.6}O_4$, regenerated $K_{0.8}Co_{0.4}Ti_{1.6}O_4$, $K_{0.8}Cu_{0.4}Ti_{1.6}O_4$ and regenerated $K_{0.8}Cu_{0.4}Ti_{1.2}O_4$ catalysts.

Products	Catalyst (% by weight of palmitic acid in catalyst)							
	KCo (18.58)		Regenerated KCo (10.84)		KCu (15.11)		Regenerated KCu (9.67)	
%Yield	70.9		51.3		68.1		47.9	
Product distribution	Unsat.	Sat.	Unsat.	Sat.	Unsat.	Sat.	Unsat.	Sat.
C1	-	-	-	-	-	-	-	-
C2	-	-	-	-	-	-	-	-
C3	0.1	-	-	-	-	-	-	-
C4	-	-	-	-	-	-	-	-
C5	-	-	-	-	-	-	-	-
C6	0.3	0.1	-	-	-	-	-	-
C7	0.1	0.1	-	-	-	-	-	-
C8	0.4	0.3	-	-	-	-	-	-
C9	0.9	0.3	0.5	0.3	0.1	0.1	-	-
C10	0.7	0.3	0.6	0.2	0.2	0.1	0.1	0.1
C11	1.2	0.5	0.7	0.5	0.3	0.2	0.2	0.1
C12	2.3	0.9	0.9	0.4	0.3	0.3	0.2	0.3
C13	3.4	1.7	1.9	1.7	0.4	0.4	0.6	0.5
C14	4.2	6.6	6.5	2.2	1.7	3.3	8.8	3.3
C15	26.0	16.8	21.0	6.3	16.2	24.9	7.4	15.6
C16	1.1	0.3	0.6	0.2	0.4	0.3	0.6	0.3
C16 alcohol	0.6		0.5		2.6		0.3	
C16 aldehyde	1.0		1.5		15.8		1.9	
C17 ketone	0.5		4.8		0.5		7.2	

It can be seen that the amount of palmitic acid adsorbed on regenerated KCo (10.84%) and regenerated KCu (9.67%) is less than that on the fresh catalysts. The liquid product yields are also reduced after regeneration. The PXRD patterns of

regenerated catalysts (**Figure 4.25**) show that the layered structure of lepidocrocite titanate is partially collapsed to the mixed metal oxide phase, resulting in the lower crystallinity. Accordingly, the peak intensity at $2\theta \approx 11$ degree (i.e., the d_{020} which is the repeating distance of the layers along the *b*-axis) of KCo is greatly reduced. Meanwhile, the layered structure of KCu is almost completely lost. Instead, diffraction peaks due to TiO_2 anatase, CuO and Cu metal can be observed. Therefore, the adsorption of palmitic acid into interlayer space would be limited. As the crystal structure is lost during regeneration, a decrease in the active site would be expected. Hence, the liquid hydrocarbon yields are decreased.

The product distributions from the deoxygenation of palmitic acid over regenerated catalysts are similar to that from the fresh catalysts. However, the yield of C17 ketone and C14 unsaturated hydrocarbons (the parallel products from cracking C31 ketone) is obtained. This result suggests that anatase phase, formed after regeneration (as seen in the PXRD pattern), can promote the ketonization as evidenced by a higher yield of cracking product of C31-ketone.

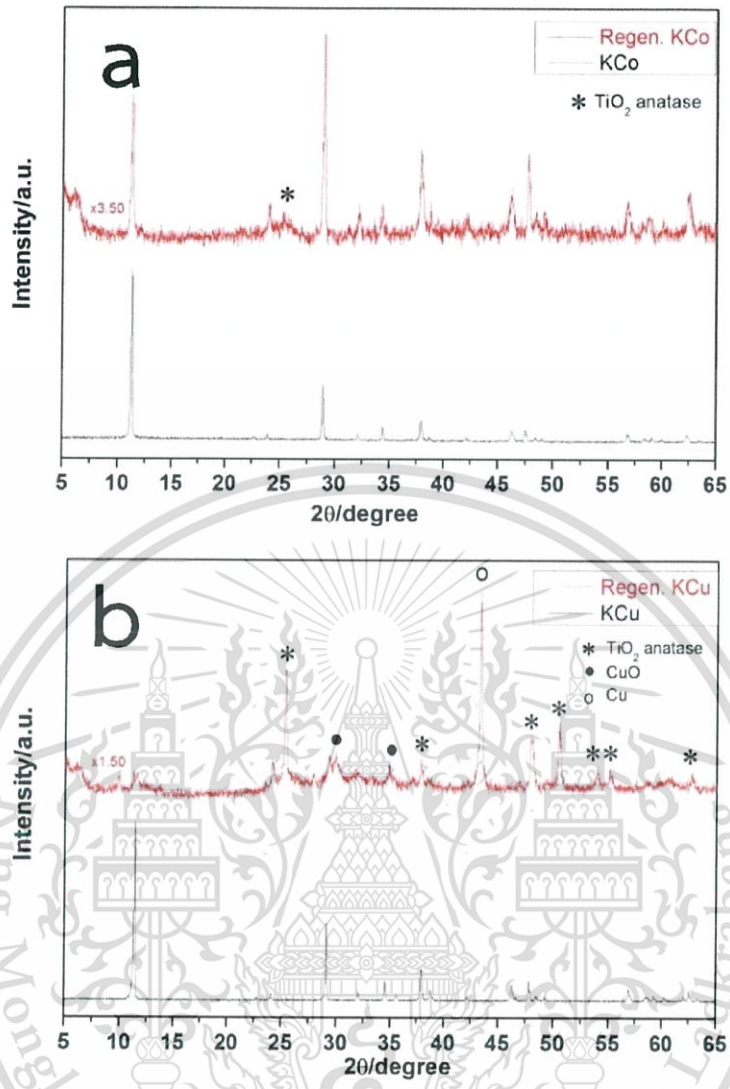

Figure 4.25 PXRD patterns of "as made" lepidocrocite titanate (bottom) vs. regenerated lepidocrocite titanate (top) after the reaction at 350 °C for 1 h: (a) KCo and (b) KCu. The patterns are rescaled such that the peaks with the highest intensity are of similar intensity. (The impurity peaks were marked with *, ● and o.)

CHAPTER 5

CONCLUSIONS AND SUGGESTIONS

5.1 Conclusions

Lepidocrocite titanates with various compositions, including $K_{0.8}Li_{0.27}Ti_{1.73}O_4$, $K_{0.8}Fe_{0.8}Ti_{1.2}O_4$, $K_{0.8}M_{0.4}Ti_{1.6}O_4$ (M = Mg^{2+}, Co^{2+}, Ni^{2+}, Cu^{2+} and Zn^{2+}), $K_{0.8}Fe_{0.7}Mn_{0.1}Ti_{1.2}O_4$, $K_{0.8}Fe_{0.4}Mn_{0.4}Ti_{1.2}O_4$, $K_{0.8}Cu_{0.2}Ni_{0.2}Ti_{1.6}O_4$ and $K_{0.8}Cu_{0.2}Zn_{0.2}Ti_{1.6}O_4$, were prepared by the conventional solid state synthesis. The lepidocrocite titanates possessed high crystallinity except $K_{0.9}Mg_{0.45}Ti_{1.55}O_4$ which was shown to have relatively low crystallinity. The crystallite size of the particles was found to be 1-7 μm. The presence of these micron-size crystals is in agreement with the low specific surface area obtained (< 6 m^2/g). The basicity of lepidocrocite titanates is ranked by the amount of negative charges at oxygen atoms (calculated using Sanderson's electronegativity value) in the order: KLi > KMg > KCo > KNi > KCu > KCuNi > KCuZn > KZn > $KFe_{0.4}Mn_{0.4}$ > $KFe_{0.7}Mn_{0.1}$ > KFe. The reduction of incorporated transition metal in lepidocrocite titanated structure (investigated by H_2 TPR) suggests the possible formation of oxygen vacancy sites. It can be seen that the reduction of $K_{0.8}Cu_{0.4}Ti_{1.6}O_4$, $K_{0.8}Ni_{0.4}Ti_{1.6}O_4$ and $K_{0.8}Fe_{0.8}Ti_{1.2}O_4$ is more facile than that of $K_{0.8}Co_{0.4}Ti_{1.6}O_4$ (with high reduction temperature) and $K_{0.8}Zn_{0.4}Ti_{1.6}O_4$ (with very small H_2 consumption).

The liquid phase adsorption of palmitic acid over KZn is as much as 37% by mass. The accompanying expansion of the interlayer space by ~0.1 nm was detected by PXRD and TEM. From PXRD and FTIR results, it can be inferred that the intercalation of palmitic acid into the interlayer region occurs as potassium palmitate.

The intercalation compound of palmitic acid and lepidocrocite titanate catalyst was prepared as a substrate for testing the catalytic deoxygenation activity. The amount of palmitic acid intercalated in several lepidocrocite titanate catalysts is increased when the crystallite size is decreased.

The deoxygenation of palmitic acid over $K_{0.8}Zn_{0.4}Ti_{1.6}O_4$ to produce long chain hydrocarbons was carried out in the semi-batch reactor. Palmitic acid can be decarboxylated and decarbonylated to C15 hydrocarbons. Gas products consisted of carbon dioxide and carbon monoxide are also detected. In addition, the overall reaction pathway including the cracking of C31 ketone to C-17 ketone and C-14 long chain hydrocarbons, the deacetylation of palmitic acid to C-14 long chain hydrocarbons, the non-catalytic reduction of palmitic acid to C16 aldehyde, C16 alcohol and C16 long chain hydrocarbon, and the cracking of these compounds to smaller hydrocarbon can be deduced. The study on reaction temperature shows that the liquid product yields and the decarboxylation are largely promoted by increasing temperature.

The deoxygenation of palmitic acid over lepidocrocite titanate catalyst with various compositions has demonstrated a linear relationship between the yields of liquid hydrocarbon products and the basicity of catalysts. The lepidocrocite titanates containing alkaline Li and alkaline earth Mg in the sheets ($K_{0.8}Li_{0.27}Ti_{1.73}O_4$ and $K_{0.8}Mg_{0.4}Ti_{1.6}O_4$) show a relatively high conversion than other lepidocrocite titanate containing transition metals in the layers and are selective to the ketonization of palmitic acid to form C31 ketone. The C31 ketone produced could be subsequently cracked to C14 unsaturated hydrocarbons and C17 ketone. For lepidocrocite titanates incorporating the transition metals, KCu and KZn are selective for the decarboxylation of palmitic acid to C15 saturated hydrocarbons, while KFe, KCo and KNi facilitates the decabonylation of palmitic acid to C15 unsaturated hydrocarbon. This is presumably because Fe, Co and Ni possess strong interaction with CO. Moreover, the high of C16 aldehyde from non-catalytic reaction of palmitic acid over oxygen vacancy site is observed in the order of KCu (15.8) > KFe (13.4) > KNi (3.6) >KCo (1.0) > KZn (0.1) which is parallel to the reducibility of the catalyst.

For lepidocrocite titanate where Ti was simultaneously substituted by two types of cations, $K_{0.8}Fe_{0.7}Mn_{0.1}Ti_{1.2}O_4$ and $K_{0.8}Fe_{0.4}Mn_{0.4}Ti_{1.2}O_4$ give the increased liquid

product yields when the basicity increased. Also, over these two compositions the ketonization of C16 aldehyde and palmitic acid to form C31 ketone increased with the increase in the Mn content. The liquid product yields from the deoxygenation of palmitic acid over $KCu_{0.2}Ni_{0.2}$ and $KCu_{0.2}Zn_{0.2}$ are not increased significantly. However, the decarboxylation of palmitic acid to C15 saturated hydrocarbon is promoted. This result implies that the activity of Cu is dominating over Ni when the two metals are co-incorporated, and reduction activity of Cu is suppressed when Zn is incorporated.

The amount of palmitic acid adsorbed on regenerated KCo (10.84%) and regenerated KCu (9.67%) is less than that on the fresh catalysts. This is because the layered structure of regenerated catalysts is greatly diminished. The liquid product yields are also reduced after regeneration as the crystal structure and active site is partially destroyed during regeneration. The product distributions from the deoxygenation of palmitic acid over regenerated catalysts are similar to that from the fresh catalysts. However, the yields of cracking products from C31 ketone were obtained. This result suggests that anatase phase, formed after regeneration, can promote the ketonization as evidenced by a higher yield of cracking products from C31 ketone.

5.2 Suggestions

1. The catalyst incorporating two metals with different valency (i.e., M^{2+} and M^{3+}) should be investigated, in order to further verify the role of basicity on the yield and selectivity of long chain hydrocarbon.

2. The lepidocrocited titanate should be synthesized using ball-mill or sol-gel technique for incresed surface area and reduced crystalline size, in order to increasing the amount of intercalated palmitic acid.

3. The deoxygenation of palmitic acid over lepidocrocite titanates under hydrogen atmosphere could be performed for the production of gasoline. The

unsaturated hydrocarbon products could be hydrogenated to saturated hydrocarbons.

4. The reduction of lepidocrocite titanates catalyst prior to the catalytic activity testing could be performed to generate a higher concentration of oxygen vacancy sites. This action might promote the ketonization or reduction of palmitic acid to synthetic lubricant oil. Also, the physical properties of the coupling products should be investigated compared to conventional lubricant oils.

References

[1] Zhang, A. Ma, Q. Wang, K. Liu, X. Shuler, P. and Tang, Y. 2006. "Naphthenic acid removal from crude oil through catalytic decarboxylation on magnesium oxide." *Applied Catalysis A: General.* 303(1): 103-109.

[2] Bo-Qing, X. Hao-Peng, W. Song-Hai, C. and Yu, L. 2007. "Sustainable production of acrolein: Gas-phase dehydration of glycerol over Nb_2O_5 catalyst." *Journal of Catalysis.* 250(2): 342-349.

[3] Felizardo, P. and Correia, M. J. N. 2005. "Production of biodiesel from waste frying oils." *Waste Management.* 26(5): 487-494.

[4] Aida, T. M. Aizawa, Y. Iida, T. Inomata, H. and Watanabe, M. 2007. "Acrolein Synthesis from Glycerol in Hot-Com- pressed Water." *Bioresource Technology.* 98(6): 1285-1290.

[5] Snåre, M. Kubickova, I. Mäki-Arvela, P. Chichova, D. Eränen, K. and Murzin, D. Y. 2008. "Catalytic deoxygenation of unsaturated renewable feedstocks for production of diesel fuel hydrocarbons." *Fuel.* 87(6): 933-945.

[6] Demirbas, A. 2011. "Waste management, waste resource facilities and waste conversion processes." *Energy Conversion and Management.* 52(1): 1280-1287.

[7] Taweesin, S. 2010. "Linear Long Chain Hydrocarbon From Deoxygenation Of Palmitic Acid Over Metal Oxide." Petrochemical and hydrocarbon master degree, Faculty of science, KMITL.

[8] Limsakul, K. Juntachairot, S. and Sangsan, S. 2013. "Deoxygenation of palmitic acid over lepidocrocite titanate catalysts." BSc. Dissertation, Industrial chemistry, Faculty of Science, KMITL.

[9] Maria, R.J. Carmen, F.M. Abraham, C. Lourdes R. and Angel, P. 2009. "Influence of fatty acid omposition of raw materials on biodiesel properties." *Bioresource Technology.* 100: 261-268.

[10] Elmhurst college. "Fatty Acids." [Online]. Available : http://www.elmhurst.edu/~chm/vchembook/551fattyacida.html.

[11] Baca, A. "Animal fat as fuel alternative." [Online]. Available : http://www.polimerieuropa.com/200page.lasso.html.2001

[12] Tamime, A. Y. 2009. "Dairy Fats and Relateed Products." Blackwell Publishing.

[13] Jerry, L. 2004. "Fats and Fatty Acids" The Gale Group, Inc.

[14] Maria, R. J. Carmen, F. M. Abraham, C. Lourdes, R. and Angel, P. 2009. "Influence of fatty acid omposition of raw materials on biodiesel properties." *Bioresource Technology*. 100: 261-268.

[15] Sarquis. "Fats and Fatty Acids." [Online]. Available : http://www.chemistryexplained.com/Di-Fa/Fats-and-Fatty-Acids.html.2010

[16] Beare-Rogers, J. Dieffenbacher, A. and Holm, J. V. 2001. "Lexicon of lipid nutrition (IUPAC Technical Report." *Pure applied chemistry*. 73: 685-744.

[17] "Palmitic acid" [Online]. Available : http://en.wikipedia.org/wiki/Palmitic_acid

[18] David, J. A. Both, S. Christoph, R. Fieg, G. Steinberner, U. and Westfechtel, A. 2006. "Fatty Acids." Ullmann's Encyclopedia of Industrial Chemistry.

[19] "Trans-Esterification" [online]. Available : www.organic-chemistry.org/namedreactions/fischer-esterification.shtm

[20] Liu, Y. Lotero, E. and Goodwin, J. J. G. 2006. "Effect of carbon chain length on esterification of carboxylic acids with methanol using acid catalysis." *Journal of Catalysis*. 243: 221-228.

[21] Yadav, G. D. and Thathagar, M. B. 2002. "Esterification of maleic acid with ethanol over cation exchange resin catalysts." *Reactive and Functional Polymers*. 52: 99-110.

[22] Marchetti, J. M. Miguel, V. U. and Errazu, A. F. 2007. "Heterogeneous esterification of oil with high amount of free fatty acids." *Fuel*. 86: 906-910.

[23] "Deoxygenation" [Online]. Available : http://en.wikipedia.org/wiki/Deoxygenation

[24] Mki-Arvela, P. Snare, M. Ernen, K. Myllyoja J. and Murzin, D. Y. 2008. "Continuous decarboxylation of lauric acid over Pd/C catalyst." *Fuel*. 87: 3543-3549.

[25] Pham, T. N. Sooknoi, T. Crossley, S. P. and Resasco, D. E. 2013. "Ketonization of Carboxylic Acids: Mechanisms, Catalysts, and Implications for Biomass Conversion." *ACS Catalysis*. 11(3): 2456-2473.

[26] Hattori, H. 2010. "Solid base catalysts: fundamentals and their applications in organic reactions." *Applied Catalysis A: General*. 504: 103-109.

[27] Schuchardta, U. Serchelia, R. and Vargas, R. M. 1997. "Transesterification of Vegetable Oils: a Review." [online]. Available : http://www.academia.edu/3402804/Transesterification_of_vegetable_oils_a_revie

[28] Cantrell, D. G. Gillie, L. J. Lee, A. F. and Wilson, K. 2005. "Structure-reactivity correlations in Mg/Al hydrotalcite catalysts for biodiesel synthesis." *Applied Catalysis A: General*. 287: 183–190.

[29] Sasaki, T. Kooli, F. Iida, M. Michiue, Y. Takenouchi, S. Yajima, Y. Izumi, F. Chakoumakos, B. C. and Watanabe, M. 1998. "A Mixed Alkali Metal Titanate with the Lepidocrocite-like Layered Structure. Preparation, Crystal Structure, Protonic Form, and Acid-Base Intercalation Properties." *Chemistry of Materials*. 10: 4123-4128.

[30] Song, H. Sjastad, A. O. Vistad, B. Gao, T. and Norby, P. 2009. "Preparation of Nb-substituted titanates by a novel sol-gel assisted solid state reaction." *Inorganic Chemistry*. 48: 6952-6959.

[31] Sasaki, T. Kooli, F. Iida, M. Michiue, Takenouchi, Y. S. Yajima, Y. Izumi, F. Chakoumakos, B. C. and Watanabe, M. 1998. "A Mixed Alkali Metal Titanate with the Lepidocrocite-like Layered Structure. Preparation, Crystal Structure, Protonic Form, and Acid-Base Intercalation Properties." *Chemistry of Materials*. 10: 4123-4128.

[32] Maluangnont, T. Matsuba, K. Geng, F. Ma, R. Yamauchi, Y. and Sasaki, T. 2013. "Osmotic Swelling of Layered Compounds as a Route to Producing High-Quality Two-Dimensional Materials. A Comparative Study of Tetramethylammonium versus Tetrabutylammonium Cation in a Lepidocrocite-type Titanate." *Chemistry of Materials*. 25: 31-37.

[33] Groult, D. Mercey, C. and Raveau, B. 1980. "Nouveaux oxydes á structure en feuillets: Les titanates de potassium non-stoechiométriques $K_x(M_yTi_{2-y})O_4$." *Journal of Solid State Chemistry*. 32: 289-296.

[34] Gao, T. Fjellvag, H. and Norby, P. 2009. "Defect chemistry of a Zinc-Doped Lepidocrocite Titanate $Cs_xTi_{2-x/2}Zn_{x/2}O_4$ (x=0.7) and its protonic Form." *Chemistry of Materials*. 21: 3503-3513.

[35] Navarro, R. Acevedo, A. Soto, M. 2008. "Synthesis and characterization of Lepidocrocite and its potential applications in the adsorption of pollutant species." *Journal of Physics*. 134: 12 -23.

[36] Leo´n, M. Dı´az, E. Bennici, S. Vega, A. Ordo´n˜ez, S. and Auroux, A. 2010. "Adsorption of CO_2 on Hydrotalcite-Derived Mixed Oxides: Sorption Mechanismsand Consequences for Adsorption Irreversibility." *Engineering Chemistry Research*. 49: 3663–3671.

[37] Speight, G. J. "The Chemistry and Technology of Petroleum." 3rd Ed., New York: Marcel Dekker.

[38] Olah, A. G. and Molnar, A. 1995. "Hydrocarbon Chemistry." New York: John Wiley & Son, Inc.

[39] Nelson, L. W. 1985. "Petroleum Refinery Engineering." 4th Ed., New York: Megraw-Hill book company.

[40] Sheehan, J. J. Dufield, J. A. Codon, R. B. and Camobreco, V. J. 1996. "Life–cycle assessment of biodieel versus petroleum diesel fuel."

[41] Paivi, M. A. Iva, K. Mathias, S. Kari, E. and Murzin, D. Y. 2007. "Catalytic Deoxygenation of Fatty Acids and Their Derivatives." *Energy & Fuels*. 21: 30-41.

[42] Snare, M. Kubickova, I. Maki-Arvela, P. Chichova, D. Eranen, K. and Murzin. D. Y. 2008. "Catalytic deoxygenation of unsaturated renewable feedstocks for production of diesel fuel hydrocarbons." *Fuel*. 87: 933-945.

[43] Simakova, I. Simakova, O. Maki-Arvela, P. Simakov, A. Estrada, M. and Murzin, D. Y. 2009. "Deoxygenation of palmitic and stearic acid over supported Pd catalysts: Effect of metal dispersion." *Applied Catalysis A: General*. 355: 100-128.

[44] Jeong-Geol, N. Bo Eun, Y. Ju Nam, K. Kwang Bok, Y. Sung-Youl, P. Jong-Ho, P. Jong-Nam, K. and Chang Hyun, K. 2010. "Hydrocarbon production from decarboxylation of fatty acid without hydrogen." *Catalysis Today*. 156: 44-48.

[45] Masaru, W. Toru, I. and Hiroshi, I. 2006. "Decomposition of a long chain saturated fatty acid with some additives in hot compressed water." *Energy Conversion and Management*. 47: 3344-3350.

[46] Dararat, C. Kulrat, T. and Soontontaweesub, S. 2013. "Deoxygenation of palmitic acid over cerium-metal mixed oxide." BSc. Dissertation, Industrial chemistry, Faculty of Science, KMITL.

[47] Asikin-Mijana, N. Lee, H. V. Juana, J. C. Noorsaadah, A. R. Abdulkareem-Alsultanc, G. Arumugam, M. and Taufiq-Yap, Y. H. 2016. "Waste clamshell-derived CaO supported Co and W catalysts forrenewable fuels production via cracking-deoxygenation of triolein." *Journal of Analytical and Applied Pyrolysis*. (Article in press).

[48] Johannesson, B. 2000. "Verification of the BET-theory by Experimental Investigations on the Heat of Adsorption." Lund Institute of Technology Division of Building Materials.

[49] Shannon, R. D. 1976. "Revised effective ionic radii and systematic studies of interatomic distances in halides and chalcogenides." *Acta Crystallographica Section A*. 32: 751–767.

[50] Haire, R. G. and Baybarz, R. D. 1973. "Identification and Analysis of Einsteinium Sesquioxide by Electron Diffraction." *Journal of Inorganic and Nuclear Chemistry*. 35(2): 489–496.

[51] Peter, L. Smith, F. and Barry, C. 2010. "Ionic radii for Group 1 and Group 2 halide, hydride, fluoride, oxide, sulfide, selenide and telluride crystals." *Dalton Transactions*. 39(33): 7786–7791.

[52] Isahak, W. Ramli, Z. Ismali, M. Ismali, K. Yusop, R. M. Hisham, M. and Armo, M. 2013. "Adsorption–desorption of CO_2 on different type of copper oxides surfaces: Physical and chemical attractions studies." *Journal of CO_2 Utilization*. 2: 8–15.

[53] Li, J. Lu, G. Wu, G. Mao, D. Guo, Y. Wang, Y. and Guo, Y. 2013. "The role of iron oxide in the highly effective Fe-modified Co_3O_4 catalyst for low-temperature CO oxidation." *ASC Advances*. 3: 12409-12416.

[54] Maluangnont, T. Arsa, P. Limsakul, K. Juntarachairot, S. Sangsan, S. Gotoh, K. and Sooknoi, T. 2016. "Surface and interlayer base-characters in lepidocrocite titanate: The adsorption and intercalation of fatty acid." *Journal of Solid State Chemistry*. 238: 175-181.

[55] Deshmanea, V. G. Owena, S. L. Abrokwah, R. Y. and Kuilaa, D. 2015. "Mesoporous nanocrystalline TiO_2 supported metal (Cu, Co, Ni, Pd, Zn and Sn) catalysts: Effect of metal-support interactions on steam reforming of methanol." *Journal of Molecular Catalysis A: Chemical*. 408: 202–213.

[56] Luo, M. Fang, P. He, M. and Xie, Y. 2005. "In situ XRD, Raman, and TPR studies of CuO/Al_2O_3 catalysts for CO oxidation." *Journal of Molecular Catalysis A: Chemical*. 239: 243–248.

[57] Bzdon, S. ralski, J. Maniukiewicz, W. Perkowski, J. Rogowski, J. and Nicze, M. S. 2012. "Radiation-induced synthesis of Fe-doped TiO_2: Characterizationand catalytic properties." *Radiation Physics and Chemistry*. 81: 322–330.

[58] Arizaga, G. G. C. Mangrich, A. S. Costa Gardolinski, J. E. F. and Wypych, F. 2008. "Chemical modification of zinc hydroxide nitrate and Zn–Al-layered double hydroxide with dicarboxylic acids." *Journal of Colloid and Interface Science*. 320: 168-176.

[59] Maluangnont, T. Bui, G. T. Huntington, B. A. and Lerner, M. M. 2011. "Preparation of a homologous series of graphite alkyl amine intercalation compounds including an unusual parallel bilayer intercalate arrangement." *Chemistry of Materials*. 23(5): 1091-1095.

[60] Witsuthammakul, A. and Sooknoi, T. 2016. "Selective Hydrodeoxygenation of Bio-Oil Derived Products: Acetic acid to propylene over hybrid CeO_2-Cu/zeolite catalysts." *Catalysis Science & Technology*. 6: 1737-1745.

[61] Pham, T. N. Sooknoi, T. Crossley, S. and Resasco, D. E. 2013. "Ketonization of Carboxylic Acids: Mechanisms, Catalysts, and Applications in Bio-oil Upgrading." *ACS Catalysis*. 3: 2456–2473.

[62] Pham, T. N. Shi, D. Sooknoi, T. and Resasco, D. E. 2012. "Aqueous-phase ketonization of acetic acid over Ru/TiO_2/carbon catalysts." *Journal of Catalysis*. 295: 169–178.

[63] Hermida, L. Abdullah, A. Z. and Mohamed, A. R. 2015. "Deoxygenation of fatty acid to produce diesel-like hydrocarbons: A review of process conditions, reaction kinetics and mechanism." *Renewable and Sustainable Energy Reviews*. 42: 1223–1233.

[64] "Chemical kinetics" [online]. Available : https://en.wikipedia.org/wiki/Chemical_kinetics

[65] Pandey, R. K. Waters, K. Nigam, S. He, H. Pingale, S. S. Pandey, A. C. and Pandey, R. 2014. "A theoretical study of structural and electronic properties of alkaline-earth fluoride clusters." *Computational and Theoretical Chemistry*. 1043: 24–30.

[66] Fielicke, A. Gruene, P. Meije, G. and Rayner, D. M. 2009. "The adsorption of CO on transition metal clusters: A case study of cluster surface chemistry." *Surface Science*. 603: 1427–1433.

[67] Glinski, M. Zalewski, G. Burnoa, E. and Jerzak, A. 2014. "Catalytic ketonization over metal oxide catalysts. XIII. Comparative measurements of activity of oxides of 32 chemical elements in ketonization of propanoic acid." *Applied Catalysis A: General*. 470: 278–284.

[68] Ambursa, M. M. Ali, T. H. Voon, L. Sudarsanam, H. P. Bhargava, S. K. and Hamid, S. B. A. 2016. "Hydrodeoxygenation of dibenzofuran to bicyclic hydrocarbons using bimetallic Cu–Ni catalysts supported on metal oxides." Fuel. 108: 767-776.

[69] Sanderson, R. T. 1976. "Chemical bond and bond energy." Department of chemistry, Arizona state university.

APPENDICES

APPENDIX A

POWDER X-RAY DIFFRACTION

Table A1 Lattice parameter and charge density of catalysts

Catalysts	*a* (nm)		*b* (nm)		*c* (nm)		Charge density (nm^{-2})
	Reported*	This work	Reported*	This work	Reported*	This work	
KZn	0.3806(4)	0.380(6)	1.569(2)	1.5(6)	0.2985(0)	0.298(5)	3.52
KCu	0.3805(4)	0.38(0)	1.563(0)	1.5(4)	0.2985(7)	0.29(8)	3.52
KNi	0.3836(1)	0.37(6)	1.555(9)	1.5(5)	0.2964(8)	0.29(5)	3.59
KCo	-	0.38(1)	-	1.5(7)	-	0.29(7)	3.52
KFe	0.3811(8)	0.37(7)	1.573(2)	1.5(2)	0.2971(5)	0.29(6)	3.56
KCuNi	-	0.37(5)	-	1.5(1)	-	0.29(5)	3.61
KCuZn	-	0.37(6)	-	1.5(0)	-	0.29(6)	3.59
$KFe_{0.7}Mn_{0.1}$	-	0.37(7)	-	1.5(1)	-	0.29(5)	3.58
$KFe_{0.4}Mn_{0.4}$	-	0.37(1)	-	1.5(2)	-	0.29(1)	3.69
KLi	0.38327(2)	0.37(6)	1.5532(1)	1.5(0)	0.29727(3)	0.29(4)	3.60
KMg	0.3820(7)	0.37(4)	1.564(1)	1.5(4)	0.2981(4)	0.29(3)	3.63

*From literature [36-38].

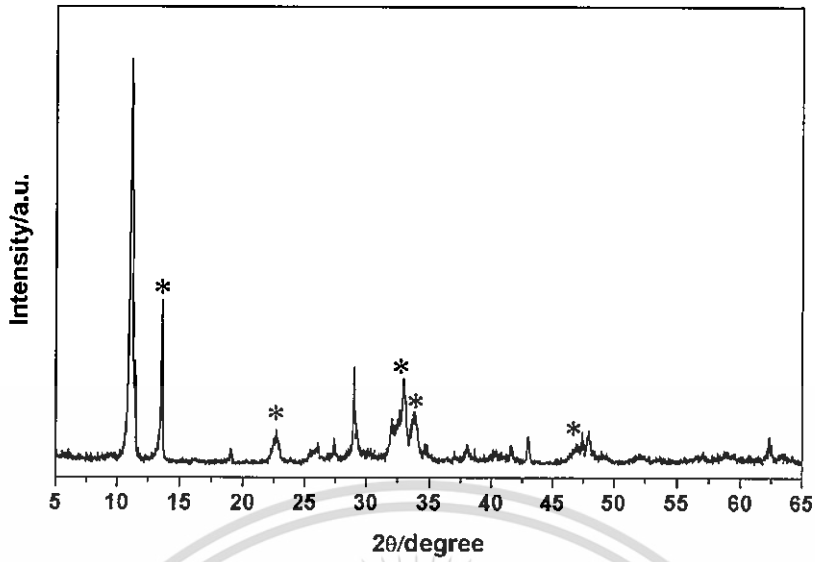

Figure A1 The PXRD pattern of reheated $K_{0.8}Mg_{0.4}Ti_{1.6}O_4$ "KMg". The KMg was first made following the reported method in Chapter 3 with low crystallinity (**Figure 4.3**). Then, it was heated at 800 °C for 20 h, resulting in KMg with an increased intensity of the impurity peaks. (The impurity peaks were marked with *.)

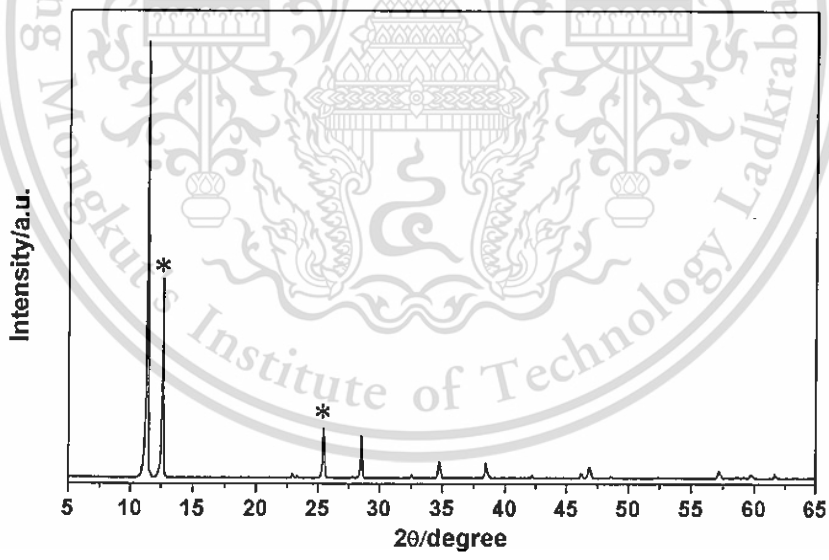

Figure A2 The PXRD pattern of $K_{0.8}Mn_{0.8}Ti_{1.2}O_4$ (the impurity peaks were marked with (*).

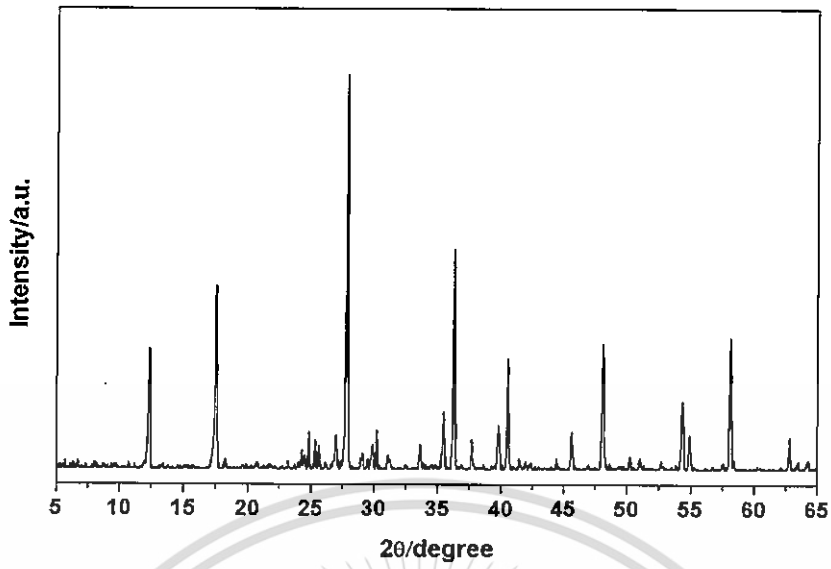

Figure A3 The PXRD pattern of the solid obtained after heating the mixture of K_2CO_3, Cr_2O_3 and TiO_2 (according to the stoichiometry $K_{0.8}Cr_{0.8}Ti_{1.2}O_4$) at 900 °C for 20 h. Lepidocrocite titanate was not formed. The phase of this solid was not examined further.

APPENDIX B

NITROGEN GAS ADSORPTION ANALYSIS

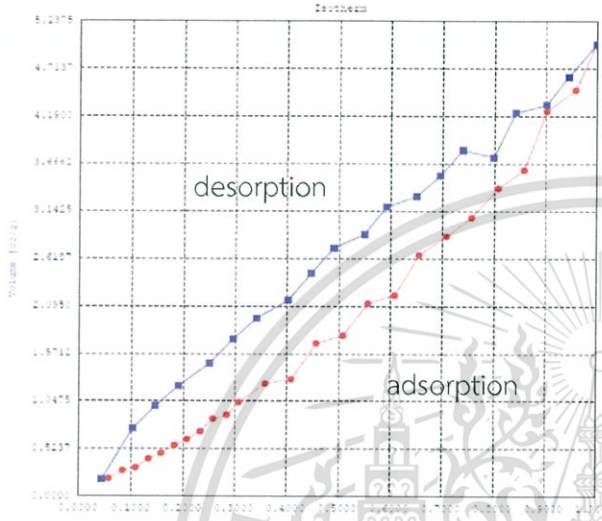

(a)

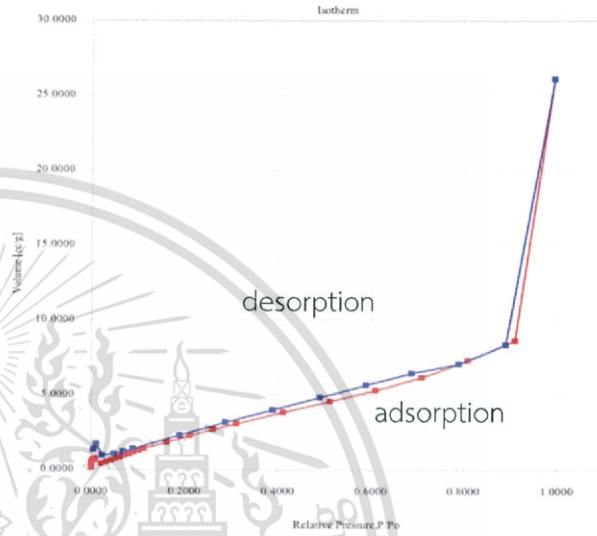

(b)

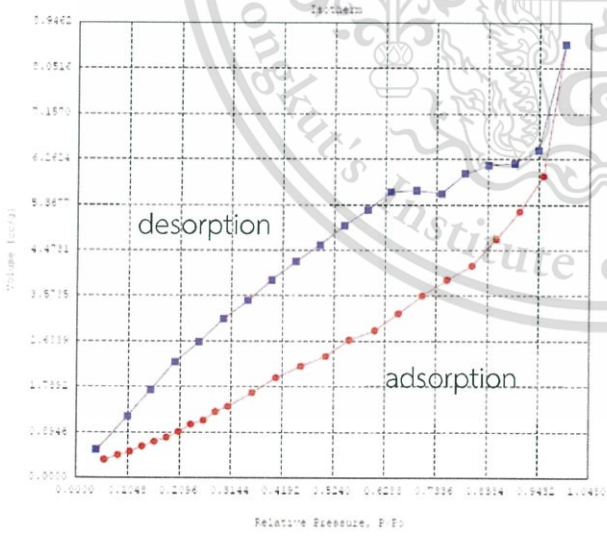

(c)

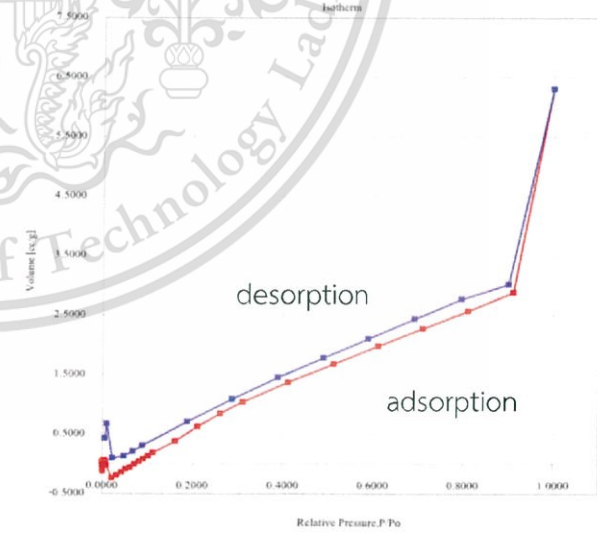

(d)

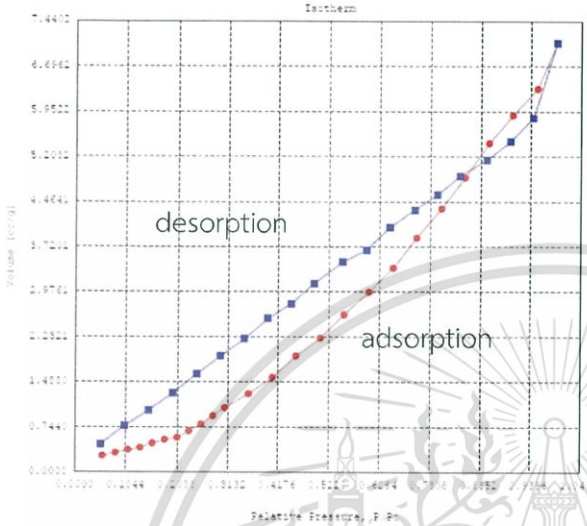

(e)

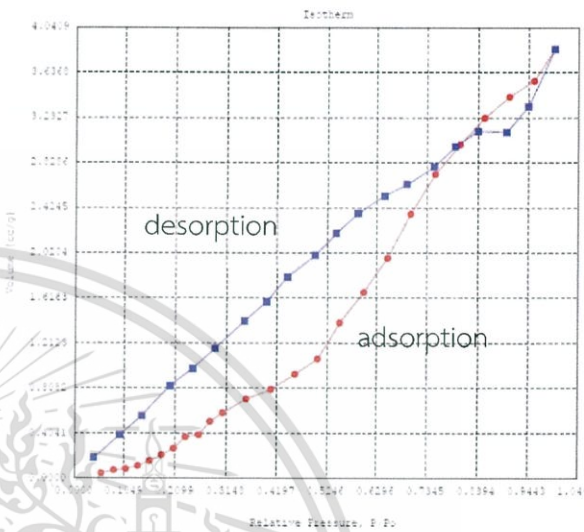

(f)

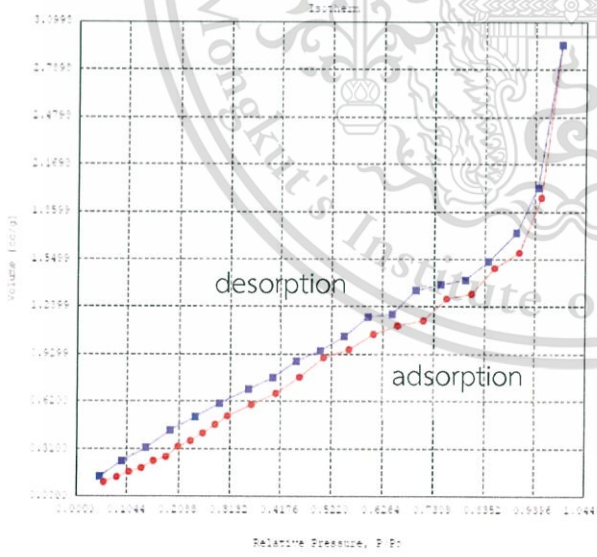

(g)

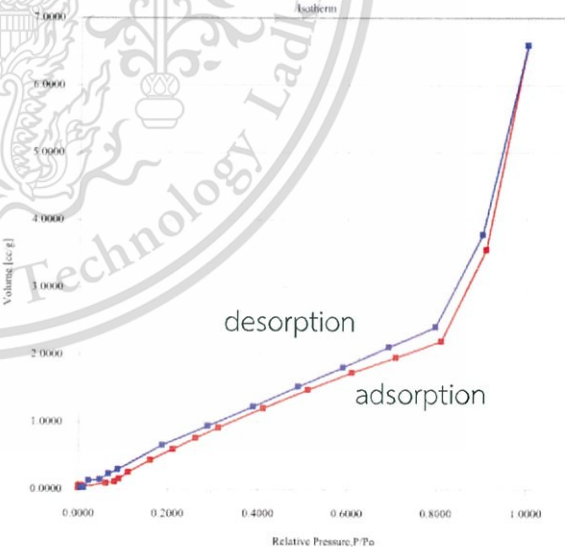

(h)

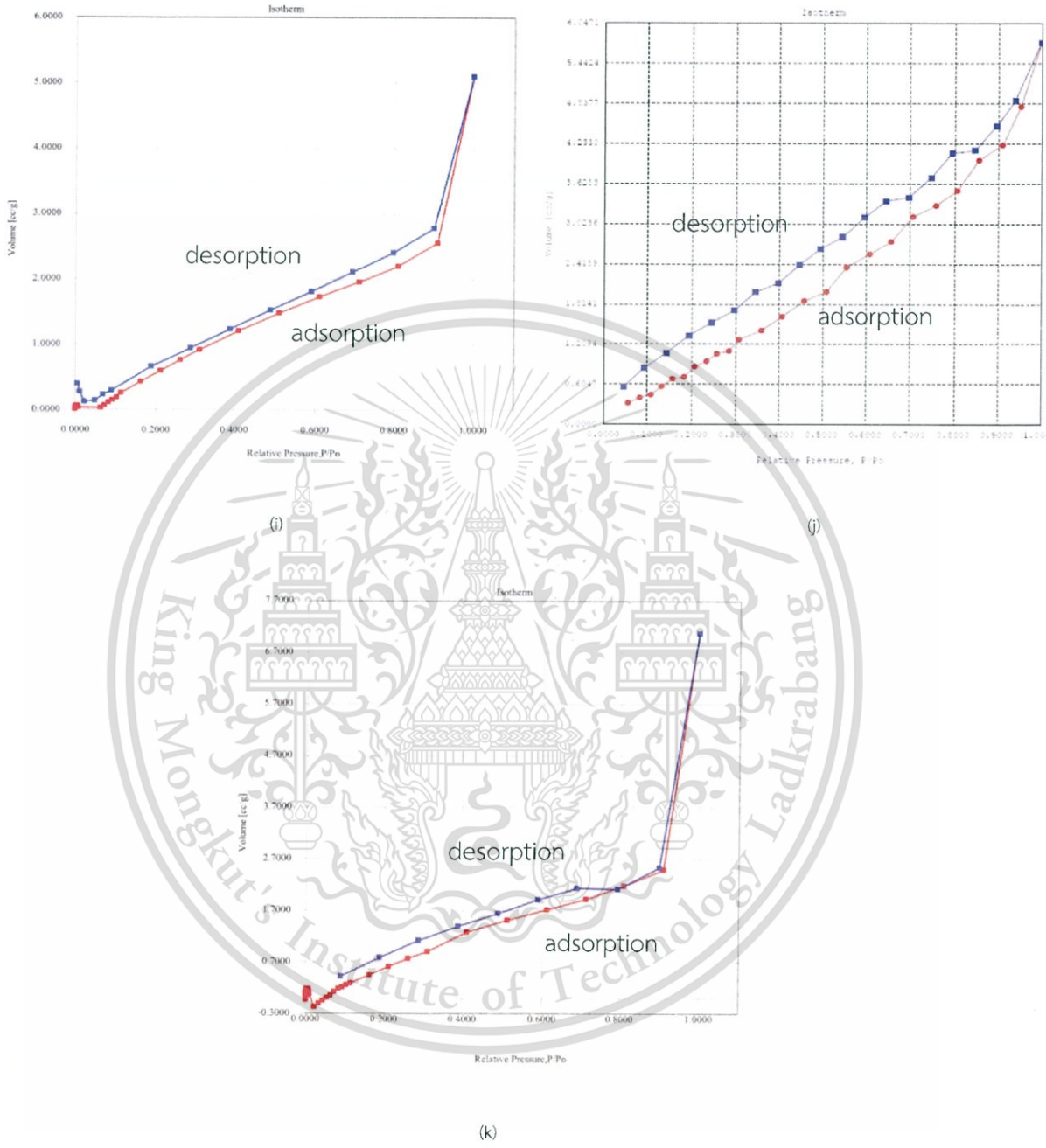

Figure B1: Adsorption-Desorption isotherm of (a) $K_{0.8}Li_{0.27}Ti_{1736}O_4$, (b) $K_{0.8}Mg_{0.4}Ti_{1.6}O_4$, (c) $K_{0.8}Fe_{0.8}Ti_{1.2}O_4$, (d) $K_{0.8}Co_{0.4}Ti_{1.6}O_4$, (e) $K_{0.8}Ni_{0.4}Ti_{1.6}O_4$, (f) $K_{0.8}Cu_{0.4}Ti_{1.6}O_4$, (g) $K_{0.8}Zn_{0.4}Ti_{1.6}O_4$, (h) $K_{0.8}Cu_{0.2}Ni_{0.2}Ti_{1.6}O_4$, (i) $K_{0.8}Cu_{0.2}Zn_{0.2}Ti_{1.6}O_4$, (j) $K_{0.8}Fe_{0.7}Mn_{0.1}Ti_{1.2}O_4$ and (k) $K_{0.8}Fe_{0.4}Mn_{0.4}Ti_{1.2}O_4$.

File name:	C:\QCdata*Å BET\58\5\580526_1.RAW				
Sample ID:	KLi	Description:	Ads 22 Pts Des 22 Pts BET 11 pts		
Comments:					
Operator:	NickK	Sample weight:	0.1647 g		
Analysis gas:	NITROGEN	X sect. area:	16.2 Å²/molec	Non-ideality:	6.50e-05
Adsbate (DRP):	Nitrogen	Bath Temp.:	77.25		
Outgas Temp:	300.0 °C	Outgas Time:	15.5 hrs	Analysis Time:	286.2 min
P/Po tolerance:	2	Equil. time:	3	End of run:	05/26/2015 15:44
Station #:	1	PC sw. version:	Pre-1.20		

Isotherm

P/Po	Volume [cc/g] STP
5.5751e-02	0.1978
9.2992e-02	0.2952
1.0854e-01	0.3130
1.9845e-01	0.4156
1.5506e-01	0.4760
1.9381e-01	0.5634
2.0509e-01	0.6295
2.2291e-01	0.7158
2.5778e-01	0.8536
2.8422e-01	0.8966
3.0755e-01	1.0377
3.5550e-01	1.2414
4.0571e-01	1.2919
4.5607e-01	1.6645
5.0542e-01	1.7730
5.5618e-01	2.1262
6.0530e-01	2.2155
6.5490e-01	2.6896
7.0770e-01	2.9642
7.5618e-01	3.3721
8.0754e-01	3.8247
8.5882e-01	3.9257
9.0200e-01	4.5484
9.5504e-01	4.4775
9.9941e-01	4.9881
9.4418e-01	4.6223
8.8096e-01	4.3144
8.2170e-01	4.2238
7.7220e-01	3.7386
7.0541e-01	3.8161
6.5481e-01	3.5511
6.4902e-01	3.0.82
5.9274e-01	3.1915
5.4550e-01	2.8872
4.9007e-01	2.7886
4.4648e-01	2.4620
4.0254e-01	2.1626
3.4048e-01	1.9698
2.9504e-01	1.7285
2.5061e-01	1.4652
2.0441e-01	1.2035
1.4858e-01	0.9851

Figure B2 Langmuir plot data on the isotherm of $K_{0.8}Li_{0.27}Ti_{1.73}O_4$

04/30/2016

Quantachrome Instruments
Quantachrome Autosorb Automated Gas Sorption System Report
Autosorb 1 for Windows 1.55

File name: C:\QCdata\PhysData\Naowarat\NWR_KMG 0 4.raw
Sample ID: Description:
Comments:
Operator: OUNSA Sample weight: 0.0339 g
Analysis gas: Nitrogen X sect. area: 16.2 A2/molec Non-ideality: 6.58e-05
Adsbate (DRP): Nitrogen Bath Temp.: 77.30
Outgas Temp: 150.0 C Outgas Time: 12.0 hrs Analysis Time: 360.2 min
P/Po tolerance: 3 Equil. time: 2 End of run: 03/16/2016 23:23
Station #: 1 PC sw. version: 1.55 TempComp: On

Isotherm

P/Po	Volume [cc/g] STP	P/Po	Volume [cc/g] STP	P/Po	Volume [cc/g] STP
1.2722e-05	0.1054	4.1690e-03	0.6805	5.1083e-01	4.5574
2.3465e-05	0.1314	5.0189e-03	0.6960	6.1080e-01	5.2907
3.7490e-05	0.1526	6.0656e-03	0.7092	7.1042e-01	6.1689
5.3758e-05	0.1697	7.1022e-03	0.7147	8.1013e-01	7.2826
7.1692e-05	0.1831	8.1575e-03	0.6922	9.0967e-01	8.6326
8.8748e-05	0.1932	9.2184e-03	0.6178	9.9389e-01	26.1022
1.0501e-04	0.2013	2.2295e-02	0.3832	8.8998e-01	8.3243
1.1912e-04	0.2070	3.2375e-02	0.4951	7.8975e-01	7.0627
1.3109e-04	0.2114	4.2379e-02	0.6107	6.8879e-01	6.4654
1.4511e-04	0.2160	5.2387e-02	0.7246	5.8935e-01	5.6619
2.2093e-04	0.2361	6.2423e-02	0.8368	4.8934e-01	4.8212
3.5741e-04	0.2547	7.2349e-02	0.9505	3.8930e-01	3.9875
5.2746e-04	0.2609	8.2340e-02	1.0623	2.8923e-01	3.1483
7.0355e-04	0.2562	9.2341e-02	1.1721	1.8929e-01	2.2907
8.9118e-04	0.2433	1.0240e-01	1.2839	8.9207e-02	1.4135
1.1022e-03	0.2228	1.1236e-01	1.3965	6.8903e-02	1.2013
1.1204e-03	0.2749	1.6192e-01	1.8264	4.8840e-02	1.0336
1.2380e-03	0.2844	2.1184e-01	2.2545	2.3263e-02	0.9442
1.0180e-03	0.5281	2.6186e-01	2.6671	9.8297e-03	1.7334
2.0187e-03	0.6026	3.1176e-01	3.0673	4.9637e-03	1.3215
3.0896e-03	0.6484	4.1109e-01	3.8301		

Figure B3 Langmuir plot data on the isotherm of $K_{0.8}Mg_{0.4}Ti_{1.6}O_4$

Date: 06/12/2014 Page 1

Quantachrome Corporation
Quantachrome Autosorb Automated Gas Sorption System Report
Autosorb for Windows® Version 1.19

Sample ID	LPC KFe				
Description	Ads 22 Pts Des 22 Pts BET 11 pts				
Comments					
Sample Weight	0.1746 g				
Adsorbate	NITROGEN	Outgas Temp	300.0 °C	Operator	Nick
Cross-Sec Area	16.2 Å²/molecule	Outgas Time	14.5 hrs	Analysis Time	278.7 min
NonIdeality	6.580E-05	P/Po Toler	2	End of Run	06/03/2014 13:00
Molecular Wt	28.0134 g/mol	Equil Time	2	File Name	570603_1.RAW
Station #	1	Bath Temp.	77.35		

Isotherm

P/Po	Volume (cc/g) STP
5.5754e-02	0.3567
8.3481e-02	0.4463
1.0859e-01	0.5133
1.3322e-01	0.6193
1.5839e-01	0.7134
1.8363e-01	0.7934
2.0814e-01	0.9054
2.3300e-01	1.0515
2.5863e-01	1.1293
2.8284e-01	1.2993
3.0822e-01	1.4024
3.5773e-01	1.6756
4.0626e-01	1.9676
4.5724e-01	2.1951
5.0829e-01	2.3914
5.5650e-01	2.7113
6.0838e-01	2.8986
6.5711e-01	3.2307
7.0589e-01	3.5630
7.5628e-01	3.8690
8.0718e-01	4.1649
8.5682e-01	4.6899
9.0477e-01	5.2294
9.5335e-01	5.9312
9.8807e-01	8.5202
9.4210e-01	6.4359
8.9327e-01	6.1685
8.4092e-01	6.1426
7.9186e-01	5.9756
7.4280e-01	5.5906
6.9291e-01	5.6478
6.4026e-01	5.6206
5.9301e-01	5.2654
5.4478e-01	4.9574
4.9505e-01	4.5780
4.4638e-01	4.2509
3.9615e-01	3.8869
3.4799e-01	3.4815
2.9782e-01	3.1249
2.4942e-01	2.6673
1.9967e-01	2.2781
1.5128e-01	1.7407
1.0241e-01	1.2115

Figure B4 Langmuir plot data on the isotherm of $K_{0.8}Fe_{0.8}Ti_{1.2}O_4$

04/30/2016

Quantachrome Instruments
Quantachrome Autosorb Automated Gas Sorption System Report
Autosorb 1 for Windows 1.55

File name: C:\QCdata\PhysData\Naowarat\NWR_KCO 0 4.raw
Sample ID: Description:
Comments:
Operator: OUNSA Sample weight: 0.0532 g
Analysis gas: Nitrogen X sect. area: 16.2 sq.A/molec Non-ideality: 6.58e-05
Adsbate (DRP): Nitrogen Bath Temp.: 77.30
Outgas Temp: 150.0 °C Outgas Time: 12.0 hrs Analysis Time: 379.6 min
P/Po tolerance: 3 Equil. time: 2 End of run: 03/16/2016 15:24
Station #: 1 PC sw. version: 1.55 TempComp: On

Isotherm

P/Po	Volume [cc/g] STP	P/Po	Volume [cc/g] STP	P/Po	Volume [cc/g] STP
5.1728e-05	0.0206	4.1874e-03	0.0596	5.1119e-01	1.6742
1.1071e-04	0.0152	5.2612e-03	0.0592	6.1099e-01	1.9857
1.4426e-04	0.0113	6.0408e-03	0.0554	7.1090e-01	2.2739
1.6142e-04	0.0089	7.0969e-03	0.0465	8.1078e-01	2.5697
1.7077e-04	0.0073	8.1654e-03	0.0220	9.1065e-01	2.8885
1.7283e-04	0.0064	9.2031e-03	-0.0314	9.9872e-01	6.3018
1.7532e-04	0.0055	2.2391e-02	-0.2437	9.0070e-01	3.0258
1.7523e-04	0.0048	3.2344e-02	-0.1927	7.9650e-01	2.7745
1.7669e-04	0.0040	4.2359e-02	-0.1418	6.9227e-01	2.4332
1.8623e-04	0.0024	5.2384e-02	-0.0909	5.8919e-01	2.1042
2.8801e-04	-0.0093	6.2406e-02	-0.0631	4.8917e-01	1.7820
4.3979e-04	-0.0276	7.2396e-02	-0.0110	3.8908e-01	1.4471
6.0888e-04	-0.0489	8.2382e-02	0.0437	2.8903e-01	1.0854
8.0392e-04	-0.0741	9.2419e-02	0.0823	1.8901e-01	0.7129
9.8624e-04	-0.0981	1.0239e-01	0.1295	8.9032e-02	0.3098
1.1839e-03	-0.1243	1.1237e-01	0.1872	6.8765e-02	0.2119
1.2312e-03	-0.1074	1.6194e-01	0.3821	4.8692e-02	0.1290
1.3370e-03	-0.1112	2.1176e-01	0.6257	2.3372e-02	0.0954
1.0154e-03	0.0430	2.6184e-01	0.8459	9.9306e-03	0.6672
2.0388e-03	0.0500	3.1184e-01	1.0392	5.0500e-03	0.4239
3.1175e-03	0.0546	4.1114e-01	1.3682		

Figure B5 Langmuir plot data on the isotherm of $K_{0.8}Co_{0.4}Ti_{1.6}O_4$

Quantachrome Corporation
Quantachrome Autosorb Automated Gas Sorption System Report
Autosorb for Windows® Version 1.19

Sample ID	LPC K0.8 Ni0.4 Ti1.6 O4				
Description	Ads 22 Pts Des 22 Pts BET 11 pts				
Comments					
Sample Weight	0.3101 g				
Adsorbate	NITROGEN	Outgas Temp	300.0 °C	Operator	Best
Cross-Sec Area	16.2 Å²/molecule	Outgas Time	23.1 hrs	Analysis Time	290.8 min
NonIdeality	6.580E-05	P/Po Toler	2	End of Run	05/07/2014 13:38
Molecular Wt	28.0134 g/mol	Equil Time	2	File Name	570507_1.RAW
Station #	1	Bath Temp.	77.35		

Isotherm

P/Po	Volume [cc/g] STP
5.5591e-02	0.2733
6.3282e-02	0.2838
1.0654e-01	0.3709
1.3855e-01	0.4066
1.5785e-01	0.4756
1.8326e-01	0.5358
2.0901e-01	0.5723
2.3286e-01	0.6808
2.5731e-01	0.7935
2.8225e-01	0.9312
3.0680e-01	1.0645
3.5608e-01	1.2960
4.0562e-01	1.5626
4.5467e-01	1.9150
5.0458e-01	2.2145
5.5290e-01	2.6017
6.0423e-01	2.9736
6.5392e-01	3.3725
7.0186e-01	3.8652
7.5355e-01	4.3509
8.0261e-01	4.8619
8.5335e-01	5.4294
9.0296e-01	5.8862
9.5403e-01	6.2268
9.9424e-01	7.0859
9.4577e-01	5.8519
8.9735e-01	5.4540
8.4916e-01	5.1631
7.9126e-01	4.8824
7.4453e-01	4.5772
6.9665e-01	4.2337
6.4755e-01	4.0455
5.9981e-01	3.6728
5.5055e-01	3.4630
4.9134e-01	3.1214
4.4493e-01	2.7869
3.9571e-01	2.5329
3.4740e-01	2.2038
2.9801e-01	1.9152
2.4861e-01	1.6272
1.9942e-01	1.2065
1.5000e-01	1.0205
1.0066e-01	0.7595

Figure B6 Langmuir plot data on the isotherm of $K_{0.8}Ni_{0.4}Ti_{1.6}O_4$

Date: 05/16/2014 Page 1

Quantachrome Corporation
Quantachrome Autosorb Automated Gas Sorption System Report
Autosorb for Windows® Version 1.19

Sample ID	LFC K0.8Cu0.4Ti1.6O4				
Description	Ads 22 Pts Des 22 Pts BET 11 pts				
Comments					
Sample Weight	0.5100 g				
Adsorbate	NITROGEN	Outgas Temp	300.0 °C	Operator	EcmB
Cross-Sec Area	16.2 Å²/molecule	Outgas Time	26.1 hrs	Analysis Time	286.5 min
NonIdeality	6.580E-05	P/Po Toler	2	End of Run	05/13/2014 20:39
Molecular Wt	28.0134 g/mol	Equil Time	2	File Name	570513_1.RAW
Station #	1	Bath Temp.	77.35		

Isotherm

P/Po	Volume [cc/g] STP
5.7015e-02	0.0461
8.3344e-02	0.0744
1.0852e-01	0.0957
1.3336e-01	0.1187
1.5830e-01	0.1572
1.8265e-01	0.2119
2.0750e-01	0.2700
2.3155e-01	0.3718
2.5845e-01	0.3925
2.8129e-01	0.5126
3.0711e-01	0.5894
3.5636e-01	0.7124
4.0740e-01	0.7995
4.5732e-01	0.9347
5.0528e-01	1.0724
5.5199e-01	1.3958
6.0223e-01	1.6693
6.5232e-01	1.9733
6.9998e-01	2.3877
7.5160e-01	2.7248
8.0222e-01	2.9897
8.5356e-01	3.2304
9.0431e-01	3.4177
9.5540e-01	3.5608
9.9930e-01	3.8485
9.4337e-01	3.3261
8.9907e-01	3.1022
8.3892e-01	3.1122
7.9259e-01	2.9733
7.4560e-01	2.7902
6.9252e-01	2.6334
6.4601e-01	2.5347
5.9008e-01	2.3741
5.4430e-01	2.1947
4.9935e-01	1.9966
4.4128e-01	1.8066
3.9702e-01	1.5830
3.5195e-01	1.4124
2.9131e-01	1.1674
2.4566e-01	0.9574
1.9961e-01	0.8387
1.4183e-01	0.5657
9.6610e-02	0.3922

Figure B7 Langmuir plot data on the isotherm of $K_{0.8}Cu_{0.4}Ti_{1.6}O_4$

Date: 05/05/2014 Page 1

Quantachrome Corporation
Quantachrome Autosorb Automated Gas Sorption System Report
Autosorb for Windows® Version 1.19

Sample ID	LPC K0.8 Zn0.4 Ti1.6 04				
Description	Ads 22 Pts Des 22 Pts BET 11 pts				
Comments					
Sample Weight	0.4968 g				
Adsorbate	NITROGEN	Outgas Temp	300.0 °C	Operator	BcmB
Cross-Sec Area	16.2 Å²/molecule	Outgas Time	16.6 hrs	Analysis Time	259.5 min
NonIdeality	6.580E-05	P/Po Toler	2	End of Run	05/04/2014 15:33
Molecular Wt	28.0134 g/mol	Equil Time	2	File Name	570504_1.RAW
Station #	1	Bath Temp.	77.35		

Isotherm

P/Po	Volume [cc/g] STP
5.6663e-02	0.0938
8.3344e-02	0.1265
1.0648e-01	0.1608
1.3367e-01	0.1851
1.5826e-01	0.2330
1.8870e-01	0.2584
2.0790e-01	0.3246
2.3348e-01	0.3621
2.5822e-01	0.4126
2.8296e-01	0.4685
3.0822e-01	0.5244
3.5783e-01	0.5987
4.0774e-01	0.6721
4.5663e-01	0.7764
5.0629e-01	0.9070
5.5851e-01	0.9580
6.0755e-01	1.0896
6.5763e-01	1.1147
7.0695e-01	1.1479
7.5650e-01	1.2521
8.0822e-01	1.3231
8.5656e-01	1.4920
9.0752e-01	1.5525
9.5324e-01	1.6511
9.9430e-01	2.9522
9.4629e-01	2.0189
9.0158e-01	1.7210
8.4298e-01	1.5335
7.9494e-01	1.4159
7.4482e-01	1.3321
6.9437e-01	1.3477
6.4750e-01	1.1910
5.9723e-01	1.1716
5.4908e-01	1.0847
4.9980e-01	0.9529
4.5015e-01	0.8851
4.0128e-01	0.7756
3.5174e-01	0.7004
2.9107e-01	0.6067
2.4230e-01	0.5186
1.9241e-01	0.4327
1.4328e-01	0.3154
9.3608e-02	0.2318

Figure B8 Langmuir plot data on the isotherm of $K_{0.8}Zn_{0.4}Ti_{1.6}O_4$

04/30/2016

Quantachrome Instruments
Quantachrome Autosorb Automated Gas Sorption System Repo
Autosorb 1 for Windows 1.55

File name: C:\QC data\PhysData\Naowarat\NWR_KCU 0 4 Ni 0 4.raw
Sample ID: Description:
Comments:
Operator: OUNSA Sample weight: 0.0481 g
Analysis gas: Nitro gen X sect. area: 16.2 A2/molec Non-ideality:
Adsorbate [DRP]: Nitro gen Bath Temp.: 77.30
Outgas Temp: 150.0 C Outgas Time: 12.0 hrs Analysis Time:
P/Po tolerance: 3 Equil. time: 2 End of run:
Station #: 1 PC sw. version: 1.55 TempComp:

Isotherm

P/Po A [cc/g]	Volume [cc/g] STP
0.00013019	0.0385
0.00016791	0.0247
0.0001813	0.0225
0.00019167	0.0206
0.00015225	0.0193
0.0010034	0.0476
0.0020367	0.0521
0.0031382	0.0563
0.0040066	0.0597
0.0050314	0.0612
0.0060729	0.0603
0.0071333	0.0547
0.0081701	0.0382
0.062325	0.09
0.052374	0.1146
0.092368	0.1505
0.11225	0.2555
0.16191	0.4282
0.2119	0.5978
0.26188	0.7613
0.31188	0.9184
0.41126	1.2015
0.51058	1.4764
0.61084	1.7312
0.71075	1.961
0.81077	2.1959
0.9162	3.5546
0.59325	6.5936
0.50111	3.7803
0.79765	2.4086

Figure B9 Langmuir plot data on the isotherm of $K_{0.8}Cu_{0.2}Ni_{0.2}Ti_{1.6}O_4$

04/29/2016

Quantachrome Instruments
Quantachrome Autosorb Automated Gas Sorption System Report
Autosorb 1 for Windows 1.55

File name: C:\QCdata\PhysData\Panarat_Naowarat\NWR_KZN 0 4 CU 0 4.raw
Sample ID: MS.Panarat Description:
Comments:
Operator: OUNSA Sample weight: 0.0685 g
Analysis gas: Nitrogen X sect. area: 16.2 sq.molec Non-ideality: 6.58e-05
Adsbate (DRP): Nitrogen Bath Temp.: 77.30
Outgas Temp: 150.0 °C Outgas Time: 12.0 hrs Analysis Time: 359.2 min
P/Po tolerance: 3 Equil. time: 2 End of run: 03/12/2016 20:22
Station #: 1 PC sw. version: 1.55 TempComp: On

Isotherm

P/Po	Volume [cc/g] STP	P/Po	Volume [cc/g] STP	P/Po	Volume [cc/g] STP
1.3019e-04	0.0289	7.1333e-03	0.0547	9.1020e-01	2.5546
1.6791e-04	0.0247	8.1701e-03	0.0382	9.9928e-01	5.0936
1.8130e-04	0.0229	6.2325e-02	0.0290	9.0111e-01	2.7805
1.8967e-04	0.0216	7.2385e-02	0.0702	7.9768e-01	2.4086
1.9221e-04	0.0210	8.2374e-02	0.1146	6.9407e-01	2.1102
1.9167e-04	0.0206	9.2368e-02	0.1509	5.9001e-01	1.8124
1.9296e-04	0.0200	1.0234e-01	0.1925	4.8933e-01	1.5217
1.9371e-04	0.0195	1.1225e-01	0.2555	3.8920e-01	1.2296
1.9225e-04	0.0193	1.6191e-01	0.4282	2.8904e-01	0.9410
2.0222e-04	0.0179	2.1190e-01	0.5978	1.8901e-01	0.6608
3.0404e-04	0.0073	2.6188e-01	0.7613	8.9114e-02	0.2938
1.0054e-03	0.0476	3.1188e-01	0.9184	6.8732e-02	0.2316
2.0567e-03	0.0521	4.1126e-01	1.2015	4.8817e-02	0.1450
3.1382e-03	0.0563	5.1098e-01	1.4764	2.3513e-02	0.1254
4.0066e-03	0.0597	6.1084e-01	1.7312	1.1425e-02	0.2762
5.0514e-03	0.0612	7.1078e-01	1.9610	5.0762e-03	0.3947
6.0729e-03	0.0605	8.1077e-01	2.1999		

Figure B10 Langmuir plot data on the isotherm of $K_{0.8}Cu_{0.2}Zn_{0.2}Ti_{1.6}O_4$

05/28/2015

Quantachrome Instruments
Quantachrome Autosorb Automated Gas Sorption System Report
Autosorb 1 for Windows 1.50

File name:	C:\QCdata\HA BET\58\5\580401_1.RAN				
Sample ID:	KMnFe	Description:	Ads 22 Pts Des 22 Pts BET 11 pts		
Comments:					
Operator:	Nick	Sample weight:	0.1583 g		
Analysis gas:	NITROGEN	X sect. area:	16.2 Å²/molec	Non-ideality:	6.58e-05
Adabate (DRP):	Nitrogen	Bath Temp.:	77.35		
Outgas Temp:	300.0 °C	Outgas Time:	11.1 hrs	Analysis Time:	301.3 min
P/Po tolerance:	2	Equil. time:	3	End of run:	04/01/2015 11:25
Station #:	1	PC sw. version:	Pre-1.28		

Isotherm

P/Po	Volume [cc/g] STP
5.6647e-02	0.3276
8.3449e-02	0.4074
1.0874e-01	0.4503
1.3303e-01	0.5751
1.5773e-01	0.6891
1.8375e-01	0.7209
2.0780e-01	0.8780
2.3410e-01	0.9556
2.5722e-01	1.0687
2.8425e-01	1.1104
3.0704e-01	1.2828
3.3866e-01	1.4195
4.0639e-01	1.6287
4.5758e-01	1.8654
5.0867e-01	2.0028
5.5432e-01	2.3703
6.0624e-01	2.5717
6.5682e-01	2.7584
7.0696e-01	3.1327
7.5561e-01	3.3028
8.0651e-01	3.5270
8.5561e-01	3.9856
9.0919e-01	4.2148
9.5227e-01	4.7918
9.9578e-01	5.7592
9.3906e-01	4.8858
8.9568e-01	4.5082
8.4598e-01	4.1915
7.9436e-01	4.0931
7.4692e-01	3.7216
6.9664e-01	3.4286
6.4541e-01	3.3715
5.9682e-01	3.1251
5.4594e-01	2.8825
4.9540e-01	2.6542
4.4678e-01	2.4096
3.9718e-01	2.1830
3.4557e-01	2.0020
2.9545e-01	1.7283
2.4462e-01	1.5364
1.9874e-01	1.3429
1.4810e-01	1.0798

Figure B11 Langmuir plot data on the isotherm of $K_{0.8}Fe_{0.7}Mn_{0.1}Ti_{1.2}O_4$

04/29/2016

Quantachrome Instruments
Quantachrome Autosorb Automated Gas Sorption System Report
Autosorb 1 for Windows 1.55

File name: C:\QCdata\PhysData\Panarat_Naowarat\NWR_KMN 0 4 FE 0 4.raw
Sample ID: Miss Naowarat Description: KMn 0.4 Fe 0.4
Comments:
Operator: OUNSA Sample weight: 0.0422 g
Analysis gas: Nitrogen X sect. area: 16.2 ㎡molec Non-ideality: 6.58e-05
Adsbate (DRP): Nitrogen Bath Temp.: 77.30
Outgas Temp: 150.0 ℃ Outgas Time: 12.0 hrs Analysis Time: 298.6 min
P/Po tolerance: 3 Equil. time: 2 End of run: 03/12/2016 13:58
Station #: 1 PC sw. version: 1.55 TempComp: On

Isotherm

P/Po	Volume [cc/g] STP	P/Po	Volume [cc/g] STP	P/Po	Volume [cc/g] STP
5.6217e-05	0.0992	2.0646e-03	0.1628	2.1205e-01	0.6150
1.0948e-04	0.0963	3.1509e-03	0.1715	2.6208e-01	0.7712
1.4392e-04	0.0928	4.0270e-03	0.1777	3.1195e-01	0.9086
1.6475e-04	0.0901	5.0774e-03	0.1781	4.1101e-01	1.2836
1.7515e-04	0.0882	6.0997e-03	0.1763	5.1153e-01	1.5117
1.8132e-04	0.0867	7.1627e-03	0.1662	6.1127e-01	1.7185
1.8475e-04	0.0856	8.2116e-03	0.1360	7.1147e-01	1.9209
1.8643e-04	0.0846	9.2745e-03	0.0664	8.1091e-01	2.1799
1.8753e-04	0.0837	2.2282e-02	-0.1668	9.1115e-01	2.4937
1.9527e-04	0.0823	3.2331e-02	-0.1040	9.9762e-01	7.0690
2.8903e-04	0.0716	4.2338e-02	-0.0468	8.9989e-01	2.5382
4.4284e-04	0.0519	5.2365e-02	0.0070	7.9440e-01	2.1180
6.1855e-04	0.0273	6.2408e-02	0.0535	6.8866e-01	2.1301
8.0847e-04	-0.0005	7.2259e-02	0.1246	5.8901e-01	1.9114
1.0072e-03	-0.0304	8.2358e-02	0.1804	4.8896e-01	1.6409
1.0342e-03	-0.0059	9.2360e-02	0.2131	3.8891e-01	1.3988
1.1420e-03	-0.0042	1.0238e-01	0.2559	2.8894e-01	1.1175
1.2352e-03	-0.0047	1.1239e-01	0.2936	1.8886e-01	0.7915
9.9939e-04	0.1513	1.6206e-01	0.4512	8.8827e-02	0.4260

Figure B12 Langmuir plot data on the isotherm of $K_{0.8}Fe_{0.4}Mn_{0.4}Ti_{1.2}O_4$

APPENDIX C

BASICITY

Standard CO_2 desorption of $CaCO_3$ (Specific surface area = 10 m^2/g):

$$CaCO_3 \longrightarrow CaO + CO_2$$

Table C1 Calibration data of standard $CaCO_3$.

$CaCO_3$ (g)	CO_2 desorption (mmolCO_2)	Peak area
0.1010	0.1009	13.28476
0.0185	0.1848	34.31688
0.0251	0.2508	42.36252

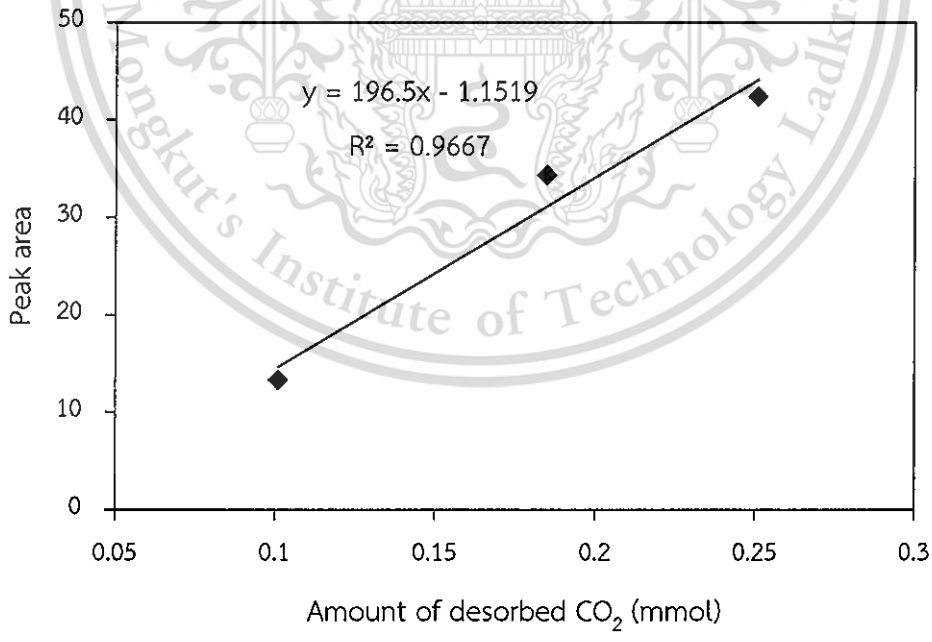

Figure C1 Calibration curve of CO_2 desorption from $CaCO_3$.

From **Figure C1:** $y = 196.5x - 1.1519$

Where; x is the amount of desorbed CO_2 ($mmolCO_2$)

y is peak area

Example C1: Calculation of basicity from CO_2 desorption of $K_{0.8}Zn_{0.4}Ti_{1.6}O_4$.

The peak area of 0.3027 g $K_{0.8}Zn_{0.4}Ti_{1.6}O_4$ from CO_2-TPD profiled is 1.1836 unit.

Therefore the amount of desorbed CO_2 is

$$1.1836 = 196.5x - 1.1519$$

$$= 0.0118\ mmolCO_2$$

$K_{0.8}Zn_{0.4}Ti_{1.6}O_4$ 0.3027 g gives CO_2 desorption $= 0.0118\ mmolCO_2$

Therefore $K_{0.8}Zn_{0.4}Ti_{1.6}O_4$ 1 g gives CO_2 desorption $= 0.0118/0.3027\ mmolCO_2/g$

$= 0.0389\ mmolCO_2/g$

Table C2 CO_2 desorption of various catalysts prepared.

Catalyst	Weight (g)	Peak area	CO_2 desorption ($mmolCO_2/g$)
KLi	0.2199	1.9059	0.0708
KMg	0.2211	0.4167	0.0361
KFe	0.6984	4.0739	0.0381
KCo	0.3133	3.8367	0.0810
KNi	0.2007	0.7831	0.0430
KCu	0.2108	1.7486	0.0700
KZn	0.3027	1.1836	0.0389
KCuZn	0.2044	0.2953	0.0360
KCuNi	0.3024	1.0645	0.0373
$KFe_{0.7}Mn0.1$	0.2077	2.5316	0.0902
$KFe_{0.4}Mn_{0.4}$	0.3008	5.2856	0.1089

Example C2: Calculation of Sanderson intermediate electronegativity and partial negative charges of framework oxygen of $K_{0.8}Zn_{0.4}Ti_{1.6}O_4$.

Table C3 Electronegativity and total composition per one Zn atom.

Element	Zn	Ti	O	K
Electronegativity from relative atomic compactness	3.00	1.40	5.21	0.42
Total composition per one Zn atom of $K_{0.8}Zn_{0.4}Ti_{1.6}O_4$	1.00	4.00	10.00	2.00

Sanderson intermediate electronegativity

$$S_{int} = [\prod_i Si^{Pi}]^{\frac{1}{\sum_i Pi}}$$

$$S_{int} = [(3.00^{1.00})(1.40^{4.00})(5.21^{10.00})(0.42^{2.00})]^{\frac{1}{17}}$$

$$= 2.7529$$

Partial negative charges of framework oxygen

$$\sigma_i = \frac{S_{int} - S_i}{2.08(S_i)^{\frac{1}{2}}}$$

$$\sigma_i = \frac{2.7529 - 5.21}{2.08(5.21)^{\frac{1}{2}}}$$

$$= -0.5175$$

Table C4 Electronegativity from relative atomic compactness.

Element	Electronegativity from relative atomic compactness*
Li	0.74
O	5.21
Mg	1.56
K	0.42
Ti	1.40
Mn	2.07
Fe	2.10
Co	2.10
Ni	2.12
Cu	2.60
Zn	3.00

*From literature [69].

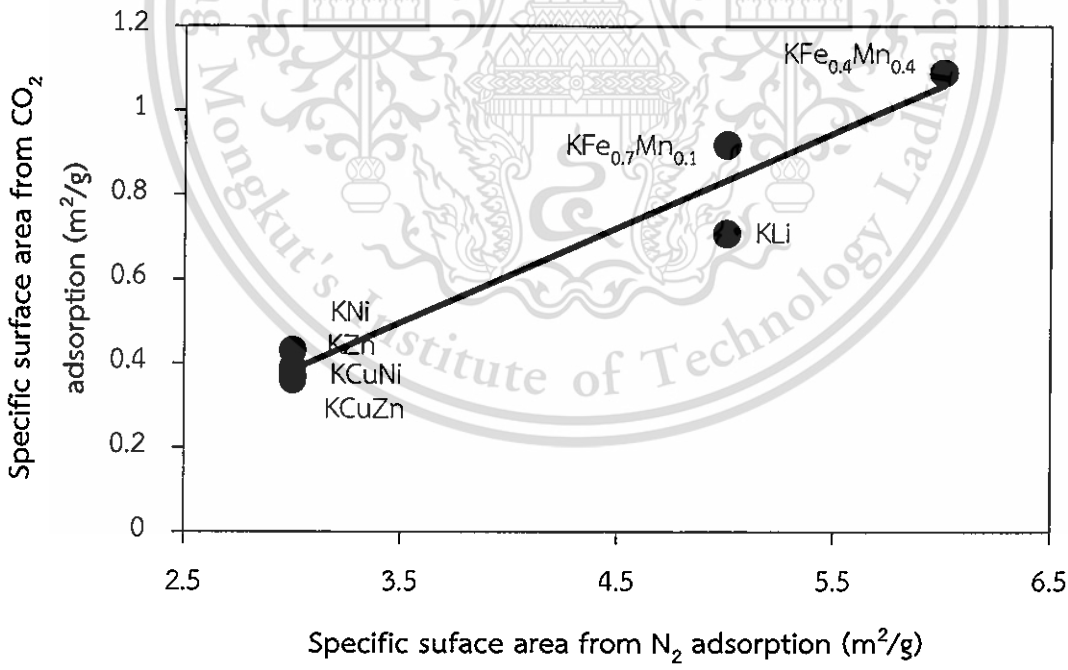

Figure C2 The relationship between the specific surface areas from N_2 adsorption vs. the specific surface areas from CO_2 desorption.

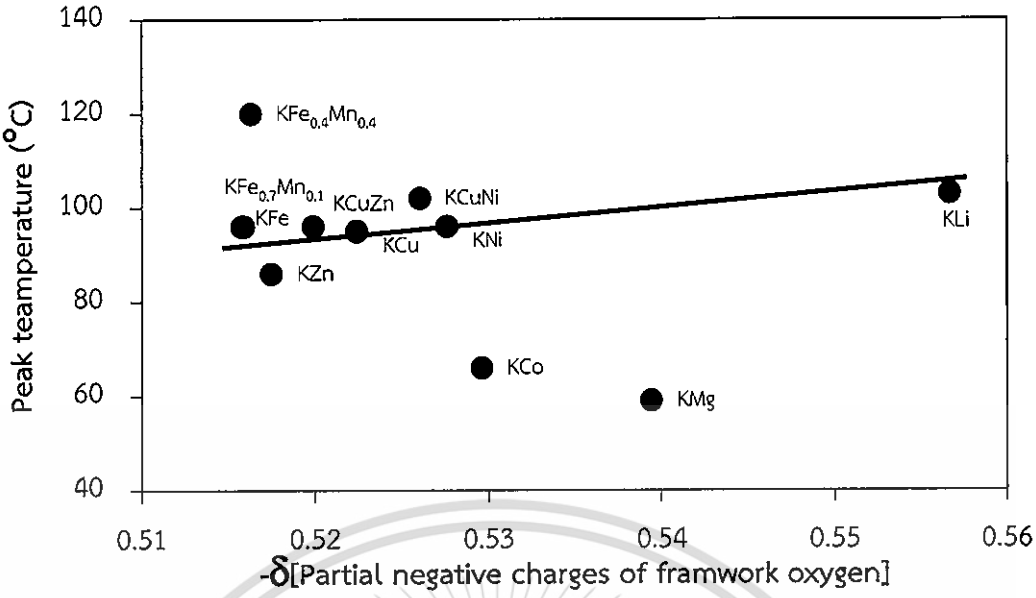

Figure C3 The relationship between the partial negative charge of framework oxygen vs. the peak temperature from CO_2-TPD

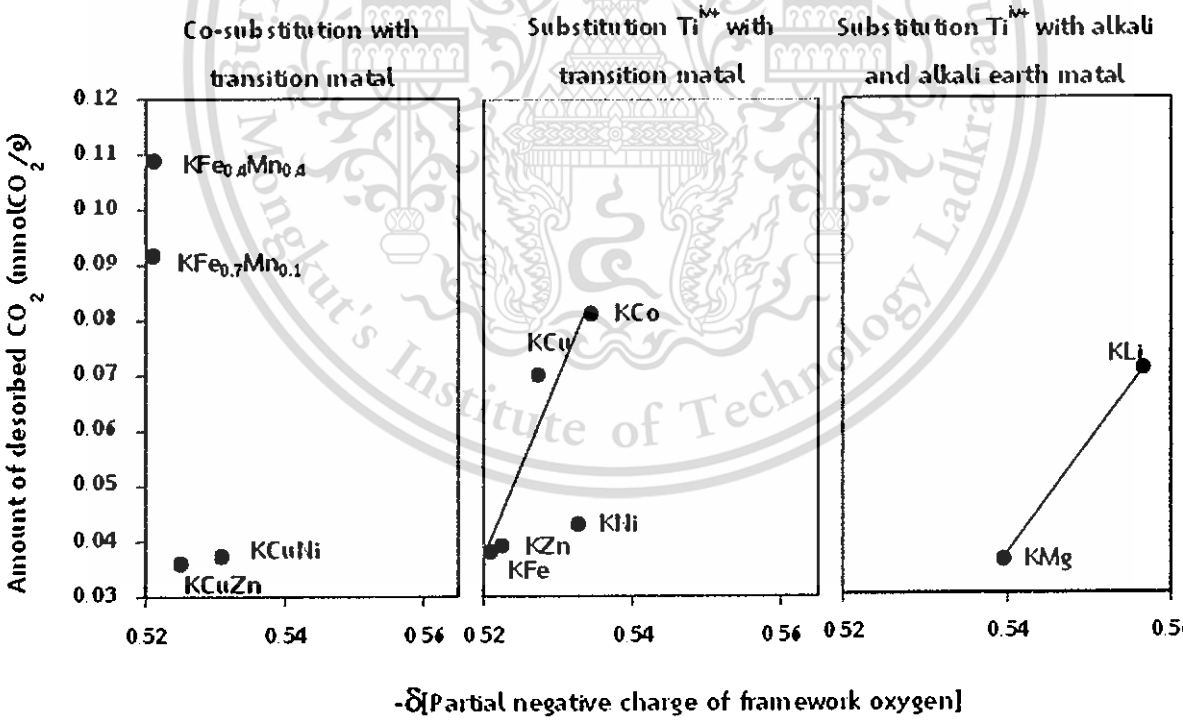

Figure C4 The relationship between the partial negative charge of framework oxygen vs. the amount of desorbed CO_2 from CO_2-TPD

APPENDIX D

REDUCIBILITY

Standard H_2 Consumption of CuO:

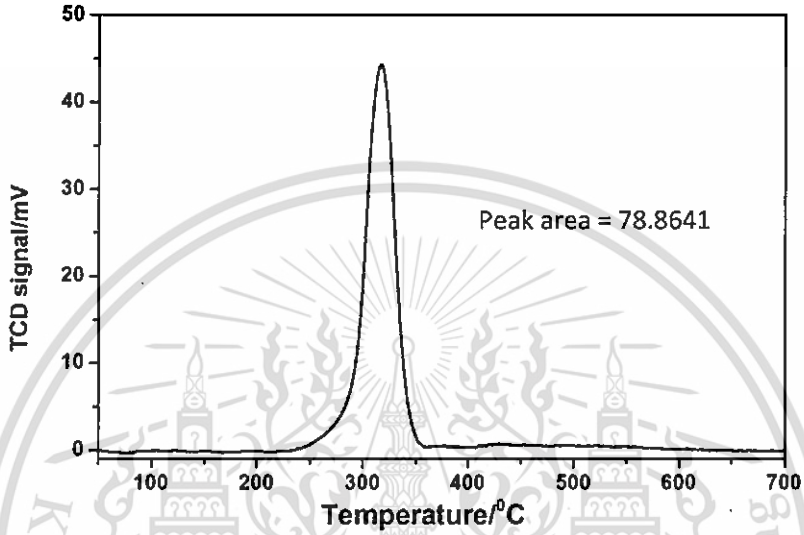

Figure D1 TPR profile of standard CuO.

$$CuO + H_2 \longrightarrow Cu + H_2O$$

CuO 0.1014 g (MW = 79.545 g/mole) could be turned into CuO 1.28 mmole.

Therefore the amount of H_2 consumption would be 1.28 mmole as well.

From TPR profile, the peak area 78.8641 is equal to H_2 consumption 1.28 mmolH_2

Example D1: Calculation of H_2 consumption (mmolH_2/g) of $K_{0.8}Zn_{0.4}Ti_{1.6}O_4$.

$K_{0.8}Zn_{0.4}Ti_{1.6}O_4$ 0.1124 g gives peak area 2.8305 unit.

It would consume H_2 = 1.28 × 2.8305/78.8641

= 0.0459 mmolH_2

$K_{0.8}Zn_{0.4}Ti_{1.6}O_4$ 1 g is consumed H_2 = 0.0459/0.1124

= 0.4087 mmolH_2/g

Table D1 Summary of the deconvolution of the TPR-profiles of some lepidocrocite titanate catalysts

Catalyst	weight (g)	Component i					Component ii					Component iii					Component iv					Component v					Component vi				
		$T_{initial}$ (°C)	T_{peak} (°C)	T_{final} (°C)	peak area	$mmolH_2/g$	$T_{initial}$ (°C)	T_{peak} (°C)	T_{final} (°C)	peak area	$mmolH_2/g$	$T_{initial}$ (°C)	T_{peak} (°C)	T_{final} (°C)	peak area	$mmolH_2/g$	$T_{initial}$ (°C)	T_{peak} (°C)	T_{final} (°C)	peak area	$mmolH_2/g$	$T_{initial}$ (°C)	T_{peak} (°C)	T_{final} (°C)	peak area	$mmolH_2/g$	$T_{initial}$ (°C)	T_{peak} (°C)	T_{final} (°C)	peak area	$mmolH_2/g$
$K_{0.8}Zn_{0.4}Ti_{1.6}O_4$	0.1124	198	550	855	2.8305	0.4087	-	-	-	-	-	-	-	-	-	-	-	-	-	-	-	-	-	-	-	-	-	-	-	-	-
$K_{0.8}Cu_{0.4}Ti_{1.6}O_4$	0.1005	357	344	447	2.2217	0.3588	328	496	652	10.4064	1.6806	-	-	-	-	-	-	-	-	-	-	-	-	-	-	-	-	-	-	-	-
$K_{0.8}Ni_{0.4}Ti_{1.6}O_4$	0.1013	297	415	508	2.9051	0.4650	324	534	724	3.4272	0.5489	545	683	826	4.5448	0.7281	650	733	800	4.4971	0.7137	-	-	-	-	-	-	-	-	-	-
$K_{0.8}Co_{0.4}Ti_{1.6}O_4$	0.1174	270	313	350	0.1485	0.0205	510	688	810	1.6050	0.2219	595	782	883	7.8549	1.0859	-	-	-	-	-	-	-	-	-	-	-	-	-	-	-
$K_{0.8}Fe_{0.8}Ti_{1.2}O_4$	0.1053	346	409	456	0.3232	0.0498	340	445	540	0.7497	0.1156	410	529	630	1.0871	0.1675	380	612	840	2.6242	0.4045	646	761	854	1.6936	0.2612	690	821	900	1.7742	0.2735

APPENDIX E

INTERCALATION COMPOUNDS

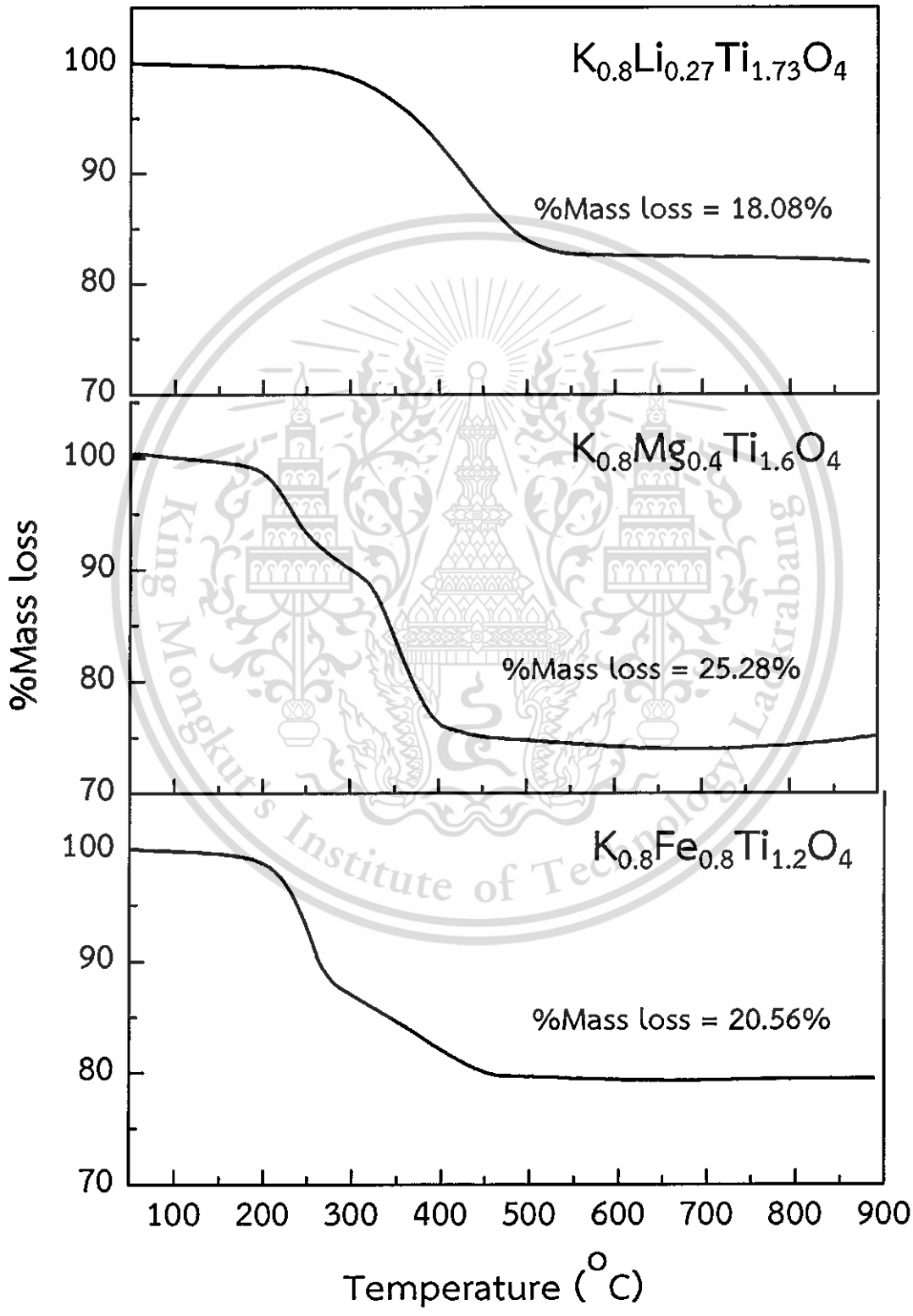

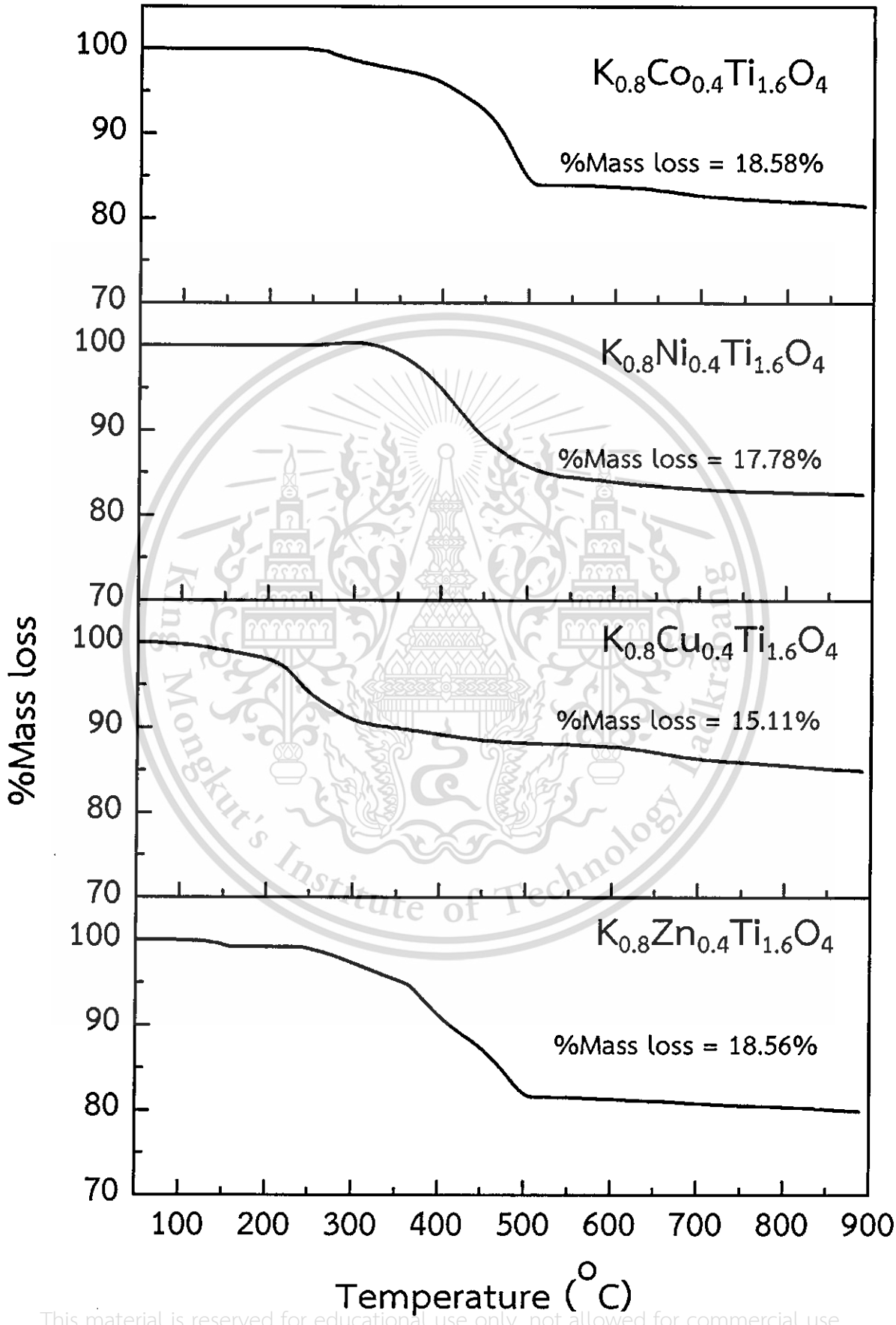

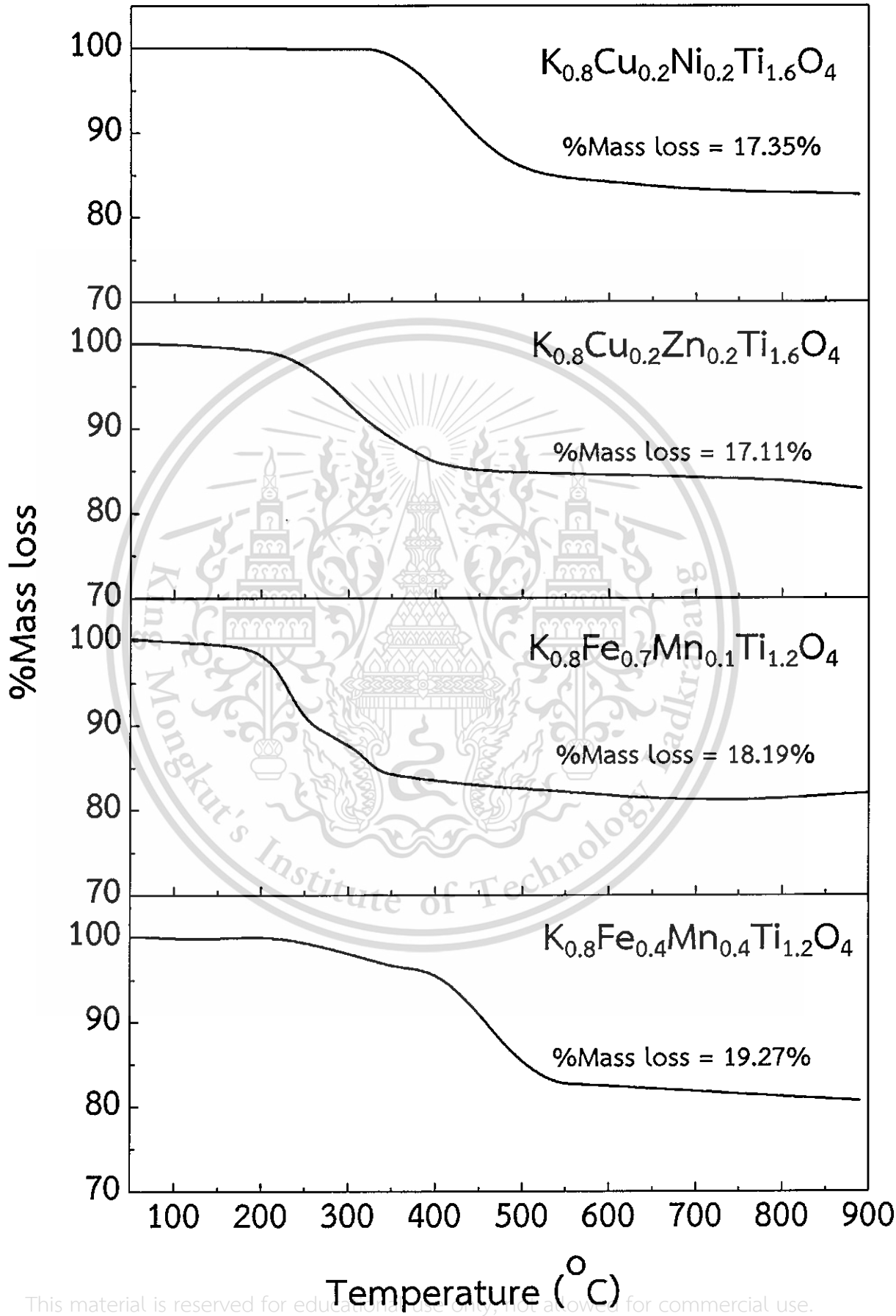

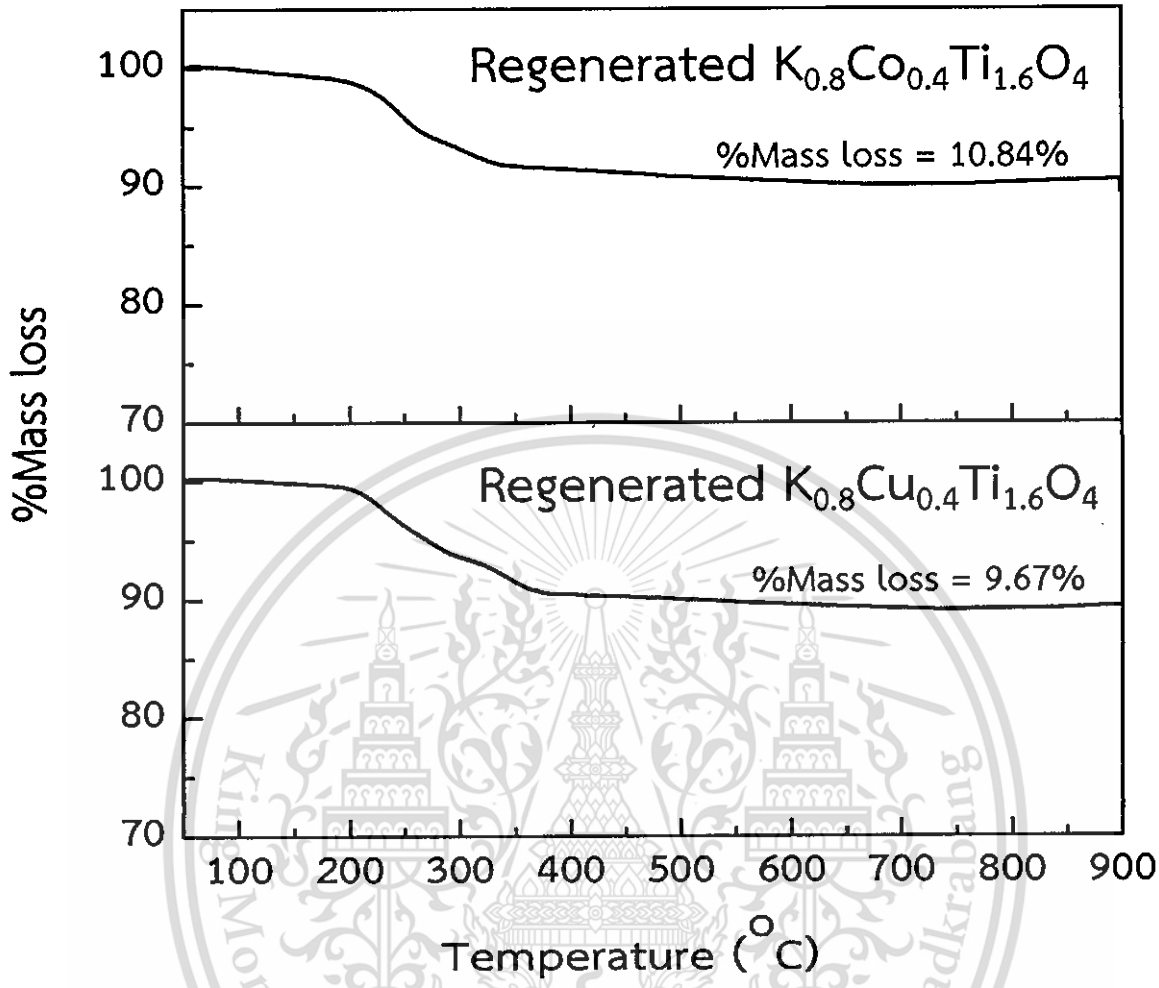

Figure E1 The TGA mass loss curve of intercalation compounds, including regenerated ones.

APPENDIX F

CALCULATION OF CATALYTIC PARAMETERS

Yield

The liquid yield is defined as the total liquid hydrocarbons obtained relative to the theoretical value of 100% conversion of palmitic acid.

Example F1: Yield from deoxygenation activity of $K_{0.8}Zn_{0.4}Ti_{1.6}O_4$ at 350°C.

Substrate;

Intercalation compound = 1.9968 g

The amount of palmitic acid intercalated from TGA = 18.56 %

Palmitic acid = $\frac{1.9968 \times 18.56}{100}$

= 0.3706 g

Products;

The total liquid products obtained = 0.1615 g

Calculation the theoretical liquid products:

Palmitic acid = 0.3706 g

MW of palmitic acid = 256.42 g/mol

MW of liquid product ($-CO_2$) = 256.42 – 44.00

= 212.42 g/mol

The theoretical liquid products = $\frac{0.3706\ g}{256.42\ g/mol} \times 212.42\ g/mol$

= 0.3070 g

$$\%\text{Yield} = \frac{\text{The total liquid products obtained}}{\text{The theoretical liquid products}} \times 100\%$$

$$= \frac{0.1615\ \text{g}}{0.3070\ \text{g}} \times 100\% = 52.60\%$$

Selectivity

Selectivity of the products is obtained from the chromatogram, and is defined as the ratio of mole of particular product to the total mole of the reactant converted. High selectivity of a desired product is preferred. %Selectivity can be obtained from the following equation.

$$\%\text{Selectivity} = \frac{yield\ of\ each\ product}{Total\ yield} \times 100\%$$

Yield of each product is defined from the selectivity as shown in the following equation.

$$\text{Yield of each product} = \frac{\%Selctivity\ x\ Total\ yield}{100}$$

Example F2: Yield of C15 saturated hydrocarbon

%Selectivity of C15 saturated hydrocarbon = 29.21 %

Total yield = 52.60 %

$$\text{Yield of C15 saturated hydrocarbon} = \frac{29.21 \times 52.60}{100}$$

$$= 15.37\ \%$$

APPENDIX G

REACTION DATA

Table G1 The amount of substrates and products from the conversion of palmitic acid over $K_{0.8}Zn_{0.4}Ti_{1.6}O_4$ at various temperatures.

Scan reaction temperature over $K_{0.8}Zn_{0.4}Ti_{1.6}O_4$				
Temperature (°C)	350	400	450	500
%Yield	52.6	56.9	63.1	67.3
%Mass loss of palmitic acid intercalated (%)	18.56	18.56	18.56	18.56
Weight of intercalation compounds (g)	1.9968	2.0182	2.0586	2.0589
Weight of liquid product (g)	0.1615	0.1765	0.1997	0.2130

Table G2 The amount of substrates and products from the conversion of palmitic acid over several composition of lepidocrocite titanate.

Reaction with several compositions of lepidocrocite titanate							
Catalysts	$K_{0.8}Li_{0.27}Ti_{1.73}O_4$	$K_{0.8}Mg_{0.4}Ti_{1.6}O_4$	$K_{0.8}Fe_{0.8}Ti_{1.2}O_4$	$K_{0.8}Co_{0.4}Ti_{1.6}O_4$	$K_{0.8}Ni_{0.4}Ti_{1.6}O_4$	$K_{0.8}Cu_{0.4}Ti_{1.6}O_4$	$K_{0.8}Zn_{0.4}Ti_{1.6}O_4$
%Yield	80.0	73.9	62.3	70.9	67.0	68.1	52.6
%Mass loss of palmitic acid intercalated (%)	18.08	25.28	20.56	18.58	17.78	15.11	18.56
Weight of intercalation compounds (g)	2.0000	1.5900	2.0813	2.0549	1.5818	2.0932	1.9968
Weight of liquid product (g)	0.2398	0.3435	0.2752	0.2243	0.1562	0.1786	0.1615

Table G3 The amount of substrates and products from the conversion of palmitic acid over co-substituted lepidocrocite titanate catalysts.

Reaction with co-substituted lepidocrocite titanate catalysts				
Catalysts	$K_{0.8}Fe_{0.7}Mn_{0.1}Ti_{1.2}O_4$	$K_{0.8}Fe_{0.4}Mn_{0.4}Ti_{1.2}O_4$	$K_{0.8}Cu_{0.2}Ni_{0.2}Ti_{1.6}O_4$	$K_{0.8}Cu_{0.2}Zn_{0.2}Ti_{1.6}O_4$
%Yield	68.5	74.3	68.8	53.9
%Mass loss of palmitic acid intercalated (%)	18.19	19.27	17.35	17.11
Weight of intercalation compounds (g)	2.041	1.6231	2.0691	2.0998
Weight of liquid product (g)	0.2107	0.2097	0.2047	0.1605

Table G4 The amount of substrates and products from the conversion of palmitic acid over regenerated lepidocrocite titanate catalysts.

Reaction with regenerated catalyst		
Catalysts	Regenerated $K_{0.8}Co_{0.4}Ti_{1.6}O_4$	Regenerated $K_{0.8}Cu_{0.4}Ti_{1.6}O_4$
%Yield	51.3	47.9
%Mass loss of palmitic acid intercalated (%)	10.84	9.67
Weight of intercalation compounds (g)	1.0849	1.0955
Weight of liquid product (g)	0.0500	0.0420

Table G5 %Selectivity of products from the deoxygenation of palmitic acid over $K_{0.8}Zn_{0.4}Ti_{1.6}O_4$ at various temperatures.

%Selectivity								
Product distribution	Reaction temperature (°C)							
	350		400		450		500	
	Unsat.	Sat.	Unsat.	Sat.	Unsat.	Sat.	Unsat.	Sat.
C1	-	0.01	-	-	-	-	-	-
C2	0.03	0.03	-	-	-	-	-	-
C3	0.07	0.04	0.01	-	-	-	-	-
C4	0.07	0.05	0.01	0.01	0.01	0.01	-	-
C5	0.08	0.05	0.01	0.00	0.01	0.01	-	-
C6	0.20	0.09	0.02	0.01	0.02	0.01	-	-
C7	0.30	0.17	0.03	0.02	0.03	0.03	-	-
C8	0.50	0.28	0.07	0.05	0.11	0.16	-	0.01
C9	0.88	0.55	0.22	0.14	0.14	0.16	0.03	0.01
C10	1.44	0.87	0.54	0.33	0.32	0.35	0.13	0.02
C11	2.12	1.23	1.29	0.08	0.67	0.72	0.52	0.07
C12	3.06	1.28	3.34	2.67	1.10	1.59	1.32	0.24
C13	3.53	4.84	5.85	5.41	2.56	5.42	1.62	0.90
C14	15.54	0.97	15.46	3.08	11.72	4.59	10.02	0.72
C15	26.18	29.22	16.30	39.80	13.55	50.42	14.43	65.12
C16	0.30	0.16	0.04	-	-	-	0.02	0.04
C16 alcohol	-		-		-		0.02	
C16 aldehyde	0.20		0.02		-		0.02	
C17 ketone	5.71		5.43		5.28		4.724	

Table G6 %Selectivity of products from the deoxygenation of palmitic acid over several compositions of lepidocrocite titanate.

%Selectivity														
Product distribution	Catalysts													
	$K_{0.8}Li_{0.27}Ti_{1.73}O_4$		$K_{0.8}Mg_{0.4}Ti_{1.6}O_4$		$K_{0.8}Fe_{0.8}Ti_{1.2}O_4$		$K_{0.8}Co_{0.4}Ti_{1.6}O_4$		$K_{0.8}Ni_{0.4}Ti_{1.6}O_4$		$K_{0.8}Cu_{0.4}Ti_{1.6}O_4$		$K_{0.8}Zn_{0.4}Ti_{1.6}O_4$	
	Unsat.	Sat.	Unsat.	Sat.	Unsat.	Sat.	Unsat.	Sat.	Unsat.	Sat.	Unsat.	Sat.	Unsat.	Sat.
C1	-	0.01	-	-	-	-	-	0.02	-	0.03	-	-	-	0.01
C2	0.02	0.02	0.00	0.01	0.01	0.01	0.05	0.02	0.05	0.02	0.00	0.00	0.03	0.03
C3	0.04	0.04	0.01	0.01	0.02	0.00	0.11	0.03	0.04	0.14	0.00	0.00	0.07	0.04
C4	0.04	0.04	0.01	0.02	0.01	0.01	0.05	0.03	0.09	0.10	0.00	0.00	0.07	0.05
C5	0.07	0.05	0.02	0.02	0.03	0.02	0.07	0.04	0.09	0.03	0.00	0.01	0.08	0.05
C6	0.26	0.12	0.07	0.04	0.11	0.04	0.40	0.19	1.89	0.86	0.01	0.01	0.20	0.09
C7	0.36	0.24	0.11	0.09	0.07	0.09	0.16	0.10	0.44	1.52	0.02	0.02	0.30	0.17
C8	0.79	0.60	0.24	0.24	0.13	0.21	0.50	0.37	0.14	1.14	0.05	0.05	0.50	0.28
C9	1.46	1.13	0.60	0.57	0.51	0.55	1.28	0.42	1.06	1.02	0.14	0.14	0.88	0.55
C10	3.08	2.28	1.39	1.28	0.53	0.45	1.02	0.40	2.02	1.01	0.25	0.21	1.44	0.87
C11	7.98	5.67	2.93	2.06	0.75	0.70	1.76	0.66	0.88	0.40	0.37	0.29	2.12	1.23
C12	12.32	7.42	3.97	2.75	1.25	1.13	3.24	1.26	1.14	1.35	0.40	0.39	3.06	1.28
C13	6.82	11.13	5.06	11.50	1.59	2.31	4.79	2.43	2.86	3.05	0.60	0.57	3.53	4.84
C14	10.36	6.68	31.94	3.69	6.52	8.63	5.87	9.35	7.10	2.92	2.53	4.81	15.54	0.97
C15	6.27	11.88	4.52	5.99	29.39	20.01	33.91	23.62	33.58	17.83	23.74	36.56	26.18	29.22
C16	0.31	0.17	0.21	0.07	1.51	3.07	1.55	0.46	4.96	4.08	0.63	0.39	0.30	0.16
C16 alcohol	0.25		0.16		1.85		0.87		1.70		3.84		-	
C16 aldehyde	0.26		0.09		21.44		1.46		5.38		23.19		0.20	
C17 ketone	1.86		20.32		1.05		3.52		1.10		0.79		5.71	

Table G7 %Selectivity of products from the deoxygenation of palmitic acid over co-substituted lepidocrocite titanate catalysts.

%Selectivity								
Product distribution	Catalysts							
	$K_{0.8}Fe_{0.7}Mn_{0.1}Ti_{1.2}O_4$		$K_{0.8}Fe_{0.4}Mn_{0.4}Ti_{1.2}O_4$		$K_{0.8}Cu_{0.2}Ni_{0.2}Ti_{1.6}O_4$		$K_{0.8}Cu_{0.2}Zn_{0.2}Ti_{1.6}O_4$	
	Unsat.	Sat.	Unsat.	Sat.	Unsat.	Sat.	Unsat.	Sat.
C1	-	-	-	-	-	-	-	-
C2	-	-	-	-	-	-	-	-
C3	-	-	0.01	0.01	-	-	-	-
C4	-	-	0.01	0.01	-	-	-	-
C5	-	-	0.01	0.01	-	-	-	-
C6	-	-	0.04	0.03	0.01	-	-	-
C7	0.01	-	0.06	0.07	0.01	0.01	0.01	0.01
C8	0.01	0.01	0.14	0.16	0.02	0.21	0.02	0.02
C9	0.11	0.16	0.38	0.41	0.06	0.06	0.04	0.04
C10	0.55	0.42	0.71	0.73	0.09	0.07	0.06	0.05
C11	1.75	1.36	1.17	1.14	0.11	0.08	0.08	0.07
C12	3.45	3.02	1.78	1.61	0.18	0.23	0.10	0.12
C13	6.44	7.77	2.88	4.96	0.20	0.29	0.11	0.18
C14	17.33	2.58	20.22	1.89	0.58	0.93	0.33	2.02
C15	17.67	12.85	28.26	12.39	21.41	74.26	25.86	69.47
C16	0.68	1.09	0.40	2.02	0.03	0.13	0.05	0.12
C16 alcohol	2.59		1.29		0.58		0.45	
C16 aldehyde	8.77		5.44		0.61		0.68	
C17 ketone	11.40		11.79		0.04		0.10	

Table G8 %Selectivity of products from the deoxygenation of palmitic acid over regenerated lepidocrocite titanate catalysts.

%Selectivity				
Product distribution	Catalysts			
	Regenerated $K_{0.8}Co_{0.4}Ti_{1.6}O_4$		Regenerated $K_{0.8}Cu_{0.4}Ti_{1.6}O_4$	
	Unsat.	Sat.	Unsat.	Sat.
C1	-	0.01	-	-
C2	0.01	0.01	0.01	-
C3	-	0.01	-	0.01
C4	0.01	0.01	-	-
C5	0.01	0.01	-	0.01
C6	0.18	0.09	0.01	-
C7	0.24	0.17	-	0.01
C8	0.24	0.35	0.11	0.01
C9	0.92	0.59	0.70	0.53
C10	1.24	0.44	1.02	0.69
C11	1.45	0.90	1.67	1.21
C12	1.73	0.69	1.82	1.98
C13	3.61	3.35	1.24	1.06
C14	12.71	4.23	15.04	6.96
C15	39.80	12.24	15.55	30.11
C16	1.10	0.45	1.20	0.58
C16 alcohol	1.02		0.62	
C16 aldehyde	2.86		3.94	
C17 ketone	9.40		12.96	

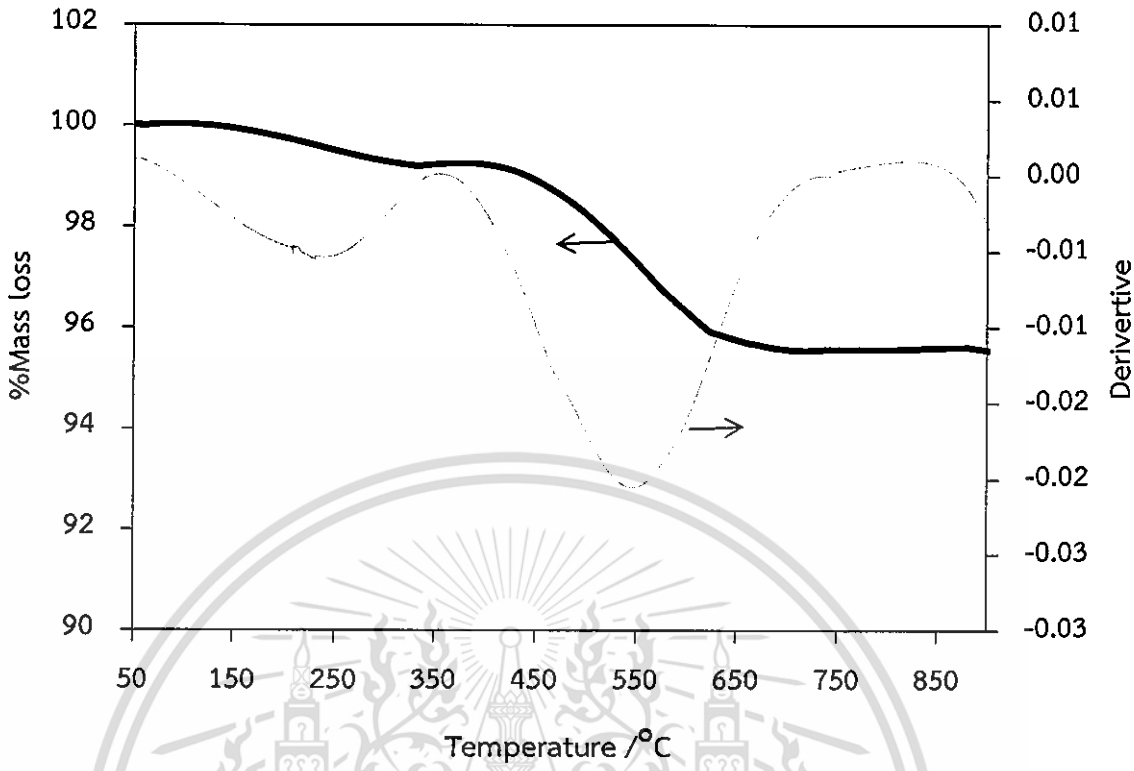

Figure G1 TGA mass loss curve of spend KCu catalyst after reaction at 350 °C for 1 h (The coke despite of spent KCu catalyst was analyzed under AirO atmosphere).

APPENDIX H

GAS CHROMATOGRAM

Analysis of gas products from gas chromatography

Prior to the analysis, the identity of the liquid products is identified by GC-MS (gas chromatography with mass spectrometer detector). Then, the quantitative analysis of products was carried by GC-FID (gas chromatography with flam ionization detector) with the condition expressed in Table H1.

Table H1 The GC condition for quantitative analysis.

Column	HP-1 (30 m x 0.32 mm x 5 μm)
Temperature program	40°C (5 min hold) to 280°C (24 min hold) at 15°C/min
Carrier gas	Nitrogen gas flow rate 2.4 mL/min (40 cm/sec)
Injector temperature	265 °C (Splitless)
Injector loop volume	250 μL
Detector temperature	FID at 280°C

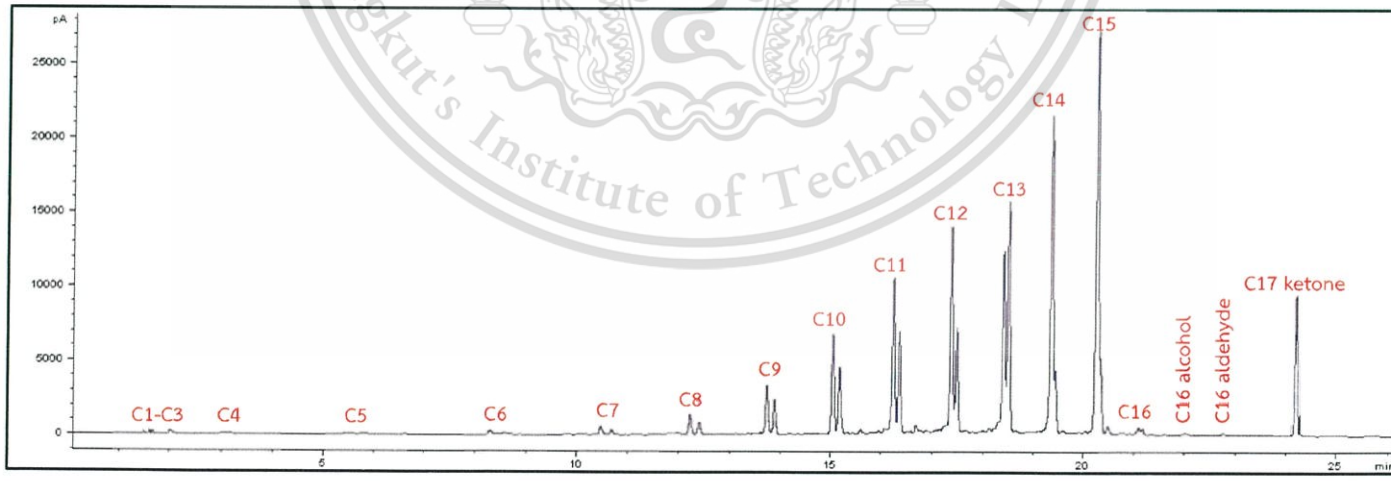

Figure H1 The GC chromatogram of products from deoxygenation of palmitic acid over $K_{0.8}Zn_{0.4}Ti_{1.6}O_4$ at 350°C.

Table H2 Chromatogram data of standard product distribution and feed for the analysis of liquid products.

Products	Retention time of standard (min)	Products	Retention time of standard (min)
C1	1.515	C10 sat	15.271
C2 unsat	1.627	C11 unsat	16.556
C2 sat	1.844	C11 sat	16.750
C3 unsat	2.031	C12 unsat	17.545
C3 sat	2.217	C12 sat	17.645
C4 unsat	3.002	C13 unsat	18.561
C4 sat	3.310	C13 sat	18.681
C5 unsat	5.396	C14 unsat	19.323
C5 sat	5.801	C14 sat	19.501
C6 unsat	8.265	C15 unsat	20.503
C6 sat	8.542	C15 sat	20.782
C7 unsat	10.842	C16 unsat	21.453
C7 sat	11.012	C16 sat	21.677
C8 unsat	12.427	C16 alcohol	21.979
C8 sat	12.581	C16 aldehyde	22.223
C9 unsat	13.755	C17 ketone	24.300
C9 sat	14.011	Palmitic acid	25.047
C10 unsat	15.075		

The gaseous products from the reaction of palmitic acid over $K_{0.8}Zn_{0.4}Ti_{1.6}O_4$ catalyst at 350°C were identified by GC-MS, which the condition expressed in Table H3.

Table H3 The GC-MS condition for quantitative analysis of gaseous products.

Column	HP-PLOT Molesieve (30 m x 0.32 mm x 25 μm)
Temperature program	35°C (10 min hold) to 250°C (24 min hold) at 20°C/min
Carrier gas	Heium gas flow rate 1.0 mL/min
Injector temperature	100 °C (split ratio 80:1)
Injector loop volume	250 μL
Detector temperature	MS at 100°C

Figure H2 The chromatogram of gaseous products from the reaction of palmitic acid over $K_{0.8}Zn_{0.4}Ti_{1.6}O_4$ catalyst.

Table H4 Chromatogram data of standard product distribution for the analysis of gaseous products.

Gaseous products	Retention time of standard (min)
Nitrogen	2.351
Carbon monoxide	5.474
Carbon dioxide	16.872

APPENDIX I

Surface and interlayer base-characters in lepidocrocite titanate: The adsorption and intercalation of fatty acid

Contents lists available at ScienceDirect

Journal of Solid State Chemistry

journal homepage: www.elsevier.com/locate/jssc

Surface and interlayer base-characters in lepidocrocite titanate: The adsorption and intercalation of fatty acid

Tosapol Maluangnont [a,b,*], Pornanan Arsa [b,c], Kanokporn Limsakul [c], Songsit Juntarachairot [c], Saithong Sangsan [c], Kazuma Gotoh [d], Tawan Sooknoi [b,c,**]

[a] College of Nanotechnology, King Mongkut's Institute of Technology Ladkrabang, Bangkok 10520, Thailand
[b] Catalytic Chemistry Research Unit, Faculty of Science, King Mongkut's Institute of Technology Ladkrabang, Bangkok 10520, Thailand
[c] Department of Chemistry, Faculty of Science, King Mongkut's Institute of Technology Ladkrabang, Bangkok 10520, Thailand
[d] Graduate School of Natural Science & Technology, Okayama University, 3-1-1 Tsushima-naka, Okayama 700-8530, Japan

ARTICLE INFO

Article history:
Received 31 January 2016
Received in revised form
5 March 2016
Accepted 18 March 2016
Available online 19 March 2016

Keywords:
Intercalation
Layered materials
Alkali titanate
basic sites
Ketonization
Fatty acid

ABSTRACT

While layered double hydroxides (LDHs) with positively-charged sheets are well known as basic materials, layered metal *oxides* having negatively-charged sheets are not generally recognized so. In this article, the surface and interlayer base-characters of O^{2-} sites in layered metal oxides have been demonstrated, taking lepidocrocite titanate $K_{0.8}Zn_{0.4}Ti_{1.6}O_4$ as an example. The low basicity (0.04 mmol CO_2/g) and low desorption temperature (50–300 °C) shown by CO_2 – TPD suggests that O^{2-} sites at the external surfaces is weakly basic, while those at the interlayer space are mostly inaccessible to CO_2. The liquid-phase adsorption study, however, revealed the uptake as much as 37% by mass of the bulky palmitic acid (C_{16} acid). The accompanying expansion of the interlayer space by ~0.1 nm was detected by PXRD and TEM. In an opposite manner to the external surfaces, the interlayer O^{2-} sites can deprotonate palmitic acid, forming the salt (i.e., potassium palmitate) occluded between the sheets. Two types of basic sites are proposed based on ultrafast ^{1}H MAS NMR and FTIR results. The interlayer basic sites in lepidocrocite titanate leads to an application of this material as a selective and stable two-dimensional (2D) basic catalyst, as demonstrated by the ketonization of palmitic acid into palmitone (C_{31} ketone). Tuning of the catalytic activity by varying the type of metal (Zn, Mg, and Li) substituting at Ti^{IV} sites was also illustrated.

1. Introduction

Solid base catalysts are capable of activating acidic reactants [1,2] in several reactions of industrial importance, or in the synthesis of fine chemicals [3,4] and first-generation biodiesel [5]. The base-characters of metal oxides originate from under-coordinated O^{2-} sites on different locations (step, corner, terrace, etc.) of the crystals. These sites could behave as the Lewis base by donating an electron pair to reactants. The formation of surface carbonate (or bicarbonate) on oxides in contact to atmospheric CO_2 is an example of the Lewis base-character of oxides. Alternatively, the O^{2-} sites act as the Brønsted base if they abstract a proton from reactants. This is the case for the formation of the surface hydroxyl group on oxides upon contacting with atmospheric water.

Common oxides such as CaO, MgO, ZrO_2 are strongly basic, inexpensive, but typically have low surface area and random distribution of the atomic planes [6]. Their catalytic activity greatly depends on the exposed facets of the crystals which have to be controlled through a delicate synthetic procedure. In contrast, a family of solids known as layered metal oxides/hydroxides [7,8] naturally crystalizes into two-dimensional (2D) plate-like objects, composed of atomically-thin sheets as elementary units. Such crystals inherently expose the faces (i.e., the basal plane) and the edges to the environment, resulting in the *external* active sites. In addition, the 2D crystals possess the *internal* interlayer space sandwiched between the sheets. These sites can be utilized only if they are accessible to reactants. However, the accessibility to internal basic sites and the thermal/chemical stability do not necessarily coexist in the same catalyst. For example, well-known 2D metal *hydroxides* such as layered double hydroxides (LDHs) or

* Corresponding author at: College of Nanotechnology, King Mongkut's Institute of Technology Ladkrabang, Bangkok 10520, Thailand.
** Corresponding author at: Department of Chemistry, Faculty of Science, King Mongkut's Institute of Technology Ladkrabang, Bangkok 10520, Thailand.
E-mail addresses: tosapol.ma@kmitl.ac.th (T. Maluangnont), kstawan@gmail.com (T. Sooknoi).

http://dx.doi.org/10.1016/j.jssc.2016.03.030
0022-4596/

layered hydroxy salts (LHSs) are considered basic largely because they exhibit high affinity toward the acidic molecule CO_2 (in the form of intercalated carbonate CO_3^{2-}), which can have the electrostatic attraction with the positively-charged sheets. However, these materials transform into (mixed) metal oxides upon contact with reactants at elevated reaction temperature [8–10], thereby losing the two-dimensionality and the associated benefits. Therefore, there is still a need to develop a new type of active and stable 2D solid base catalysts whose the external and the internal surfaces could be effectively utilized.

Lepidocrocite titanates ($A_xM_yTi_{1-y}O_4$, where A=K, M=Zn, Mg, Ni, Cu, Fe^{III}, Mn^{III}; [11,12] A=Cs, M=Zn, [13] Ni, [14] Mg, [15,16] Nb; [17] A=K, Rb, and Cs, M=Li; [18,19] A=Cs, M=cationic vacancy [20]) show great potential as thermally stable, 2D basic catalysts. The basal plane (either external or internal) is on the *ac* plane of an orthorhombic unit cell. Two types of bridging basic oxygen atoms can be found. The first one is O_{2c} coordinating to two Ti^{IV} atoms nearby, while the second one is O_{4c} and coordinates to four Ti^{IV} atoms. It is natural to assume that the negative charges on the sheets would localize at O_{2c} and O_{4c}, contributing to the base characters. Moreover, the edges of crystals also contain under-coordinated oxygen atoms of which the exact geometry depends on the extent of hydroxylation. Therefore, the nature of basic sites (O^{2-}) in layered metal oxides is fundamentally different from that in LDHs/LHSs mentioned above. Still, with the exception of a simple ion exchange of interlayer alkali cations with aqueous mineral acids [19,21–25], reports on base characters of layered metal oxides and their behavior toward other acidic probe molecules are lacking.

In this work, the surface basicity of lepidocrocite titanate $K_{0.8}Zn_{0.4}Ti_{1.6}O_4$ has been characterized by CO_2 temperature programmed desorption (CO_2 TPD). In combination with FTIR and ^1H ultrafast MAS NMR, surface hydroxyl can be revealed. Results were compared to TiO_2 and the well-known basic catalyst such as MgO. Bulky acidic probe molecule, palmitic acid (C_{16} acid), was employed to test the accessibility to the interlayer basic sites via liquid phase adsorption (intercalation). We further demonstrated the application of some lepidocrocite titanates ($K_{0.8}Zn_{0.4}Ti_{1.6}O_4$, $K_{0.8}Mg_{0.4}Ti_{1.6}O_4$ and $K_{0.8}Li_{0.27}Ti_{1.73}O_4$) as catalysts for the gas-phase ketonization of palmitic acid, in comparison to the mixed Mg/Al oxides from the decomposition of LDH. The ketonization of carboxylic acids to the respective ketones is of industrial importance as a processing step in biomass conversion to hydrocarbon fuels [26–29].

2. Material and methods

2.1. Synthesis

Lepidocrocite titanate $K_{0.8}Zn_{0.4}Ti_{1.6}O_4$ was synthesized [11] by the calcination of the stoichiometric mixture of K_2CO_3, ZnO, and TiO_2 at 900 °C for 20 h. Two other compositions, $K_{0.8}Mg_{0.4}Ti_{1.6}O_4$ and $K_{0.8}Li_{0.27}Ti_{1.73}O_4$, can be prepared similarly but replacing ZnO with MgO [11] and Li_2CO_3 [18,19], respectively. The layered double hydroxide with Mg/Al mole ratio of 2.5 was synthesized by a co-precipitation method [30] and was calcined at 450 °C for 6 h, giving the mixed Mg/Al oxide "MgAl2.5". Potassium palmitate was obtained as the white powder from the reaction between KOH(aq) and palmitic acid. The PXRD patterns of other materials in addition to $K_{0.8}Zn_{0.4}Ti_{1.6}O_4$ can be found in Figs. S1 and S2 in Supporting Information. All chemicals are of reagent grade and were used as received, except K_2CO_3, Li_2CO_3, KOH and palmitic acid which were dried 120 °C overnight prior to use.

2.2. CO_2 temperature programmed desorption

Approximately 200–300 mg of the sample was activated in situ at 450 °C for 2 h under air zero in a quartz tube reactor, followed by a cooling to room temperature under N_2 gas. Gaseous CO_2 was then flown through the sample at the flow rate 30 mL/min for an hour, followed by a flow of helium at the same flow rate for another hour. Next, the temperature was raised from room temperature to 600 °C at 5 °C/min using pure helium as a carrier gas. The CO_2 desorption profile was recorded by a thermal conductivity detector and was normalized by mass of the sample employed. The basicity was expressed as mmol of CO_2 per g of the sample. The peak area obtained was compared to that from a known amount of $CaCO_3$ which decomposes completely and quantitatively to CaO and CO_2. All gases are the commercial products of Praxair with the purity of 99.99% and were used as received.

2.3. Adsorption of palmitic acid

An amount of 2.0 g of $K_{0.8}Zn_{0.4}Ti_{1.6}O_4$ was heated with 150 mL of a 5% w/w palmitic acid (Fluka, 97%+) in isopropanol at 60 °C from 1 to 36 h. The liquid was withdrawn at certain intervals, and the content of adsorbed palmitic acid was determined based on Eq. (1), together with an appropriate conversion of concentration to mass. Here, A_0 is the corrected peak area of palmitic before the adsorption, and A_t is the corrected peak area of palmitic acid remaining in the mother liquor after the adsorption time t.

$$\%\text{Adsorption} = [(A_0 - A_t)/A_0] \times 100\% \quad (1)$$

The solid was filtered, washed with isopropanol, and then dried at 70 °C overnight. The experiment with decanoic acid was performed similarly. A control experiment was performed by heating $K_{0.8}Zn_{0.4}Ti_{1.6}O_4$ with isopropanol at 60 °C in the absence of any carboxylic acid. Another control experiment was also performed, where $K_{0.8}Zn_{0.4}Ti_{1.6}O_4$ was magnetically stirred with 1 M HCl (3 times, 12 h each, with the fresh HCl loaded between repetition) [24] so as to obtain the proton-containing lepidocrocite where K^+ is ion exchanged with $H^+ \cdot H_2O$.

2.4. Characterization

Powder X-ray diffraction (PXRD) measurements were conducted on a Rigaku DMAX 2200/Ultima+ diffractometer, employing a Cu-Kα radiation at 40 kV and 30 mA. The sample was scanned in the range 2θ=5–65° at a 0.05°/step and a detection time of 0.6 second/step. BET specific surface area of the sample was determined by a Gas Adsorption Analyzer (Autosorb-1C, Quantachrome). For TGA (Perkin-Elmer, Pyris 1), the sample was heated from room temperature to 900 °C (10 °C/min) under nitrogen gas flowing at 20 mL/min. FTIR spectra of the pelletized samples (prepared by grinding with KBr) were collected on a Spectrum GX (Perkin Elmer) spectrometer. SEM images were acquired on a Zeiss EVO/MA10 scanning electron microscope, while TEM images were acquired on a JEOL JEM 2010 transmission electron microscope. ^1H MAS NMR (spinning speed: 100 kHz) of $K_{0.8}Zn_{0.4}Ti_{1.6}O_4$ was recorded using a JEOL ECA-600 spectrometer with a 0.75 mmϕ MAS sample rotor. Depth2 pulse sequence with 1.3 μs of 90° pulse length and 5.0 s of repetition time were applied to obtain a spectrum.

2.5. Catalytic activity testing

Catalytic activity testing was conducted in a continuous fixed bed down-flow reactor made of glass (length, 50 cm; outer diameter, 8 mm; inner diameter, 6 mm) under atmospheric pressure

of N_2. The catalyst was activated to 800 °C in air zero for an hour, followed by a cooling to the reaction temperature (375 °C) under air zero. Then, 5% palmitic acid in *p*-xylene was fed into the reactor by an HPLC pump at a flow rate of 0.025 mL/min. The catalyst activity testing was conducted at atmospheric pressure, at the contact time (*W/F*) of 1500 g h/mol, and the flow rate of palmitic acid plus carrier gas (N_2) of 30 mL/min, for a total of 360 min. The liquid products were trapped by an ice bath and collected every 45 min before the analysis by an HP6890 gas chromatograph (Hewlett-Packard). The catalyst recovered after the activity testing at the mentioned condition is hereafter called "spent".

3. Results and discussion

Calcination of the stoichiometric mixture of K_2CO_3, ZnO, and TiO_2 at 900 °C for 20 h results in the lepidocrocite titanate $K_{0.8}Zn_{0.4}Ti_{1.6}O_4$ with high crystallinity, as shown by the PXRD pattern in Fig. 1a. This product will be hereafter called "as made" $K_{0.8}Zn_{0.4}Ti_{1.6}O_4$. The diffraction pattern can be indexed based on the orthorhombic symmetry, with unit cell parameters (refined by Cellcalc) of $a=0.3809(3)$, $b=1.567(1)$, and $c=0.2981(2)$ nm, in agreement with the previous work (suggested space group [11] $Cmc2_1$). The first peak at $2\theta=11.34°$ ($d=0.78$ nm) corresponds to the 020 reflection which is the repeating distance of the edge-shared TiO_6 (or $(Ti/Zn)O_6$) sheets stacking along the *b*-direction.

Fig. 2a shows that the plate-like crystals of the as made $K_{0.8}Zn_{0.4}Ti_{1.6}O_4$ with the lateral size up to 2 μm × 2 μm form aggregates, likely due to the use of high temperature in the synthesis. $K_{0.8}Zn_{0.4}Ti_{1.6}O_4$ had an extremely low specific surface area of 3 m^2/g.

The CO_2 desorption profiles of $K_{0.8}Zn_{0.4}Ti_{1.6}O_4$ and other tested materials are shown in Fig. 3. CO_2 desorbs from $K_{0.8}Zn_{0.4}Ti_{1.6}O_4$ in the range 50–300 °C (with the peak temperature T_p at 89 °C), which is close to the range reported for mixed sodium/potassium titanate nanotubes [31]. A relatively low T_p suggests that the majority of CO_2 adsorption occurs physically. Lepidocrocite titanate $K_{0.8}Zn_{0.4}Ti_{1.6}O_4$ is therefore a relatively weak base solid, similar to other reported titanate-based materials [31,32]. On the other hand, CO_2 desorption from TiO_2 anatase ($T_p=120$ °C) and "MgAl2.5", which is the mixed (Mg/Al) oxide from the decomposition of layered double hydroxide ($T_p=170$ °C), span a wider range (both in the range 50–400 °C). CO_2 molecules adsorbed on these two materials could contain a minor fraction which was adsorbed chemically, in addition to the major fraction which was adsorbed physically. While MgO shows the small peak at $T_p=196$ °C somewhat similar to $K_{0.8}Zn_{0.4}Ti_{1.6}O_4$, TiO_2 and MgAl2.5, a very strong CO_2 desorption at 400–700 °C is due to the decomposition of $MgCO_3$ which was produced in situ from the exposure of MgO to CO_2. The strength of the basic sites which are accessible to CO_2 can be estimated from T_p, and is in the order: $K_{0.8}Zn_{0.4}Ti_{1.6}O_4 < TiO_2 < MgAl2.5 < MgO$.

The basicity (mmol CO_2/g, in parenthesis) is in the order:

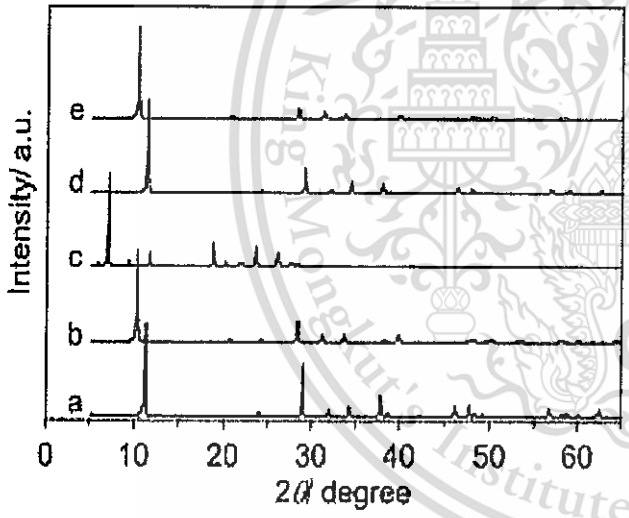

Fig. 1. PXRD patterns of (a) as made $K_{0.8}Zn_{0.4}Ti_{1.6}O_4$, (b) the solid product after the adsorption of the 5% w/w palmitic acid/isopropanol solution at 60 °C for 36 h, (c) potassium palmitate, (d) the solid product heated with isopropanol only, and (e) similar to (b) but with decanoic acid.

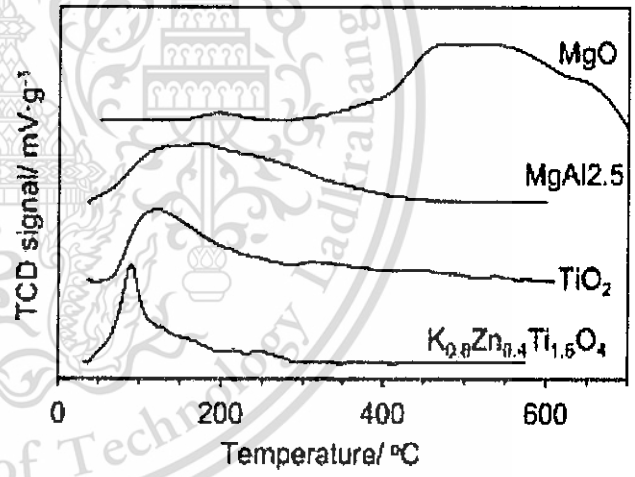

Fig. 3. CO_2 desorption profiles of as made $K_{0.8}Zn_{0.4}Ti_{1.6}O_4$, TiO_2 (anatase), MgAl2.5 which is a mixed (Mg/Al) oxide from the decomposition of a layered double hydroxide with MgAl=2.5, and MgO. The y-axis is the signal from the thermal conductivity detector normalized by the mass of the sample.

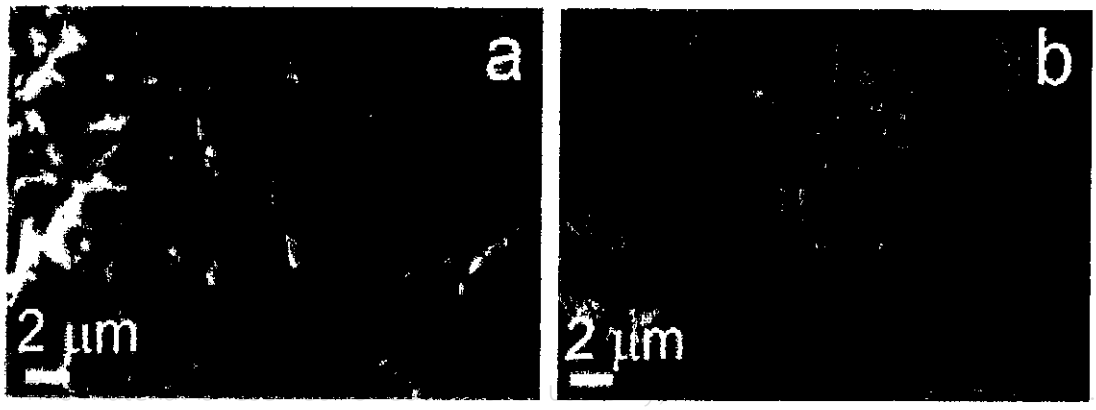

Fig. 2. SEM images of (a) as made, and (b) spent $K_{0.8}Zn_{0.4}Ti_{1.6}O_4$.

$K_{0.8}Zn_{0.4}Ti_{1.6}O_4$ (0.04) < TiO_2 (0.07) < MgAl2.5 (0.82) < MgO (1.18). Excluding MgO whose the CO_2 desorption has a contribution from the bulk, these values parallel the surface area (m^2/g) of each material which is in the order $K_{0.8}Zn_{0.4}Ti_{1.6}O_4$ (3) < TiO_2 (6) < MgAl2.5 (122). Our results imply the inaccessibility of the O^{2-} sites at the interlayer region of $K_{0.8}Zn_{0.4}Ti_{1.6}O_4$ with respect to gaseous CO_2. Consequently, the adsorption of CO_2 should take place at the sites located on the external surfaces of the crystals only. It is important to note that CO_2– TPD detects the basic sites accessible by CO_2 without discriminating whether they are O^{2-} or OH sites. These basic sites could react with CO_2, forming carbonate (for O^{2-}) or bicarbonate (for OH) in various configurations [33]. Interestingly, the basicity of $K_{0.8}Zn_{0.4}Ti_{1.6}O_4$ (0.04 mmol/g) with a low surface area of 3 m^2/g is just slightly different from some of the values reported for titanate nanotubes (0.03–0.05 mmol/g) [31] despite a much larger surface area of the nanotubes (generally more than 100 m^2/g) [31].

The FTIR spectrum of $K_{0.8}Zn_{0.4}Ti_{1.6}O_4$ is shown in Fig. 4a. The sharp peak at 811 cm^{-1} is due to Ti-O lattice vibration [18,19]. For comparison, the peak at 899 cm^{-1} was reported [34] and assigned similarly in a lepidocrocite titanate with interlayer Na^+ cations. The band at 3418 and 1624 cm^{-1} can be ascribed to the stretching and bending vibration of adsorbed H_2O [18,19] respectively. The hydroxyl group attached to the layered titanates can be found generally at 900–1000 cm^{-1} [18,19,35,36,37]. It is likely that the sharp peak at 1018 cm^{-1} in $K_{0.8}Zn_{0.4}Ti_{1.6}O_4$ (Fig. 4a) has similar origin. The relatively high wavenumber of this peak in relation to others [18,19,35,36,37] suggests a strong bonding between the oxygen atom (i.e., O^{2-} sites) and the hydrogen atom (presumably from adsorbed water molecules). In addition to the formation of a hydroxylated surface, a small band at 1388 cm^{-1} due to the asymmetric stretching of monodentate carbonate (vs 1378 cm^{-1} as calculated by Mino et al. [38]) can be observed. Here, the O^{2-} sites are the Lewis basic donating an electron pair to gaseous CO_2 in the atmosphere. Other peaks at ~2300–2375 cm^{-1} are due to the asymmetric stretching of gaseous CO_2. Several bands at 2850–3000 cm^{-1} are due to CH stretching of the thin organic films coated on an FTIR window.

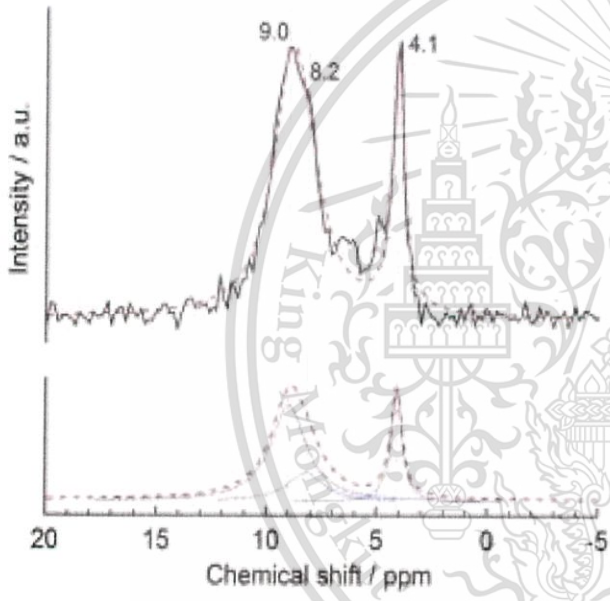

Fig. 5. ^1H MAS NMR spectrum of as made $K_{0.8}Zn_{0.4}Ti_{1.6}O_4$ (solid line) and the fitting spectrum (broken line). The deconvoluted Lorentzian components are shown by blue dotted lines at the bottom spectrum. (For interpretation of the references to color in this figure legend, the reader is referred to the web version of this article.)

The solid state ^1H ultrafast MAS NMR spectrum of as made $K_{0.8}Zn_{0.4}Ti_{1.6}O_4$ is shown in Fig. 5. The peak at 4.1 ppm (FWHM = 0.6 ppm) is assigned to protons of physisorbed water [39,40]. The presence of water molecules as detected by NMR agrees with results by FTIR just mentioned. The broad signal at ~9 ppm can be deconvoluted into two peaks at 8.2 and 9.0 ppm (FWHMs of both peaks are 2.0 ppm), suggesting that these two protons are in very similar yet different chemical environments. These signals can be inferred to water molecules interacting with two types of O^{2-} sites in as made $K_{0.8}Zn_{0.4}Ti_{1.6}O_4$. Since there are two types of structural oxygen atoms, each bound to different number of Ti^{IV} atoms, two partially overlapped H signals could be expected. For comparison, the peaks at 7.9 and 10.0 ppm have been reported in protonated titanate nanotubes [41], and at 6.0 and 8.0 ppm in $H_2Ti_3O_7$ [42]. However, in these materials [41,42] the signals are due to protons introduced via acid ion exchange, while in our case the presence of protons (or hydroxyl groups) is most likely a result of the affinity between O^{2-} sites and atmospheric water.

In order to demonstrate the accessibility of interlayer basic sites, we performed a liquid-phase adsorption study of a 5% w/w palmitic acid in isopropanol on as made $K_{0.8}Zn_{0.4}Ti_{1.6}O_4$ at 60 °. As shown in Fig. 6, the uptake of "palmitic acid" gradually increases to 34.5% (12 h) by weight, and remains constant after that (34.9%, 36 h). Such a large adsorption *solely* to the external surfaces is unlikely considering the extremely low surface area of 3 m^2/g.

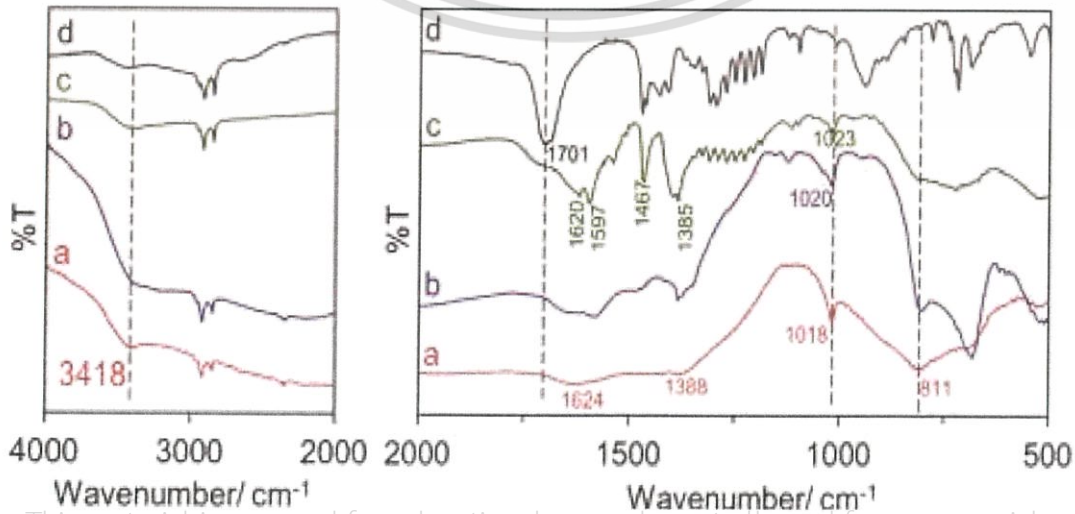

Fig. 4. FTIR spectrum of (a) as made $K_{0.8}Zn_{0.4}Ti_{1.6}O_4$. (b) the solid product after being heated with isopropanol only, (c) the solid product after the adsorption of the 5% w/w palmitic acid/isopropanol solution at 60 °C for 36 h, and (d) palmitic acid.

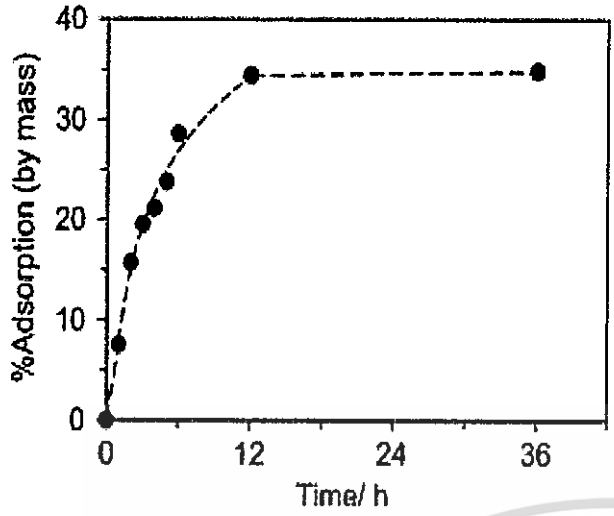

Fig. 6. The %adsorption by mass of palmitic acid by $K_{0.8}Zn_{0.4}Ti_{1.6}O_4$ at 60 °C, determined from the corrected peak area of palmitic acid before the adsorption (A_0) and at time t (A_t) of the mother liquor.

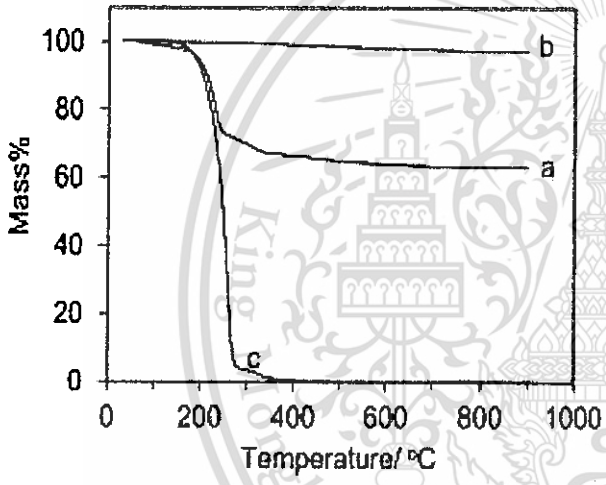

Fig. 7. Mass loss curves of (a) the solid product after the adsorption of the 5% w/w palmitic acid/isopropanol solution to $K_{0.8}Zn_{0.4}Ti_{1.6}O_4$ at 60 °C for 36 h, (b) the solid product treated with isopropanol only, and (c) palmitic acid.

Instead, the internal surfaces must involve in this uptake. We will show later on that "palmitic acid" is adsorbed as palmitate species, and that the adsorption involves the interlayer space, i.e., intercalation. In agreement with %adsorption determined from the mother liquor, the solid after contact with palmitic acid at 36 h shows 37.0% mass loss in the range 200–400 °C (Fig. 7a), ascribed to the loss of the adsorbed "palmitic acid". The mass loss curve of palmitic acid is shown for comparison in Fig. 7c. Besides, Fig. 7b shows a negligible mass loss from the control experiment in the absence of palmitic acid where only isopropanol was in the liquid phase.

In line with above view, PXRD pattern of the sample after palmitic acid adsorption in Fig. 1b shows an expansion of the interlayer. The PXRD pattern can also be indexed based on the orthorhombic symmetry, but with $a=0.3763(1)$ nm, $b=1.7190(7)$ nm, and $c=0.3005(1)$ nm. While the orthorhombic unit cell of pristine $K_{0.8}Zn_{0.4}Ti_{1.6}O_4$ is *C* based-centered [11] (hkl reflections observed following $h+k=2n$), such restriction is no longer hold considering the presence of reflections such as 121, 141, 161, 211 and 251. Instead, the unit cell of this product is likely primitive orthorhombic. (See also Fig. S3 and Table S1.) Unfortunately, the quality of the data does not allow us to do Rietveld analysis. Two parameters (*a* and *c*) are close to those in as made $K_{0.8}Zn_{0.4}Ti_{1.6}O_4$, suggesting that the host layer was kept unchanged during the adsorption. The most obvious feature is the shift of the first peak (i.e., d_{020}) to a lower angle $2\theta=10.36°$ (i.e, larger spacing $d=0.85$ nm), resulting from the expansion of ~0.1 nm. While this expansion is rather small compared to typical values (0.3–0.4 nm) reported [43,44] for the intercalation compounds having an alkyl chain, the 0.23 nm-expansion due to the pressure-induced intercalation [45] of ethanol into $K_{0.8}Ni_{0.4}Ti_{1.6}O_4$ has been reported. For comparison, the unit cell parameters $a=0.378(3)$ nm, $b=1.79(2)$ nm, and $c=0.298(4)$ nm can be deduced from the PXRD pattern (Fig. S4) of the proton-containing solid prepared via repeated ion exchange with aqueous HCl. The relatively large *d* spacing ($d_{020}=0.90$ nm at $2\theta=9.82°$) is due to the intercalation of $H^+ \cdot H_2O$ in agreement with the literature [46], but is in sharp contrast to the small d_{020} in Fig. 1b.

In $K_{0.8}Zn_{0.4}Ti_{1.6}O_4$ having the *C* based-centered unit cell (space group $Cmc2_1$) [11], potassium cations sit at the 4*a* site within the trigonal prismatic cavity. Since the two adjacent sites are too small to be occupied simultaneously, the site occupancy [11] of only 40% was achieved. So, there are rooms available for the subsequent intercalation of the guest species into the interlayer space. Upon intercalation, we observed the change of the symmetry from *C*-base centered to the primitive one. Recently, Shirpour et al. [47] have reported a similar change as $K_{0.8}Li_{0.27}Ti_{1.73}O_4$ intercalates the bulky *hydrated* sodium cations. This change occurs via the lateral gliding of the lepidocrocite layers along the *a* axis by *a*/2, generating a relatively larger cubic cavity for the guest species. Based on this cited work [47], we propose that the cubic cavity could *locally* accommodate palmitic acid (palmitate) while limiting the long-range expansion along the *b*-direction. It could be deduced that the strong guest-host interaction (i.e., acid-base interaction between palmitic acid and O^{2-} sites) overcomes the weaker host-host interactions such that the gliding of the layers is possible. Other examples [18,45,48] of the change of symmetry of the orthorhombic unit cell in lepidocrocite titanate upon the intercalation of guest species have also been reported.

The PXRD pattern of the solid product heated with isopropanol only (Fig. 1d) is similar to that of the as made $K_{0.8}Zn_{0.4}Ti_{1.6}O_4$, suggesting the essential role of palmitic acid in such topotactic transformation. The FTIR spectrum of the isopropanol-treated $K_{0.8}Zn_{0.4}Ti_{1.6}O_4$ in Fig. 4b is generally similar to as made $K_{0.8}Zn_{0.4}Ti_{1.6}O_4$, with some variations in the relative peak intensities. We also exclude the possibility that the expanded product be potassium palmitate, as evidenced from the notable differences between Fig. 1c and b. Additionally, replacing palmitic acid ($C_{15}H_{31}COOH$) by decanoic acid ($C_9H_{19}COOH$) gave the product with a similar PXRD pattern (Fig. 1e) and unit cell parameters ($a=0.3760(4)$ nm, $b=1.716(2)$ nm, and $c=0.3002(3)$ nm). The similar interlayer spacing in these two cases suggests the orientation where the long molecular axis of the acids is parallel to inorganic sheets.

Further evidence for the interlayer expansion is the TEM image. It can be seen that as made $K_{0.8}Zn_{0.4}Ti_{1.6}O_4$ shows a repeating distance of ~0.8–0.9 nm (Fig. 8a), while the solid after the adsorption of palmitic acid exhibits a repeating distance of ~1.0 nm (Fig. 8b). These distances agree reasonably with the *d*-spacing of the first peak in the respective PXRD patterns.

The characteristics peaks in the FTIR spectrum of palmitic acid in Fig. 4d include the strong C=O stretching at 1701 cm^{-1}, and the OH stretching at 3420 cm^{-1}. The co-presence of these two peaks is widely accepted as the signature of a carboxylic acid. Several other peaks serve as a fingerprint especially at 1000–1250 cm^{-1}. Unfortunately, the peaks due to CH_2 symmetric and asymmetric stretching (~2850–2960 cm^{-1}) overlap with the thin organic films coated on the FTIR window. Interestingly, while the OH stretching is still visible, the C=O stretching is very weak in $K_{0.8}Zn_{0.4}Ti_{1.6}O_4$ refluxed with palmitic acid (Fig. 4c). Instead, the peaks at 1597 and

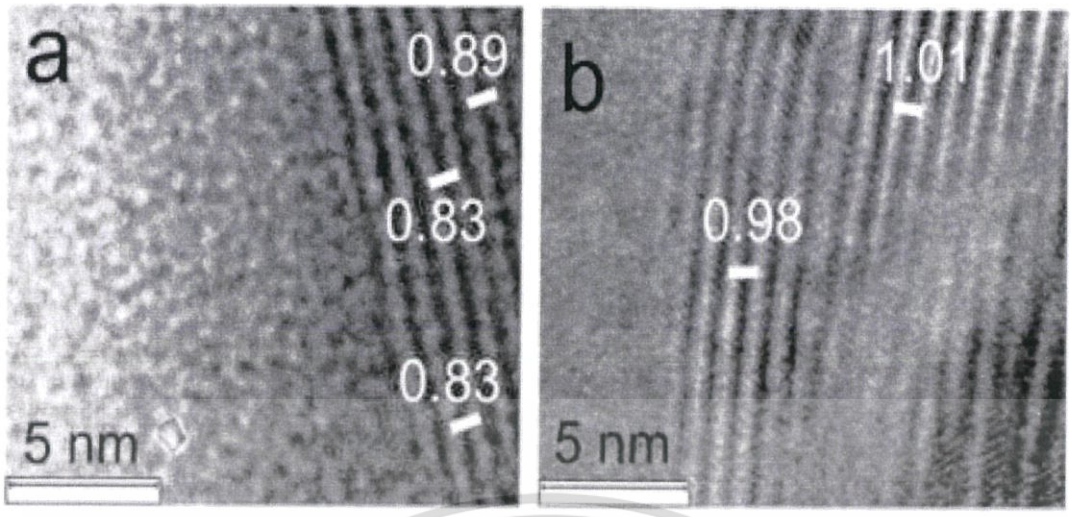

Fig. 8. TEM images of (a) as made $K_{0.8}Zn_{0.4}Ti_{1.6}O_4$, and (b) the solid product after adsorption of palmitic acid at 60 °C for 36 h.

1385 cm^{-1} were detected and assigned to the asymmetric and symmetric stretching of the carboxylate anion [49], respectively. These results suggest the existence of *palmitate species*. Besides, two other peaks (1620 and 1467 cm^{-1}) at the positions slightly shifted from the previous ones (1597 and 1385 cm^{-1}) indicate that palmitate species are in two environments. Several vibrations in the range 1000–1250 cm^{-1} are maintained, confirming the integrity of the skeleton of the intercalated palmitate species after the intercalation into $K_{0.8}Zn_{0.4}Ti_{1.6}O_4$.

Basic sites at several positions in $K_{0.8}Zn_{0.4}Ti_{1.6}O_4$ crystals might involve in the uptake of palmitic acid. Initially, palmitic acid would be adsorbed onto the external basic sites at the basal plane or the edges. The adsorption at the latter site might specifically lead to the rearrangement/activation of palmitic acid into the geometry suitable for the subsequent intercalation *into* the interlayer region. The internal O^{2-} sites at the interlayer region act as a Brønsted base, abstracting the proton from palmitic acid. Meanwhile, the charge-balancing potassium cations at the interlayer region migrate close to the newly-formed palmitate anion, so as to preserve charge neutrality of the system as shown by Eq. (2):

$$K_{0.8}[Zn_{0.4}Ti_{1.6}O_4] + 0.8C_{15}H_{31}COOH \rightarrow H_{0.8}[Zn_{0.4}Ti_{1.6}O_4] + 0.8C_{15}H_{31}COOK \quad (2)$$

where the species in the bracket represents the immobilized layers of lepidocrocite titanate. This reaction might be driven by the acid-base interactions between interlayer O^{2-} sites and proton of palmitic acid, and also by the electrostatic attraction between palmitate anion and K^+. Our observation is somewhat different from that reported [50] by Chou et al., where only the complexation of the carboxylate with divalent (but not monovalent) cations in smectite clays drives the formation of the occluded salt. Upon the intercalation, an internal hydroxylated surface would be formed, together with the palmitate species. The peak at 1023 cm^{-1} in Fig. 4c could be the O-H stretching of the hydroxyl group attached to the layered titanates, similar to the one in as made $K_{0.8}Zn_{0.4}Ti_{1.6}O_4$ at 1018 cm^{-1}. According to Eq. (2), and using the formula mass of 198.02 g/mol ($K_{0.8}Zn_{0.4}Ti_{1.6}O_4$) and 256.42 g/mol (palmitic acid), the content of fully intercalated palmitic acid would be as high as $[(0.8 \times 256.42)/(198.02 + 0.8 \times 256.42)] \times 100\% = 50.9\%$. So, it is reasonable that the uptake of 37% from GC analysis and TGA (Figs. 6 and 7) virtually originates from the "palmitic acid" adsorbed at the interlayer space of this material.

The fact that $K_{0.8}Zn_{0.4}Ti_{1.6}O_4$ intercalates carboxylic acids into the interlayer space has prompted us to investigate its use as a catalyst in the gas-phase ketonization of palmitic acid. The removal of oxygen atom by ketonization (i.e., the transformation of two molecules of the acid into the ketone) could be coupled with the cracking of the corresponding ketone to C_{10} to C_{14} hydrocarbons applicable for use as a diesel fuel. Table 1 compares the conversion of palmitic acid and the distribution of products obtained over tested materials. The 86% conversion of palmitic acid was achieved over $K_{0.8}Zn_{0.4}Ti_{1.6}O_4$, giving palmitone $C_{15}H_{31}(C=O)C_{15}H_{31}$ as the major product via ketonization process. Other groups of products include heavy ketone (mostly C_{17} ketone $CH_3(C=O)C_{15}H_{31}$), C_{10} to C_{14} hydrocarbons, and light hydrocarbons ($< C_{10}$). These products were formed via the cracking at the α,β-position of palmitone, followed by further cracking and/or hydrogen transfer. A detailed reaction pathway for the formation of these products is under investigation and will be reported in a near future. Fig. S5 shows the PXRD pattern of spent $K_{0.8}Zn_{0.4}Ti_{1.6}O_4$, confirming that the lepidocrocite structure is preserved under the heat treatment in air at 800 °C and subsequent contact with palmitic acid at 375 °C (see section 2.5). The stability of $K_{0.8}Zn_{0.4}Ti_{1.6}O_4$ is in contrast to other layered materials such as layered double hydroxide (LDH) [9] or layered hydroxy salt (LHS) [10] which undergo structural transformation upon contact with liquid fatty acids at 100–140 °C. We also tested the catalytic activity of the mixed (Mg/*Al*) oxide "MgAl2.5", which is known to catalyze the ketonization of carboxylic acids by its basic sites [51–53]. MgAl2.5 gave an almost complete conversion of palmitic acid with a smaller yield of

Table 1
Conversion of palmitic acid and the distribution of liquid products over three compositions of lepidocrocite titanate and MgAl2.5.[a]

Catalyst	$K_{0.8}Zn_{0.4}Ti_{1.6}O_4$	$K_{0.8}Mg_{0.4}Ti_{1.6}O_4$	$K_{0.8}Li_{0.27}Ti_{1.73}O_4$	MgAl2.5
Conversion	85.6	96.5	97.9	96.9
Product distribution				
Palmitone	58.6	41.5	39.2	35.5
Heavy ketone[b]	7.1	28.1	23.4	37.0
C_{10} to C_{14} hydrocarbons	17.7	26.5	34.5	22.6
Light hydrocarbons	1.0	1.0	2.9	5.0

[a] Reaction conditions: 5% palmitic acid in *p*-xylene; flow rate of feed plus carrier gas (N_2) 30 mL min^{-1}; reaction temperature 375 °C, atmospheric pressure; W/F = 1500 g h/mol. The values shown were averaged at the time on stream 225–360 min where conversion and product distributions were stabilized.
[b] C_{17} ketone $CH_3(C=O)C_{15}H_{31}$ and others.

palmitone (36%, vs 59% over $K_{0.8}Zn_{0.4}Ti_{1.6}O_4$), together with the larger yield of hydrocarbon products.

Besides, an almost complete conversion of palmitic acid over two other compositions of lepidocrocite titanate was obtained (Table 1). This result can be explained by their larger specific surface area ($K_{0.8}Mg_{0.4}Ti_{1.6}O_4$, 13 m^2/g; $K_{0.8}Li_{0.27}Ti_{1.73}O_4$, 28 m^2/g), among several factors. Since the adsorption of palmitic acid must take place initially before subsequent diffusion and activation at the interlayer space, the catalysts with higher surface area would facilitate the latter two processes. The increase in palmitic acid conversion over these two catalysts is hence accompanied by a decrease in the yield of palmitone, as compared to that over $K_{0.8}Zn_{0.4}Ti_{1.6}O_4$. Yet, the yields of hydrocarbons over Mg and Li-containing lepidocrocite titanate (26–34%) are higher than those over MgAl2.5 (22%). This result indicates a better selectivity of Mg- and Li-containing lepidocrocite titanate toward cracked hydrocarbons, as compared to typical basic oxides.

The high conversion (86%) of palmitic acid over $K_{0.8}Zn_{0.4}Ti_{1.6}O_4$ with a low specific surface area (3 m^2/g) suggests that the observed activity is a result of the active sites at the interlayer space. In line with this view, an SEM image (Fig. 2b) shows that the surface of spent $K_{0.8}Zn_{0.4}Ti_{1.6}O_4$ was roughened and the crystals expanded, in comparison to the dense crystals of as made $K_{0.8}Zn_{0.4}Ti_{1.6}O_4$ with a smooth surface. We propose that as made $K_{0.8}Zn_{0.4}Ti_{1.6}O_4$ intercalates palmitic acid vapor, as it does in the liquid phase. The intercalated palmitic acid and the reaction products might exert appreciable mechanical stress to the layers sandwiching them, such that the layers are deformed and then the crystals expanded. However, the preservation of the crystal structure and the associated two-dimensionality is clearly beneficial.

4. Conclusions

The surface and interlayer basic characters in lepidocrocite titanate $K_{0.8}Zn_{0.4}Ti_{1.6}O_4$ was investigated. $K_{0.8}Zn_{0.4}Ti_{1.6}O_4$ is a weak base as evaluated by CO_2 TPD. Besides, the low basicity implies the major contribution from O^{2-} sites at the external surfaces, while those at the interlayer region are not accessible to CO_2. Yet, the liquid-phase adsorption study suggests the intercalation of palmitic acid into the interlayer region as palmitate salts. The accessibility of interlayer basic sites in $K_{0.8}Zn_{0.4}Ti_{1.6}O_4$ was further demonstrated by its use as a catalyst in the gas phase ketonization of palmitic acid. Despite of small (external) surface area and low basicity, this lepidocrocite titanate was active and selective for the conversion of palmitic acid to hydrocarbons via ketonization-cracking. The layered structure was also preserved in contrast to other 2D basic catalysts reported so far. Moreover, the catalytic activity of lepidocrocite titanate can be tuned by the variation of the metal M^{I} and M^{II} substituting at Ti^{IV} sites.

Acknowledgements

The financial support from The Thailand Research Fund to T.M. (TRG5780160) and T.S. (BRG5680007) is acknowledged. The ^1H ultra-fast MAS NMR experiments were supported by the Natural Science Center for Basic Research and Development, Hiroshima University.

Supplementary Material: PXRD patterns and additional material and methods available.

Appendix A. Supporting information

Supplementary data associated with this article can be found in the online version at http://dx.doi.org/10.1016/j.jssc.2016.03.030.

References

[1] H. Hattori, J. Jpn. Petrol. Inst. 47 (2004) 67–81.
[2] D. Barthomeuf, Catal. Rev. Sci. Eng. 38 (1996) 521–612.
[3] Y. Ono, J. Catal. 216 (2003) 406–415.
[4] J. Weitkamp, M. Hunger, U. Rymsa, Microporous Mesoporous Mater. 48 (2001) 255–270.
[5] D.-W. Lee, Y.-M. Park, K.-Y. Lee, Catal. Surv. Asia 13 (2009) 63–77.
[6] L. Chen, J. Zhao, S.-F. Yin, C.-T. Au, RSC Adv. 3 (2013) 3199–3814.
[7] D.P. Debecker, E.M. Gaigneaux, G. Busca, Chem. Eur. J. 15 (2009) 3920–3935.
[8] R. Ma, T. Sasaki, Acc. Chem. Res. 48 (2015) 136–143.
[9] C.S. Cordeiro, F.R. da Silva, R. Marangoni, F. Wypych, L.P. Ramos, Catal. Lett. 142 (2012) 763–770.
[10] C.S. Cordeiro, G.G.C. Arizaga, L.P. Ramos, F. Wypych, Catal. Commun. 9 (2008) 2140–2143.
[11] D. Groult, C. Mercey, B. Raveau, J. Solid State Chem. 32 (1980) 289–296.
[12] A.F. Reid, W.G. Mumme, A.D. Wadsley, Acta Cryst. B24 (1968) 1228–1233.
[13] T. Gao, H. Fjellvåg, P. Norby, Chem. Mater. 21 (2009) 3503–3513.
[14] T. Gao, P. Norby, H. Okamoto, H. Fjellvåg, Inorg. Chem. 48 (2009) 9409–9418.
[15] W.A. England, J.E. Birkett, J.B. Goodenough, P.J. Wiseman, J. Solid State Chem. 49 (1983) 300–308.
[16] T. Gao, H. Fjellvåg, P. Norby, J. Mater. Chem. 19 (2009) 787–794.
[17] H.Y. Song, A.O. Sjastad, O.B. Vistad, T. Gao, P. Norby, Inorg. Chem. 48 (2009) 6952–6959.
[18] T. Sasaki, F. Kooli, M. Iida, Y. Michiue, S. Takenouchi, Y. Yajima, F. Izumi, B. C. Chakoumakos, M. Watanabe, Chem. Mater. 10 (1998) 4123–4128.
[19] T. Sasaki, M. Watanabe, Y. Michiue, Y. Komatsu, F. Izumi, S. Takenouchi, Chem. Mater. 7 (1995) 1001–1007.
[20] I.E. Grey, C. Li, I.C. Madsen, J.A. Watts, J. Solid State Chem. 66 (1987) 7–19.
[21] M. Kitano, K. Nakajima, J.N. Kondo, S. Hayashi, M. Hara, J. Am. Chem. Soc. 132 (2010) 6622–6623.
[22] T.I. Draskovic, T. Wang, C.N. Henderson, T.E. Mallouk, Int. J. Hydrog. Energy 39 (2014) 4576–4580.
[23] K. Fukuda, K. Akatsuka, Y. Ebina, R. Ma, K. Takada, I. Nakai, T. Sasaki, ACS Nano 2 (2008) 1689–1695.
[24] T. Maluangnont, K. Matsuba, F. Geng, R. Ma, Y. Yamauchi, T. Sasaki, Chem. Mater. 25 (2013) 3137–3146.
[25] T. Sasaki, M. Watanabe, J. Am. Chem. Soc. 120 (1998) 4682–4689.
[26] C.A. Gaertner, J.C. Serrano-Ruiz, D.J. Braden, J.A. Dumesic, J. Catal. 266 (2009) 71–78.
[27] L. Deng, Y. Fu, Q.X. Guo, Energy Fuels 23 (2009) 564–568.
[28] T.N. Pham, T. Sooknoi, S.P. Crossley, D.E. Resasco, ACS Catal. 3 (2013) 2456–2473.
[29] M. Renz, Eur. J. Org. Chem. (2005) 979–988.
[30] M.J. Climent, A. Corma, S. Iborra, K. Epping, A. Velty, J. Catal. 225 (2004) 316–326.
[31] A.V. Grigorieva, V.Y. Yuschenko, I.I. Ivanova, E.A. Goodilin, Y.D. Tretyakov, J. Nanomater. (2012) 920483.
[32] J.A. Santos-Lopez, B.E. Handy, R. García-de-León, Thermochim. Acta 567 (2013) 85–92.
[33] G.B. Raupp, J.A. Dumesic, J. Phys. Chem. 89 (1985) 5240–5246.
[34] W. Hu, L. Li, G. Li, Y. Liu, R.I. Withers, Sci. Rep. 4 (2014) 6582.
[35] H. Izawa, S. Kikkawa, M. Koizumi, J. Phys. Chem. 86 (1982) 5023–5026.
[36] T. Sasaki, M. Watanabe, Y. Komatsu, Y. Fujiki, Inorg. Chem. 24 (1985) 2265–2271.
[37] T. Sasaki, Y. Komatsu, Y. Fujiki, Chem. Mater. 4 (1992) 894–899.
[38] A. Markovits, A. Fahmi, C. Minot, J. Mol. Struct.: THEOCHEM 371 (1996) 219–235.
[39] A. Takagaki, M. Sugisawa, D. Lu, J.N. Kondo, M. Hara, K. Domen, S. Hayashi, J. Am. Chem. Soc. 125 (2003) 5479–5485.
[40] G. Yu, Y. Zhou, R. Yang, M. Wang, L. Shen, Y. Li, N. Xue, X. Guo, W. Ding, L. Peng, J. Phys. Chem. C 119 (2015) 12325–12334.
[41] D.V. Bavykin, M. Carravetta, A.N. Kulak, F.C. Walsh, Chem. Mater. 22 (2010) 2458–2465.
[42] D.J.D. Corcoran, D.P. Tunstall, J.T.S. Irvine, Solid State Ion. 136–137 (2000) 297–303.
[43] T. Maluangnont, G.T. Bui, B.A. Huntington, M.M. Lerner, Chem. Mater. 23 (2011) 1091–1095.
[44] T. Maluangnont, W. Sirisaksoontorn, M.M. Lerner, Carbon 50 (2012) 597–602.
[45] S. Nakano, T. Sasaki, K. Takemura, M. Watanabe, Chem. Mater. 10 (1998) 2044–2046.
[46] K. Fujimoto, N. Tobito, S. Ito, J. Ion Exch. 25 (2015) 12–15.
[47] M. Shirpour, J. Cabana, M. Doeff, Chem. Mater. 26 (2014) 2502–2512.
[48] T. Sasaki, F. Izumi, M. Watanabe, Chem. Mater. 8 (1996) 777–782.
[49] G.G.C. Arizaga, A.S. Mangrich, J.E.F. da Costa Gardolinski, F. Wypych, J. Colloid Interface Sci. 320 (2008) 168–176.
[50] C.-C. Chou, M.-L. Chiang, J.-J. Lin, Macromol. Rapid Commun. 26 (2005) 1841–1845.
[51] E. Kandare, J.M. Hossenlopp, Inorg. Chem. 45 (2006) 3766–3773.
[52] K. Parida, J. Das, J. Mol. Catal. A 151 (2000) 185–192.
[53] J. Das, K. Parida, React. Kinet. Catal. Lett. 69 (2000) 223–229.

AUTHOR BIOGRAPHY

Mr. Porn-a-nan Arsa was born on August 28, 1990 in Bankoko. He graduated a Bachelor degree in Inductrial Chemical Science from the Department of Chemical, Faculty of Science, King Mongkut's Institute of Technology Ladkrabang in 2012. He has been a graduate student in Petrochemicals and Hydrocarbon Chemistry program of Faculty of Science, King Mongkut's Institute of Technology Ladkrabang, since 2012.

Work experiences:

2012 –2016 Teacher Assistant, King Mongkut's Institute of Technology Ladkrabang.

Conferences

2015 **Pornanan Arsa**, Tosapol Maluangnont and Tawan Sooknoi, Adsorption and swelling of lepidocrocite titanate by palmitic acid and heptanoic acid, Poster presentation, Pure and Applied Chemistry International Conference 2015 (PACCON 2015), January 21-23, 2015, Amari watergate hotel, Bangkok, Thailand.

Publication

2016 Tosapol Maluangnont, **Pornanan Arsa**, Kanokporn Limsakul, Songsit Juntarachairot, Saithong Sangsan, Kazuma Gotoh, Tawan Sooknoi. 2016. "Surface and interlayer base-characters in lepidocrocite titanate: The Adsorption and intercalation of fatty acid." *Journal of Solid State Chemistry*. 238: 175–181.